SEDIMENTATION AND TECTONIC EVOLUTION OF CENOZOIC SEQUENCES

FROM BENGAL AND ASSAM FORELAND BASINS, EASTERN HIMALAYAS

Except where reference is made to the work of others, the work described in this thesis is my own or was done in collaboration with my advisory committee. This thesis does not include proprietary or classified information.

_____

Mohammad Wahidur Rahman

Certificate of Approval:

_____	_____
Charles E. Savrda Professor Geology and Geography	Ashraf Uddin, Chair Associate Professor Geology and Geography
_____	_____
Willis E. Hames Professor Geology and Geography	George T. Flowers Interim Dean Graduate School

SEDIMENTATION AND TECTONIC EVOLUTION OF CENOZOIC SEQUENCES FROM BENGAL AND ASSAM FORELAND BASINS, EASTERN HIMALAYAS

Mohammad Wahidur Rahman

A Thesis

Submitted to

the Graduate Faculty of

Auburn University

in Partial Fulfillment of the

Requirement for the

Degree of

Master of Science

Auburn, Alabama
August 9, 2008

SEDIMENTATION AND TECTONIC EVOLUTION OF CENOZOIC SEQUENCES

FROM BENGAL AND ASSAM FORELAND BASINS, EASTERN HIMALAYAS

Mohammad Wahidur Rahman

_____
Mohammad Wahidur Rahman

August 9, 2008
Date of Graduation

VITA

Mohammad Wahidur Rahman, son of Mr. Bazlur Rahman and Mrs. Begum Shamsunnahar Chowdhury, was born in 1978 in Comilla, Bangladesh. He passed his Higher Secondary Certificate Examination in 1995 from Comilla Victoria Govt. College with distinctions. He received his Bachelor of Science and Master of Science degrees in Geology in 2003 and 2006, respectively, from the University of Dhaka, Bangladesh. He entered the graduate school at Auburn University to pursue his second Masters degree from the Department of Geology and Geography in Fall 2006.

THESIS ABSTRACT

SEDIMENTATION AND TECTONIC EVOLUTION OF CENOZOIC SEQUENCES FROM BENGAL AND ASSAM FORELAND BASINS, EASTERN HIMALAYAS

Mohammad Wahidur Rahman

Master of Science, August 9, 2008
(Master of Science, University of Dhaka, Bangladesh, 2006)
(Bachelor of Science, University of Dhaka, Bangladesh, 2003)

180 Typed pages

Directed by Ashraf Uddin

The Himalayan Mountains developed due to the collision of the Indian and Eurasian plates. There are two large foreland basins south of the eastern Himalayas: Assam Basin, located near the eastern syntaxis of the Himalayas, and the Bengal Basin further to the south. The Indo-Burman Ranges lie to the southeast of Assam and east of the Bengal Basin. The Indian craton is located to the west of the Bengal Basin. Mineralogical, geochemical, and geochronological studies provide critical information for the evolution of the Tertiary sequences of these basins.

Sandstone modal analyses document that Eocene Disang ($Qt_{56}F_5L_{40}$), Oligocene Barail ($Qt_{59}F_7L_{34}$), Miocene Surma ($Qt_{68}F_3L_{29}$), and Mio-Pliocene Tipam ($Qt_{53}F_9L_{38}$) from Assam Basin, and Oligocene Barail ($Qt_{83}F_3L_{14}$), Miocene Surma ($Qt_{59}F_{18}L_{23}$), Mio-Pliocene Tipam ($Qt_{57}F_{14}L_{29}$), and Pliocene Dupi Tila ($Qt_{54}F_{21}L_{25}$) from the Bengal Basin

plot in the “recycled orogenic” provenance field of Dickinson, indicating an orogenic source from the Himalayas and/or Indo-Burman Ranges. Studies of detrital heavy-minerals, including garnets, also suggest orogenic source terranes with input from low- to medium-grade metamorphic rocks. Chrome spinels from the Bengal Basin were probably derived either from Himalayan arc material or Indo-Burmese Alpine-type ophiolites, while those of Assam were mostly derived from the Indo-Burman Ranges. Oligocene muscovite grains from Assam give a cooling age range from 35 to 204 Ma, indicating that they likely sourced from the Gangdese batholith of Tibet and the Mogok Metamorphic Belt of Indo-Burman Ranges (Myanmar). Cooling ages of Miocene muscovites from Assam range from 28 Ma to 81 Ma, with noticeable modes at 28-50 Ma and 65-80 Ma. This suggests that source rocks for Assam Miocene units, most likely the Gangdese batholith of Tibet and the Mogok belt of Myanmar, are older than that from the Bengal Basin. Whole-rock chemistry data reveal that sediments from the Assam Basin and the post-Oligocene sediments from the Bengal Basin were derived from granitic source rocks. Oligocene samples from Bengal Basin, however, show high silica contents suggesting intense chemical weathering during deposition closer to the equator.

Depocenters in the foreland basins of the eastern Himalayas progressed generally south and west through time (in Assam during the Paleogene and in the Bengal Basin during the Neogene). The right-lateral Kaladan fault may have brought these two depositional systems closer in the Miocene.

ACKNOWLEDGMENTS

I am pleased to thank the almighty God who has been with me all the way and given me the scope to study about the mystery of the Earth. I would like to express my thanks and gratitude to my dear teacher Dr. Ashraf Uddin for bringing me to Auburn University and giving me the chance to get a Master's degree in Geology. Dr. Uddin helped me not only as the principal advisor but also as a real guardian to get the best outcome of this research.

I would like to express my sincere thanks to Dr. Charles Savrda, who helped with significant editing in this thesis. It would have been difficult to get this research work done without Dr. Savrda. I also would like to thank Dr. Willis Hames for help with geochronology part of this thesis.

This research was funded by the U.S National Science Foundation (NSF-EAR-0310306), Geological Society of America, and the Department of Geology and Geography of Auburn University. I also acknowledge Mr. Chris Fleisher of University of Georgia for help during microprobe analysis. I thank Dr. Humayun Akhter and few friends, specially Himel, Bahar, and Babu for help in field. All faculty members and fellow graduate students here at Auburn gave me moral support.

I show gratitude to my beloved Mother, my loving sisters and brothers for their endless love, encouragement, and inspiration. I dedicate this thesis to my Mother.

Style manual or journal used

Geological Society of America Bulletin

Computer software used

Adobe Acrobat 6 Professional

Adobe Illustrator 8.0

Adobe Photoshop 5.5

ArcGIS 9.1

Golden Software Grapher 3.0

Golden Software Surfer 8.0

Microsoft Excel 2003

Microsoft Word 2003

TABLE OF CONTENTS

LIST OF FIGURES

LIST OF TABLES

CHAPTER 1: INTRODUCTION

1.1 INTRODUCTION

Provenance analysis is based on the assumption that the composition of detrital sediments records the composition of the source region from which those sediments were derived (Dickinson and Suczek, 1979). This theoretical relationship enables interpretation of paleogeography (Uddin and Lundberg, 1998a), ancient plate tectonic settings (Graham et al., 1976; Dickinson and Suczek, 1979), and rock-uplift and exhumation histories (Graham et al., 1976) from the sedimentary record. In some cases, such as those involving deeply denuded source terranes, sedimentary rocks may be the only known resource for acquiring such information. Whereas the validity of this assumption has been demonstrated for numerous detrital sediments and sedimentary rocks (Dickinson, 1970a, 1982; Dickinson and Suczek, 1979), provenance interpretation of compositional data requires attention to the influence of other factors (Suttner, 1974).

Sandstone composition analyses are very important in tracing sediment provenance (Dickinson and Suczek, 1979). Sandstone compositional analyses, in which proportions of detrital framework grains within a sand (stone) sample are plotted on various ternary plots (QtFL, QmFLt, etc.), can distinguish various tectonic settings of source areas (Ingersoll et al., 1995). This approach helps to understand and interpret plate interactions in the geologic past. Provenance studies that focus on some key attributes of detrital mineralogy provide important constraints on basin evolution and unroofing

history of mountain belts (Dorsey, 1988; Uddin and Lundberg, 1998a, b). Reconstruction of provenance from detailed mineralogical analyses is based on the assumption that modes of transport, depositional environments, climates, and diagenesis have not significantly altered detrital grain composition (Basu, 1976).

The Himalayan mountain chain is one of the world's comparatively young geological features and contains the highest peak on Earth. This chain developed due to the collision of the Indian and Eurasian plates (Fig. 1) in an area once occupied in part by the Tethys Sea. Orogenesis is partly recorded in sediments derived from the eastern part of the Himalayas and deposited in subsiding troughs to the south, the Assam-Bengal Basin system (Fig. 1). The Bengal basin originated due to the collision of India with Eurasia and Burma, which built the extensive Himalayan and Indo-Burman Ranges and loaded the lithosphere to form flanking sedimentary basins. The northeastern part of this basin contains a thick (12-16 km) fill of late Mesozoic and Cenozoic strata (Hiller and Elahi, 1984). The Early Paleogene history of the Bengal Basin was characterized by sedimentation on a passive continental margin formed during Mesozoic rifting and opening of the Indian Ocean (Sclater and Fisher, 1974). Cenozoic sediments filled the Assam Basin, which probably was a remnant ocean basin during the early stages of its development (Graham et al., 1975). Stratigraphic sequences deposited in Assam Basin preserve a continuous record of orogenic events. As a result of collision and sedimentation in the basin, tectonic events, such as flexural loading and basement faulting, led to the formation of a complex foreland basin characterized by dramatic topographic relief and complex geometry (Evans, 1964).

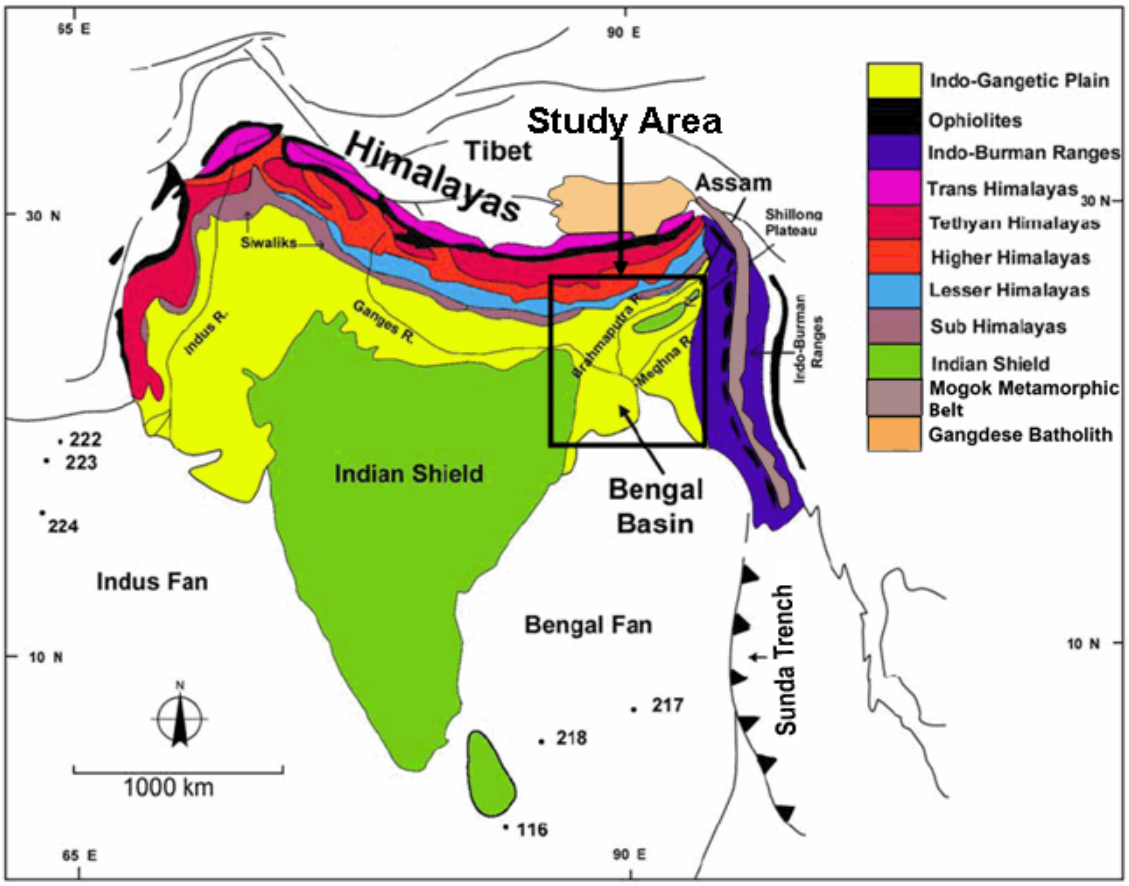

Figure 1. Map showing major tectonic elements near the study area, including the Bengal Basin, Assam Basin, the Himalayas, and the Indo-Burman Ranges (after Uddin and Lundberg, 1998a). The Gangdese Batholith is located at the southeastern part of Tibet (after Copeland et al., 1995) and the Mogok Metamorphic Belt (MMB) is located in the Indo-Burman Ranges (after Mitchell et al., 2007).

The right-lateral Kaladan fault (Figs. 2 and 3) demarcates the boundary between the Bengal basin (Indian plate) in the west and the fold belt of Mizoram and lower Assam of India (Indo-China plate) in the east (Zutshi, 1993). Because of its location in the eastern part of the Mizoram-Tripura-Chittagong Folded belt, the Kaladan fault may have played a significant role in the tectonic evolution of Bengal-Assam basin system. This fault trends northeast-southwest along the Kaladan River down to the Arakan coast. This fault is identified by the geologists of the Bangladesh Oil, Gas, and Mineral Corporation, (BOGMC: Exploration Promotion Brochure) as a dextral transform fault, but the basis of this identification is not known. Focal plan solution of moderate size earthquakes that have occurred in that region also suggest that this is a strike-slip fault (Fig. 2).

The provenance histories of Cenozoic sediments in the Bengal and Assam basins are not adequately known. Reconstruction of the paleogeography of this region constitutes an important goal of the proposed research. This study investigates the petrology of Cenozoic sedimentary sequences exposed on both eastern and western sides of the Kaladan fault (Figs. 2 and 3).

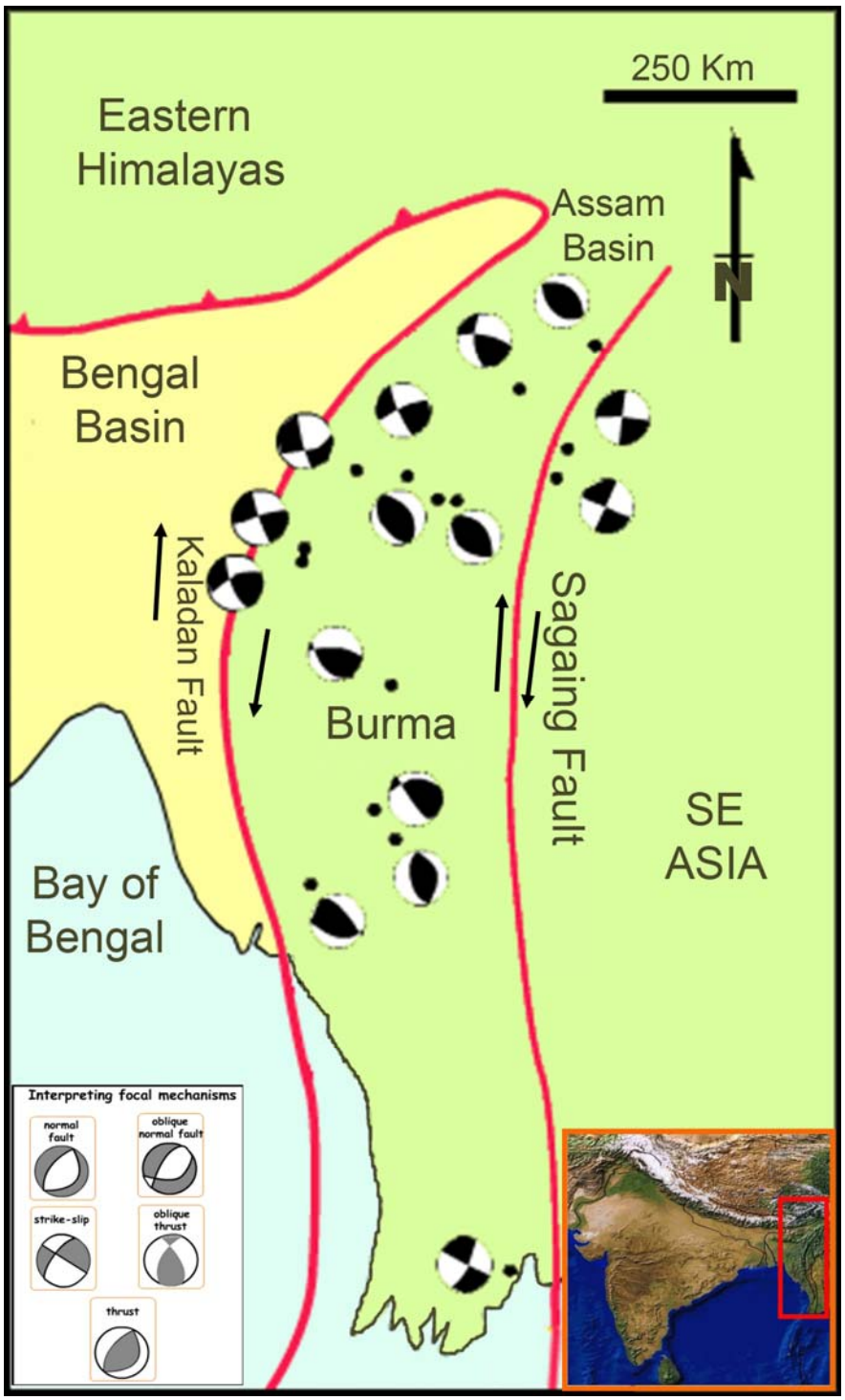

Figure 2. Nature and orientation of the Kaladan fault, which separates the Bengal Basin from Assam Basin. Diagram also shows another prominent fault, the Sagaing fault, east of the Kaladan fault (after www.see.leeds.ac.uk/structure/dynamicearth).

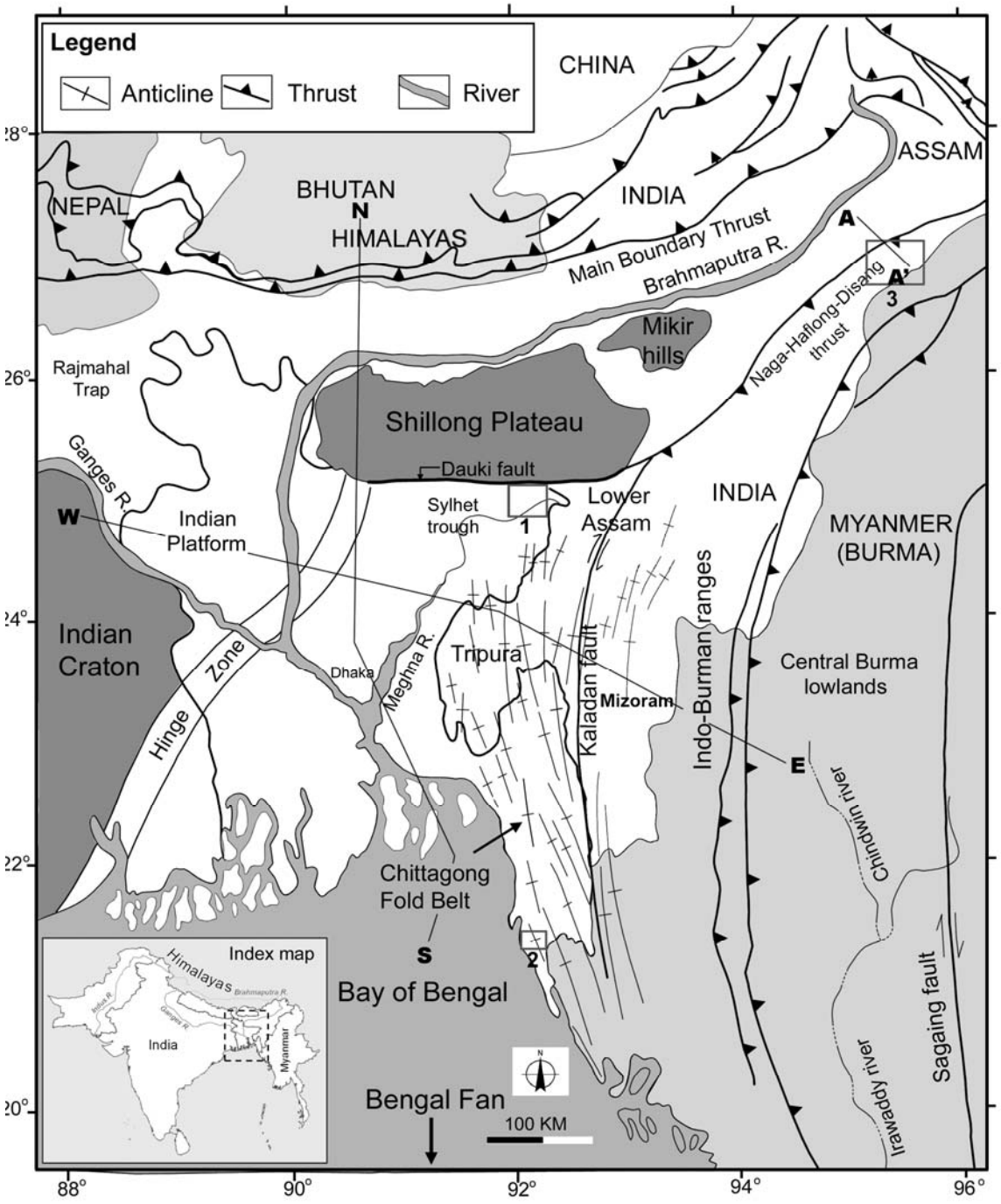

Figure 3. Map showing major tectonic elements in and around the Bengal-Assam basins. The Kaladan fault separates the eastern part of the Bengal Basin from Assam Basin, and other east Indian states. Boxes 1, 2, 3 in the figure show sample locations. Cross-sections along N-S, E-W, and A-A' lines are shown in Figures 4, 5, and 6 (after Uddin and Lundberg, 1998b).

Although the source areas of Paleogene sediments in the Assam Basin have been inferred to be orogenic terranes in the eastern Himalayas and the Indo-Burman Ranges (Kumar, 2004), the provenance history of Paleogene sediments of the Bengal Basin is still debatable. Johnson and Nur Alam (1991) proposed that the Paleogene sandstones from the Bengal Basin were derived from the eastern orogenic belts. In contrast, Uddin and Lundberg (1998a) suggest that these sediments were derived from the Indian craton. Zahid (2005), however, suggested a mixed provenance, with derivation from both the Indian craton and the Indo-Burman Ranges. Neogene sediments from both the Bengal and Assam basins indicate an orogenic source (Rahman and Faupl, 2003; Kumar, 2004), and thus suggest that orogenic activity had certainly began in eastern Himalayan areas by the early Miocene.

The hypothesis addressed in this research is that Eocene-Oligocene sandstones from the Assam Basin and rocks of similar age from the Bengal Basin of Bangladesh were on two different plates during their deposition. These two basins may have been brought adjacent to each other during the lower Miocene along the Kaladan fault. This hypothesis was tested through sandstone compositional studies of the two sequences and detrital geochronologic analyses to document the nature of the disparate source terranes. This work also provides constraints on the early unroofing history of the Indo-Burman Ranges and eastern Himalayas.

1.2 LOCATION OF THE STUDY AREA

The Bengal Basin, located in Bangladesh and in the West Bengal state of India, is situated at the confluence of the two great river systems of the eastern South Asia, the Ganges from the west and the Brahmaputra from the north. The Shillong Plateau stands at the immediate north and the Himalayas to the distant north (Figs. 1 and 3). The Indo-Burman Ranges are to the east and the Indian Shield is to the west (Figs. 1 and 3). The area is open to the south and extends into the Bay of Bengal and the Bengal deep sea fan.

The Assam Basin, located at the northeastern part of the joint Assam-Bengal system, is bounded by the eastern Himalayas to the north, Mishmi Hills to the northeast, Indo-Burman Ranges to the east, Bengal Basin to the south, and Shillong Plateau to the southwest (Fig. 2). The studied Digboi-Margherita area is situated in the northeastern part of Assam basin, in the Schuppen belt, which consists of a series of NE-SW imbricate thrust faults between the Naga and Disang thrust belts (Rangarao, 1983). The sedimentation pattern, geomorphology, and geometry of the Assam Basin are influenced by the Brahmaputra River. Uplift of the Shillong Plateau in the Pliocene and has since controlled major sedimentation and structural features of the Assam Basin (Fig. 2; Johnson and Nur Alam, 1991).

The history of development of the Assam-Bengal Basin is directly related to uplift of the Himalayas and the Indo-Burman Ranges. The east-west Himalayan arc is over 2500 km long and 300 km wide (Fig. 1). The area is convex toward the south and made up of four longitudinal litho-tectonic units juxtaposed along generally north-dipping thrust faults (Fig. 1). The Indo-Burman Ranges trend generally north to south, with a width of approximately 230 km. These ranges encroach the Assam-Bengal basin from the

east, associated with subduction of the Indian plate beneath the Burmese platelet (Fig. 3; Sengupta et al., 1990). The Indo-Burman Ranges are composed of Cretaceous to Eocene pelagic sediments overlain by a thick Eocene to Oligocene flysch and upper Miocene to Pleistocene molasse (Brunnschweiller, 1974).

Representative sandstone samples from both sides of the Kaladan fault were analyzed for this research. Most of the samples were collected from the northeastern Sylhet trough (box 1, Fig. 3; Fig. 4) and the southeastern Ulahtaung Anticline (box 2, Fig. 3; Fig. 5) of the Bengal Basin. Samples from the Assam Basin were collected from the Digboi-Margherita area (box 3, Fig. 3; Fig. 6), where almost all the Cenozoic sequence is well exposed along the following four sections: (1) Tipang Pani section (Naogaon Formation); (2) Namdang section (Naogaon and Baragolai formations); (3) Dirak section (Baragolai Formation); and (4) Margherita – Changlang section (Disang, Naogaon, and Baragolai formations). Samples were collected based on recommendations from experts familiar with the region and existing literature.

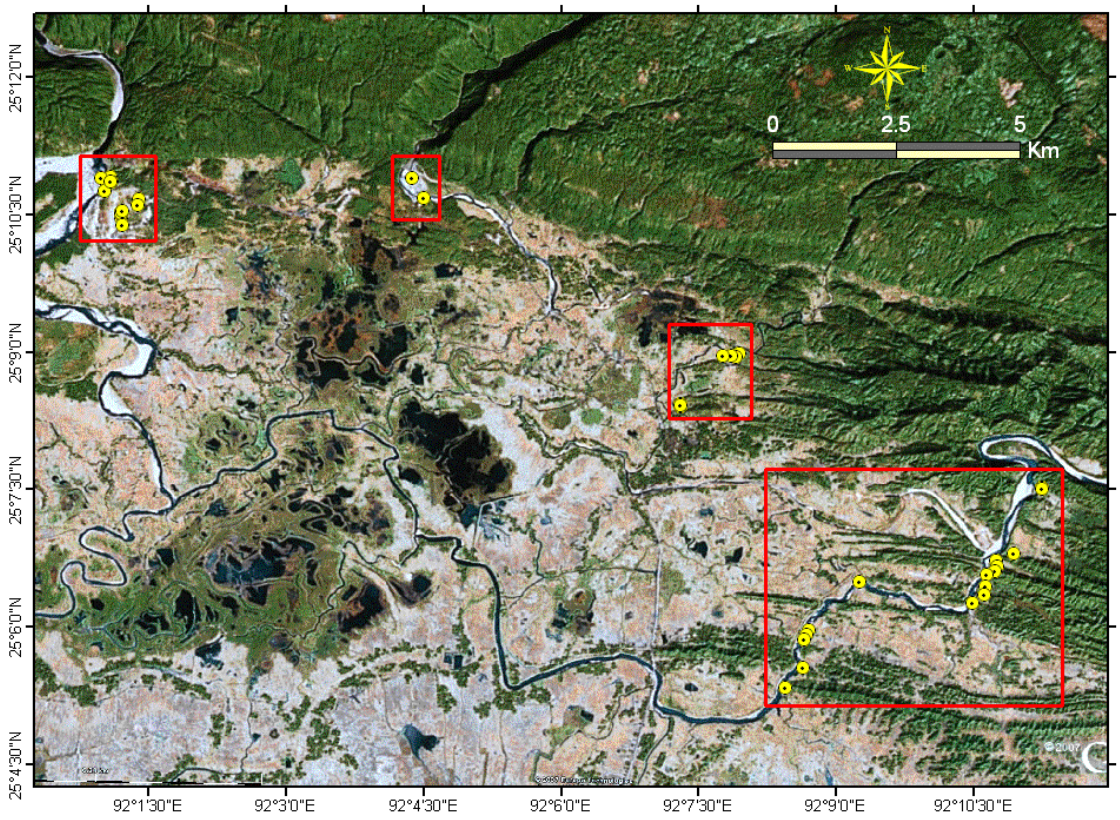

Figure 4. Map showing the northeastern part of the Bengal Basin where samples of Oligocene to Pliocene were collected (box 1 in Fig. 3) (from Google Earth).

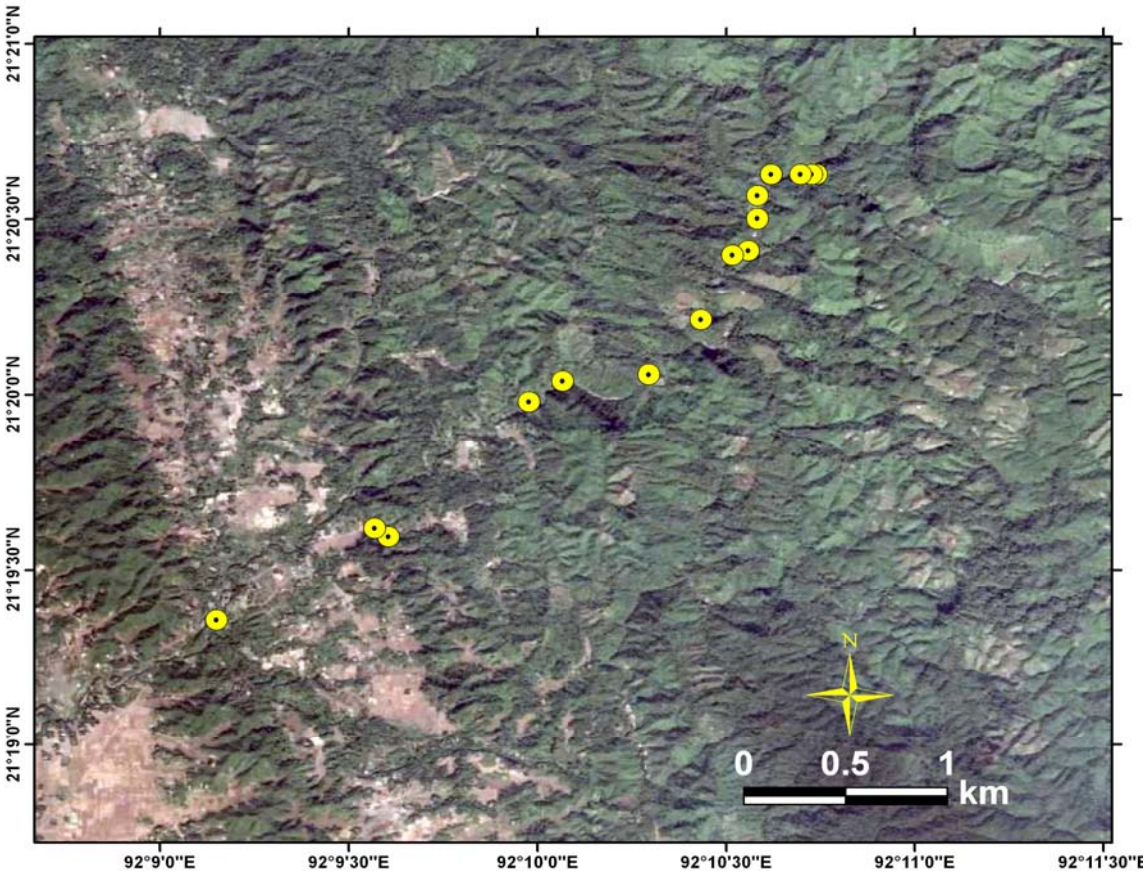

Figure 5. Location of samples collected from the Ulahtaung anticline, located in the eastern fold belts of southeast Bengal Basin (box 2 in Fig. 3). Middle Miocene and younger samples are exposed in these sections (from Google Earth).

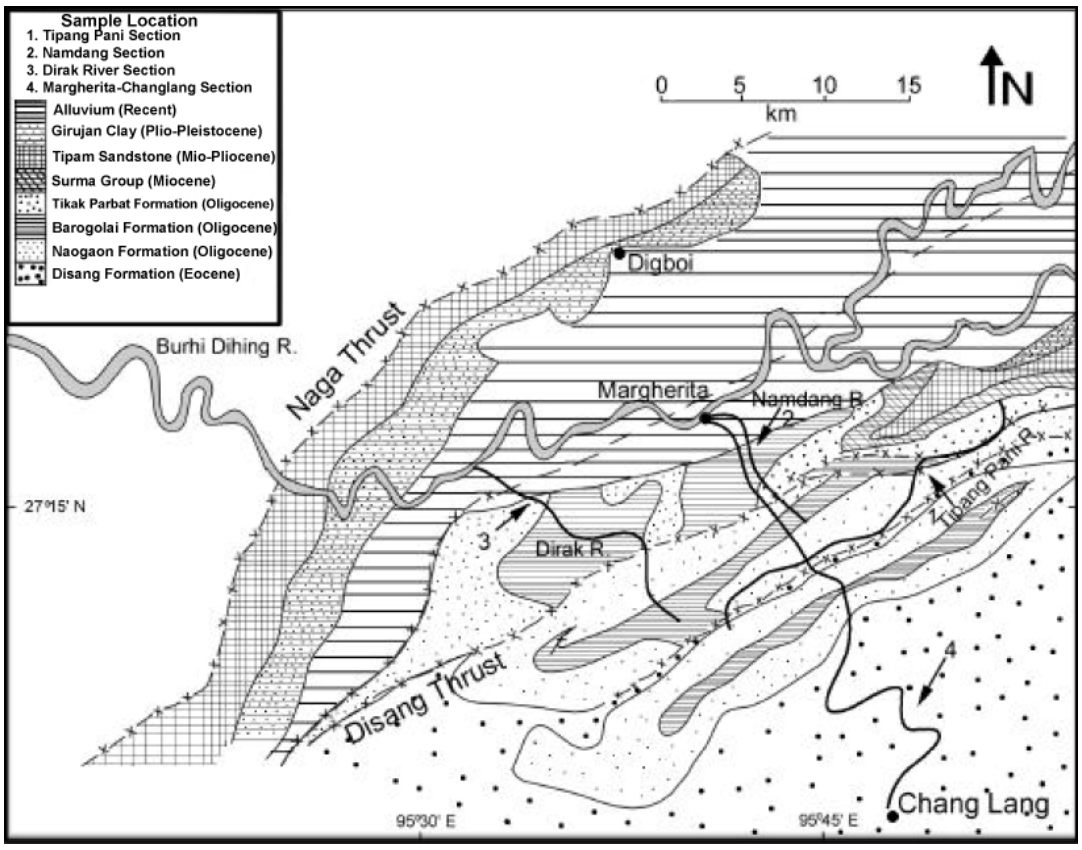

Figure 6. Map showing the geology of part of Assam Basin (box 3 in Fig. 3) and four sections along which samples were collected (after Kumar, 2004).

1.3 PREVIOUS WORKS

Johnson and Nur Alam (1991) studied sediments from the Sylhet trough of Bangladesh and suggested that the Dauki fault was a thrust fault and that the Shillong Plateau was uplifted in the Pliocene. Copeland and Harrison (1990) found the ages of muscovite grains from the Bengal Fan sediments to be around 30 Ma. Uddin and Lundberg (1998a, b) studied Cenozoic sediments from Bengal Basin and found that the pre-Miocene sediments were not derived from Himalayas, but rather probably were transported short distances from the Indian craton to the west. Godwin et al. (2001) and Uddin et al. (2002) did preliminary work on sediments from the Assam Basin and suggested that the provenance history is controlled by localized tectonic activity. Rahman and Faupl (2003) reported cooling ages of muscovite grains for Miocene sediments from the northeastern Bengal Basin as ca. 25 Ma to 35 Ma. The $^{40}Ar/^{39}Ar$ ages for detrital muscovite grains of the early Miocene Bhuban sediments of the Bengal Basin range from ca 16 Ma to 516 Ma and consistently reflect peaks at ~16 Ma to ~22 Ma, suggesting a young episode of orogenic activity in the Himalayas (Uddin et al., 2005). Zahid (2005) studied Oligocene and lower Miocene sequences of the Bengal Basin and suggested a mixed provenance.

The Digboi oil field, which was the first oil discovery in Assam area, was drilled in 1889 (Selly, 1998). Sinha and Sastri (1973) worked on heavy minerals to assess provenance for the southeastern Assam basin. Geologists from India and abroad explored this basin to understand its tectonic history and related events (Baksi, 1965; Karunakaran and Rangarao, 1976). Tectonic framework of the Assam-Burma-Bengal basins and major tectonic events were studied by Hutchison (1989). Kent and Dasgupta (2004) discussed

the relationship between sequence stratigraphy and structure of the upper Assam valley. Kumar (2004) focused on the provenance history of Cenozoic sediments of the north Assam area, near the eastern Himalayan syntaxis. Uddin et al. (2006) studied U/Pb dates on zircon crystals from Assam Basin and inferred predominant sources from the Himalayas and Tibetan Plateau. Very little work has been done on evaluating the stratigraphic sequences on opposite sides of the Kaladan fault.

CHAPTER 2: TECTONIC SETTING AND REGIONAL GEOLOGY

2.1 INTRODUCTION

The tectonic evolution of the Bengal and Assam basins is controlled by north-south convergence along the Himalayas and east-west convergence along the Indo-Burman Ranges. The tectonic nature of these basins can be attributed to the interaction of the three major plates: Indian, Tibetan (Eurasian), and Burma (West Burma) plates. The Bengal Basin started its development at the beginning of the Late Cretaceous when the Indian plate rifted away from Antarctica along an inferred northeast-southwest-trending ridge system (Sclater and Fisher, 1974). Later, the Indian plate began migrating rapidly northward, leading to its collision with Asia, which probably began during the Eocene between 55 to 40 Ma ago (Curray et al., 1982; Molnar, 1984; Rowley, 1996). In the eastern part of the Bengal Basin, the subduction complex of the Indo-Burman arc emerged above sea level, although major uplift of the Himalayas may not have begun until the Miocene (Gansser, 1964). The history of the Assam and Bengal basins is clearly related to the rifting and separation of the Indian plate from Gondwanaland and to the uplift and erosion of the Himalayas and the Indo-Burman Ranges.

The Indo-Burman Ranges are very active organic belts that trend generally north to south with a width of approximately 230 km. These ranges are encroaching the Assam-Bengal basin from the east, associated with subduction of the Indian plate beneath the Burmese platelet (Fig. 2, Sengupta et al., 1990). They are composed of Cretaceous to Eocene pelagic sediments overlain by the thick Eocene to Oligocene

synorogenic sediments, and upper Miocene to Pleistocene post-orogenic sediments (Brunnschweiller, 1966).

2.2 INDIAN CRATON

The Cretaceous has widely been considered as the time of initial rifting of the Indian continent from the East Gondwana block (Curry and Moore, 1974), although the time of collision between the Indian plate and the Eurasian plate is a subject of considerable controversy. The Indian block collided terminally with the Tibetan block during Early to Middle Eocene, initiating Himalayan orogenesis (Dasgupta and Nandy, 1995). There were two episodes of extensive continental flood basalt extrusion, reflected by the Rajmahal Trap (~118 Ma; Kent et al., 2002) and Deccan Trap (70-65 Ma; Mahoney et al., 1983). The Shillong Plateau is a major tectonic feature in between Assam and Bengal basins and was uplifted to its present height in the Pliocene (Johnson and Nur Alam, 1991). This plateau is bounded to the west by the Rajmahal trough fault (Fig. 3) and to the south by the Dauki fault (Fig. 3; Johnson and Nur Alam, 1991). Precambrian rocks of the Shillong Plateau are divided into two groups: (1) an Archean Gneissic Complex; and (2) the Proterozoic Shillong Group (Rahman, 1999). The boundary between the Gneissic Complex and Shillong Group is marked by a lithologic and structural break. The Shillong Group was overlain by Mesozoic to Miocene sediments prior to Pliocene uplift of the Shillong Plateau (Johnson and Nur Alam, 1991). Late Mesozoic and Cenozoic sedimentary rocks drape portions of the southern Shillong Plateau and generally dip south in a monocline. As much as 15-18 km of structural relief between the Shillong Plateau and the basement of the Sylhet trough has been postulated (Murthy et al., 1976; Hiller and Elahi, 1988). The poorly exposed Dauki fault forms the contact between the Shillong Plateau and

the Sylhet trough (Fig. 3). Cratonic continental crust is exposed in the Shillong Plateau, Mikir hills, and various other small isolated outcrops.

2.3 INDO-BURMAN RANGES

The 230 km wide, generally north-south trending Indo-Burman Ranges make up an active orogenic belt that encroaches the Bengal Basin from the east in response to subduction of the Indian plate beneath the Burmese platelet (Fig. 3, Curray et al., 1979; Sengupta et al., 1990). Several authors, like Curray et al. (1979), Ni et al. (1989) and Sengupta et al. (1990), suggested that the Indo-Burman Ranges were trench deposits containing ophiolitic melanges scraped off the Indian plate. East-west crustal compression is still active in the Indo-Burman Ranges as evidenced by north-south trending folds of very young (Plio- Pleistocene) sediments (Le Dain, 1984). Earthquake studies suggest that the basement of the Indian plate below the Indo-Burman Ranges is moving north with respect to Asia (Ni et al., 1989), producing right-lateral slip along the Sagaing fault and other faults located east of these ranges (Fig 2, Le Dain et al., 1984).

2.4 BENGAL BASIN

The Bengal Basin has two broad tectonic divisions: (1) the Precambrian ‘Indian Platform’ (also known as the ‘stable shelf’) to the northwest and west; and (2) the ‘Bengal Foredeep’ in the southeast (Fig. 3). These two provinces are separated by a 25-to-100-km-wide, NE-trending ‘hinge zone’ (Bakhtine, 1966), which follows the ‘Calcutta-Mymensingh Gravity High’ (Alam, 1972; Khandoker, 1989) produced by deep-seated basement faults. Within the narrow hinge zone, the basin slope increases from 2-3° to 6-12° and the thickness of overlying deposits increases from 1800 m to

4000 m.

The ‘Bengal Foredeep’, a zone of very thick sediment overlying deeply subsided basement, is subdivided into two zones based on gravity studies: (1) the northwestern Platform Flank; and (2) the eastern Folded flank. The zones are separated by another NE-SW-trending gravity high known as the ‘Barisal-Chandpur Gravity High' (Khandaker, 1989). The Platform Flank of the Bengal Foredeep is occupied by two structural troughs and an intervening high, including the Sylhet trough (also known as the Surma basin), and in the northeastern Bengal Basin is important for its petroleum reservoirs. The Folded Flank of the Bengal foredeep mainly comprises sub-Himalayan orogenic detritus, folded tightly (as a wrench belt) about north-trending axes, with structural complexity increasing eastward toward the Indo-Burman Ranges. The dividing line between the extensional western basin and the compressive wrenched eastern margin is approximately marked by the 90th Meridian.

The eastern fold belt marks the outermost part of the zone of compression between the west Burma block and the Indian plate (Fig. 7). The north-south-trending folds in this belt decrease in amplitude and become broader and less complex westward. Intensity of folding rapidly attenuates westwards; the central and western parts of the basin are relatively undeformed. Some structures show evidence of more than one phase of deformation. The age of folding ranges from the Pliocene to Recent.

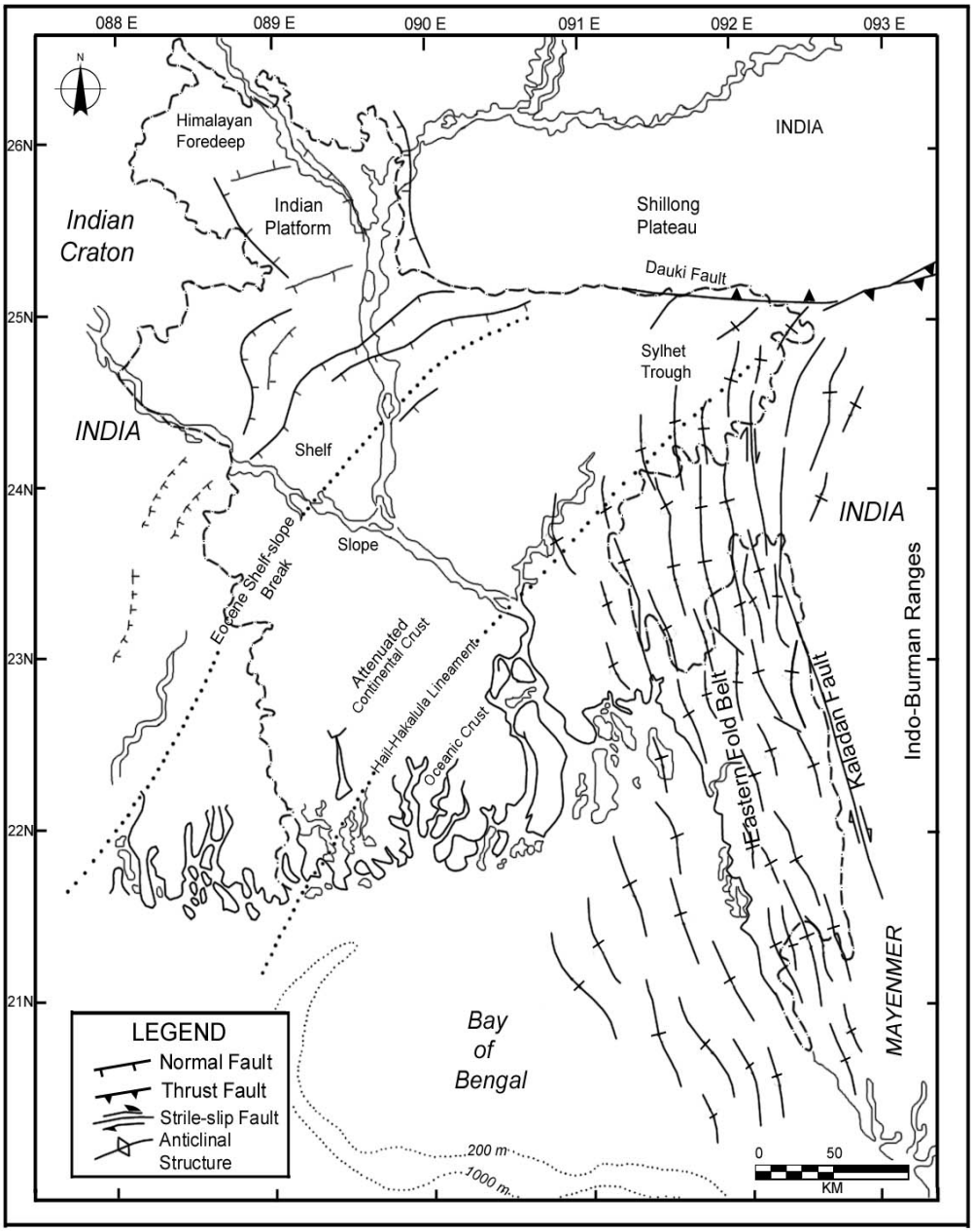

Figure 7. Structural elements of Bengal basin showing the extent of continental and oceanic crusts, Eocene shelf-slope break, Dauki fault separating Shillong Plateau and Sylhet trough, and anticlinal trends in eastern Bengal basin (after Hoque, 1982).

The Sylhet trough is a subbasin of the Bengal Basin in northeastern Bangladesh. It is characterized by a large, closed, negative gravity anomaly (as low as -84 milligals; Mirkhamidov and Mannan, 1981; Fig. 8). The Sylhet trough has minimal topography and is actively subsiding (Holtrop and Keizer, 1970). Estimates of sediment thickness in the Sylhet trough range from about 12 to 16 km (Hiller and Elahi, 1984). The eastern part of the Sylhet trough lies in the frontal zone of the Indo-Burman Ranges.

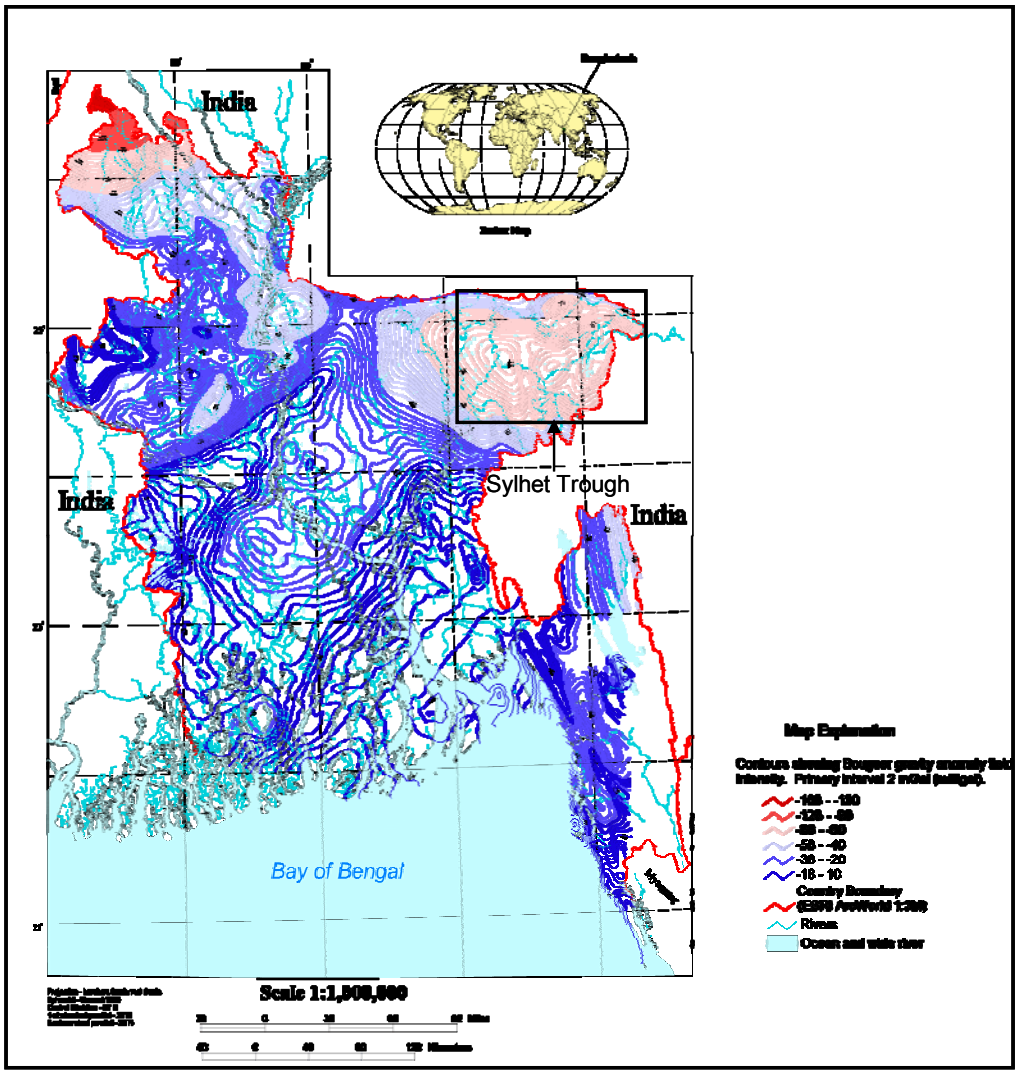

Figure 8. Bouguer gravity-anomaly map of the Bengal Basin (after Geological Survey of Bangladesh and USGS, 1990).

2.5 ASSAM BASIN

The following structural elements are important in and around the Assam Basin: (1) Upper Assam Plains; (2) Schuppen Belt; (3) Kohima-Patkai synclinorium; and (4) Eastern Zone, including the Ophiolitic Belt (Fig. 1). The upper Assam Plains is the alluvial plain of the Brahmaputra River and forms a part of the shelf of the Assam-Arakan Basin. It represents a depressed, northeastern extension of Shillong-Mikir Hills that was down-faulted sometime during the Upper Cretaceous (Das Gupta and Biswas, 2000). The plain is bounded by the Himalayas to the north, by the Mishmi hills to the east, and by the raised rim of the Assam-Arakan Basin to the south (Fig. 3).

The Schuppen belt in the Upper Assam Plains, which contains the Assam Basin localities addressed in the current study, is an imbricate fault belt bounded by the Naga thrust in the northwest and Disang thrust in the southeast (Fig. 9). The belt is 20 to 25 km wide and extends for more than 200 km along strike from the Mishmi thrust in the NE to the Maibong thrust in the SW, where the Naga and Disang-Haflong thrusts meet. Each thrust slice has a homoclinal dip towards the southeast. The Naga thrust is a complex set of westerly faults that have preserved anticlinal folds with steep NW flanks and gentle SE flanks. The southeastern margin of the Schuppen belt is marked by the Disang thrust. The southwestern continuation of the Naga thrust and the Disang thrust is known as the Haflong thrust, which farther westward becomes part of the Dauki fault (Fig. 3; Johnson and Nur Alam, 1991).

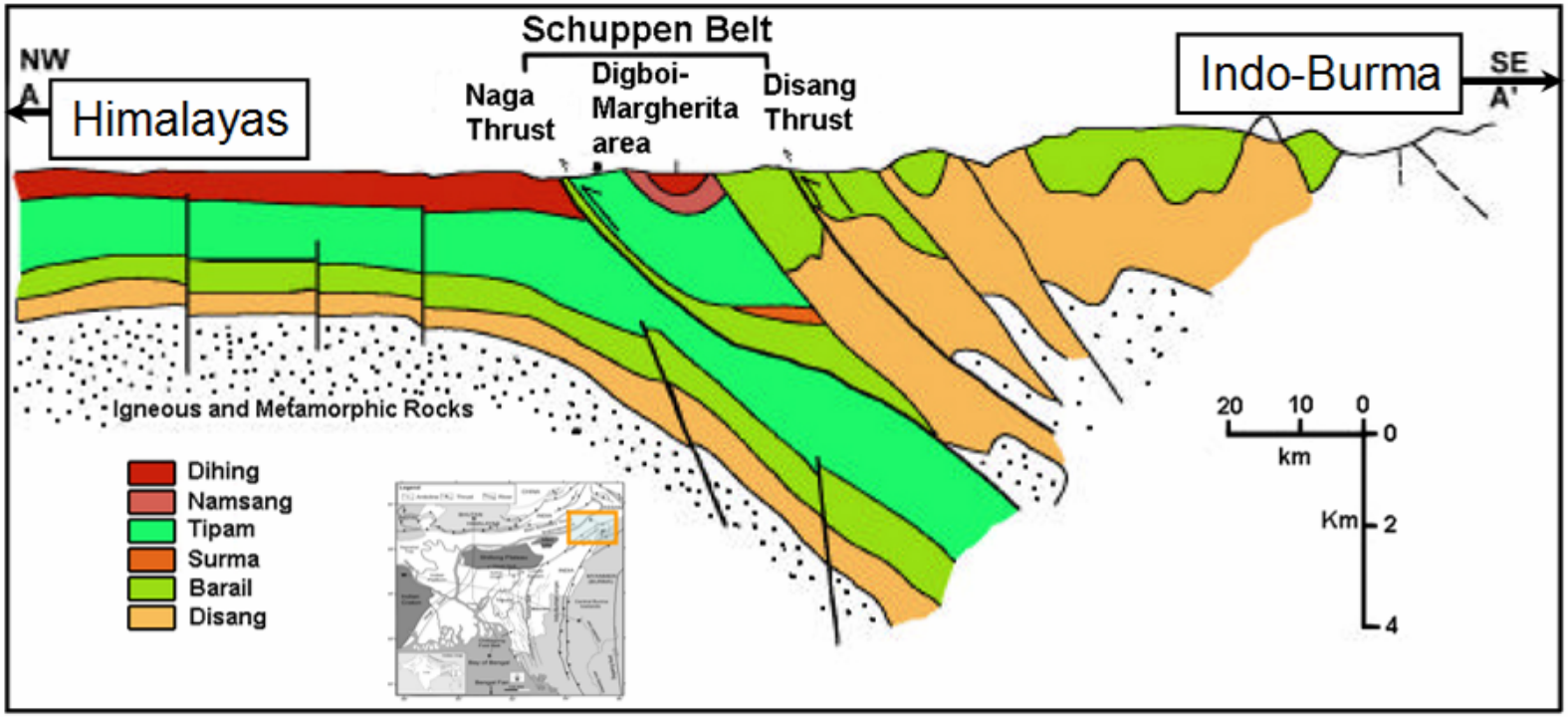

Figure 9. Cross-section across the Assam basin, including the Schuppen belt, which is bounded by the Naga thrust and Disang thrust, and includes the study area (after Hutchison, 1989). A-A' refers to figure 3. Late Miocene overthrusts are developed on down-to-basin faulting.

The Kohima-Patkai synclinorium is developed in the southern and southeastern parts of the Schuppen belt and includes the folded belt of the Surma basin (Fig. 3; Dasgupta, 1984). This Miocene basin contains a series of north-south-trending anticlinal ridges and a synclinal valley forming an arcuate belt with convexity towards the west. Structural complexity of the fold belt increases towards the east. Large-scale, regional folds of the Surma basin and the imbricate thrust belt of the Naga Hills developed in response to subduction of the Indian plate underneath the Burmese plate (Saikia, 1999).

The Eastern Zone, including the Ophiolite belt, consists of the Naga Metamorphic belt, ophiolite belt, and the Disang belt. The pre-Mesozoic Naga Metamorphic belt consists of low- to medium-grade metamorphic rocks that are thrust westward over the Ophiolite belt. The Ophiolite belt reaches a maximum width of 15 km and extends for 200 km in Nagaland and Manipur (Fig. 10; Hutchison, 1975). The following lithotectonic units have been recognized in the Ophiolite belt by Venkataraman et al. (1986): (1) ultramafic complexes consisting of tectonized peridotite and cumulate ultramafics; (2) a gabbro complex, divided into layered and massive gabbro; (3) diabase dikes; (4) a mafic volcanic complex; (5) plagiogranite occurring as veins, dikes, and small stocks within mafic rocks; and (6) associated sediments such as radiolarian cherts, limestones, and shales interbedded with volcanics. Rock types, their mode of occurrence, and their petrological characteristics suggest that these ophiolites are of alpine-type affinities (Duarah et al., 1983).

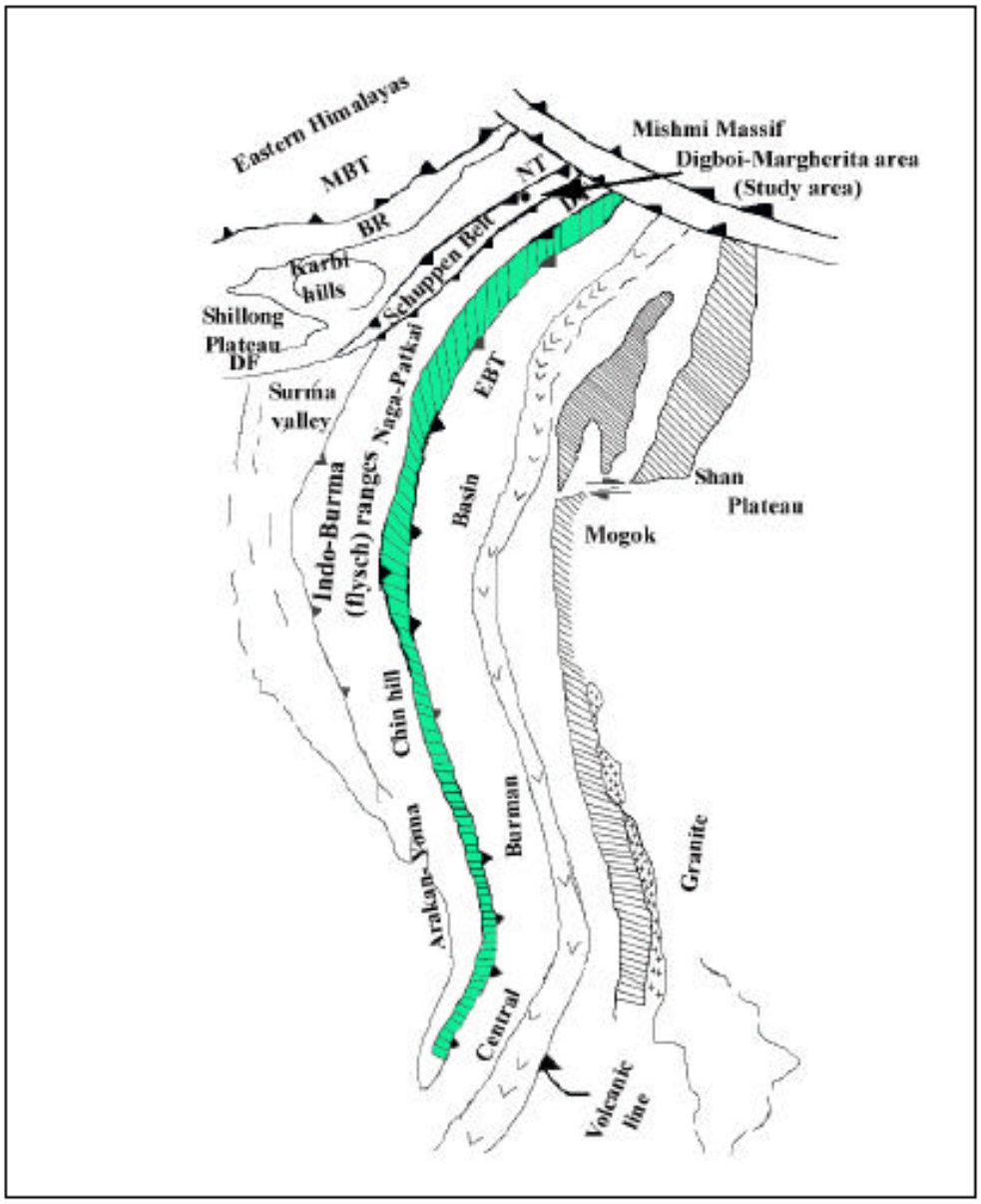

Figure 10. Map showing important structural units of the Indo-Burman orogenic belt (after Saikia, 1999). MBT-Main Boundary Thrust, EBT-Eastern Boundary Thrust, NT-Naga Thrust, DT-Disang Thrust, DF-Dauki Fault, LT-Luhit Thrust, MT-Mixu Thrust, BR-Brahmaputra River.

CHAPTER 3: STRATIGRAPHY AND SEDIMENTATION

3.1 INTRODUCTION

The stratigraphic scheme of the Bengal Basin was originally established based on exposures along the fold belt in the eastern part of the basin and lithostratigraphic correlation to type sections of the Assam Basin (Evans, 1964; Khan and Muminullah, 1980). Seismostratigraphic correlations have subsequently refined the conventional stratigraphic framework for most parts of the Bengal Basin (Hiller and Elahi, 1984). The Bengal Basin is also well known for the development of a thick (22 km) sedimentary succession (Curray, 1991; Curray and Munasinghe, 1991) that has long been of interest to the petroleum exploration industry. Sedimentation in the Bengal Basin is considered to have occurred in five phases: (1) Permo-Carboniferous to early Cretaceous; (2) Cretaceous-Mid-Eocene; (3) Mid-Eocene-Early Miocene; (4) Early Miocene-Mid-Pliocene; and (5) Mid-Pliocene-Quaternary (Alam et al., 2003). Each of these sedimentation phases was controlled by tectonic cycles, which involved the interaction and collision of the major plates. In terms of the tectonic evolution of the basin, these five phases correspond to the following tectonic stages, respectively: (1) syn-rift stage; (2) drifting stage; (3) early collision stage; and (4) and (5) late collision stage.

The stratigraphy of the Assam Basin was developed on the basis of extensive lithological and paleontological studies (Sinha and Sastri, 1973, Bhandari et al., 1973, Rangarao, 1983). Like clastic wedges in other foreland basins, stratigraphic units of the Assam-Bengal basin system are generally time-transgressive and reflect broad

changes in depositional environments (Evans, 1964). Paleozoic and Pre-Cretaceous rocks have not been recorded in any of the wells drilled in the Assam Valley, although their presence in front of the Assam Himalayas and Mishmi hills has been inferred (Rangarao, 1983).

Cenozoic stratigraphic successions in the Assam-Bengal basins are shown in Tables 1 and 2 and Figure 11.

Table 1. Generalized Cenozoic stratigraphy of the Bengal Basin (after Uddin et al., 2007).

Age	Unit		Thickness (m)	Lithology
Pliocene to Pleistocene	Dihing		129	Yellow and grey, medium-grained, occasionally pebbly sandstone
	Dupi Tila Sandstone		300-500	Medium-to coarse-grained, massive to cross-bedded, polychromatic sand(stone) with pebbles and clay galls
Late Miocene to Pliocene	Tipam Group	Girujan Clay	70-1000	Brown to blue mottled clay with calcareous nodules
		Tipam Sandstone	80-1100	Yellow-brown to orange, medium- to coarse-grained, massive and cross-bedded, sand(stone) with pebbles and coal fragments
Middle to Late Miocene	Surma Group	Boka Bil Formation	300-1400	Alternation of bedded and rippled mudstone, siltstone, and sandstone with calcareous concretions; top is marked by the "upper marine shale"
Early to Middle Miocene		Bhuban Formation	250-1700	Light gray to light yellow, bedded siltstone, sandstone and sandy mud in top unit; blue to yellowish gray silty and sandy mudstone in the middle unit; bedded siltstone, sandstone and sandy mud in the lower unit
Oligocene	Barail Formation		45-1600	Pink, massive, medium-to coarse-grained sand(stone)
Late Eocene	Kopili Formation		7-150	Thinly bedded, fossiliferous mudstone
Middle Eocene	Sylhet Limestone		90-240	Nummulitic limestone
Early Eocene	Tura/Cherra Sandstone		240	White, pink to brown, coarse-grained, cross bedded, carbonaceous sandstone

Table 2. Generalized Cenozoic stratigraphy of the Assam Basin (after Uddin et al., 2007).

Age	Unit		Thickness (m)	Lithology
Pleistocene	Moran Group	Dihing Formation	>500	Sandstones with carbonaceous shale
Pliocene		Namsang Formation	>1000	Sandstones and clays with thin bands of coal
Mio-Pliocene	Tipam Group	Girujan Clay	2300	Clay with siltstone and sandstone "alternations"
		Tipam Sandstone	2300	Sandstones with rare thin clay bands
Miocene	Surma Group	Boka Bil Formation	400	Gray shale, associated with sandstone
		Upper Bhuban Formation	400	Fine-grained sandstone, silt, shale, and mudstone
		Lower Bhuban Formation	>450	Sandy shale, mudstone, and siltstone
Eocene to Oligocene	Barail Group	Tikak Parbat Formation	700	Sandstones, thin-bedded grey sandy siltstone
		Baragolai Formation	2700	Predominantly shale with subordinate thin sandstone beds and prominent coal seams
		Naogaon Formation	1040	Thinly bedded sandstone, thin subordinate shale
Eocene	Disang	Upper Disang Formation	>1000	Dark-gray, splintery shale rich in carbonaceous matter and massive siltstone with concretions
		Lower Disang Formation (not exposed)	>1000	Fine-grained sandstone with subordinate shale
Pre-Eocene	Deragaon Formation (not exposed)		~250	Inferred to be fine grained sandstones and argillites

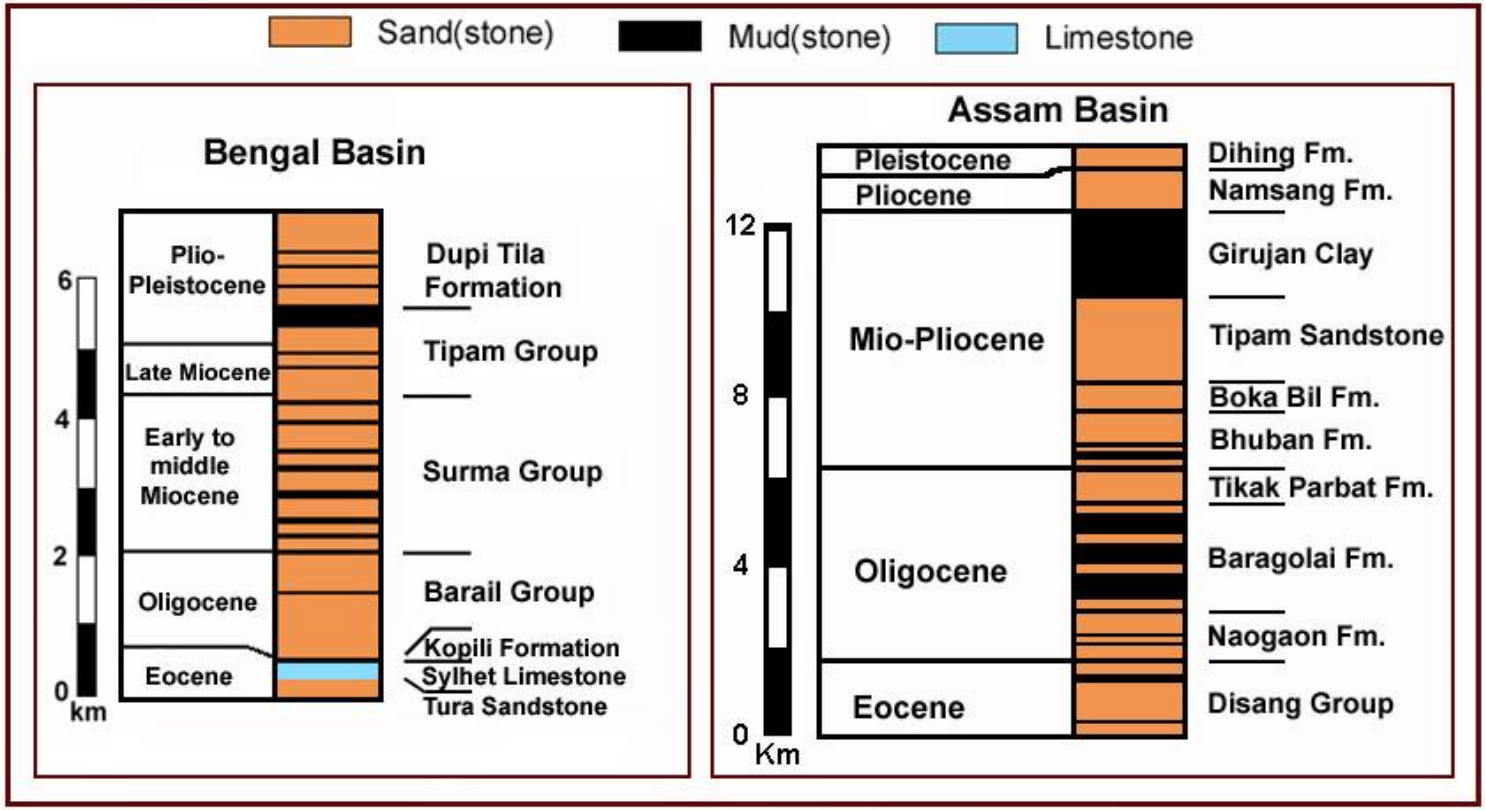

Figure 11. Composite Cenozoic stratigraphic succession of Assam and Bengal basins (after Uddin et al., 2007).

3.2 BENGAL BASIN

The oldest sediments in the Bengal Basin comprise a Gondwanan [Late Carboniferous (?) to Permian] continental succession deposited prior to the continental break-up and preserved in intrashelf grabens (Banerjee, 1981; Salt et al., 1986, Lindsay et al., 1991; Shamsuddin and Abdullah, 1997). This continental succession is overlain by Jurassic basaltic and andesitic volcanics of the Rajmahal Trap Formation. The succeeding Late Cretaceous to Eocene sediments correspond to a post break-up but precollision phase (drift stage). These are represented in the Platform area by a 300-m-thick interval of Cretaceous-Early Eocene shallow-marine sandstones and shales assigned to the Cherra/Tura Formation. These are overlain by the Middle Eocene open-marine Sylhet Limestone (presence of nanno-fossils and foraminifera) and the Late Eocene marine Kopili Shale (Reimann, 1993; Shamsuddin et al., 2001; Chowdhury et al., 2003).

The Oligocene Barail Group has been interpreted to have been deposited in predominantly tide-dominated shelf environments (Alam, 1991). These strata are exposed along the northern fringe of the Sylhet trough near the Dauki fault area (Fig. 12) and range in thickness from 800 meters (Johnson and Nur Alam, 1991) to 1600 meters (Table 1; Ahmed, 1983). In the platform area, Barail equivalent rocks are less than 200 m thick and are known as the Bogra Formation (Khan and Muminullah, 1980). The upward transition the Barail Group to the Surma Group in Assam appears to reflect transgressive onlap (Banerji, 1981; Salt et al., 1986). This marine transgression on the shelf may be the result of major upthrust movement along the Dauki fault in the Early Miocene or subsidence associated with the approach of the subduction zone (Murthy et al., 1976; Fig. 13).

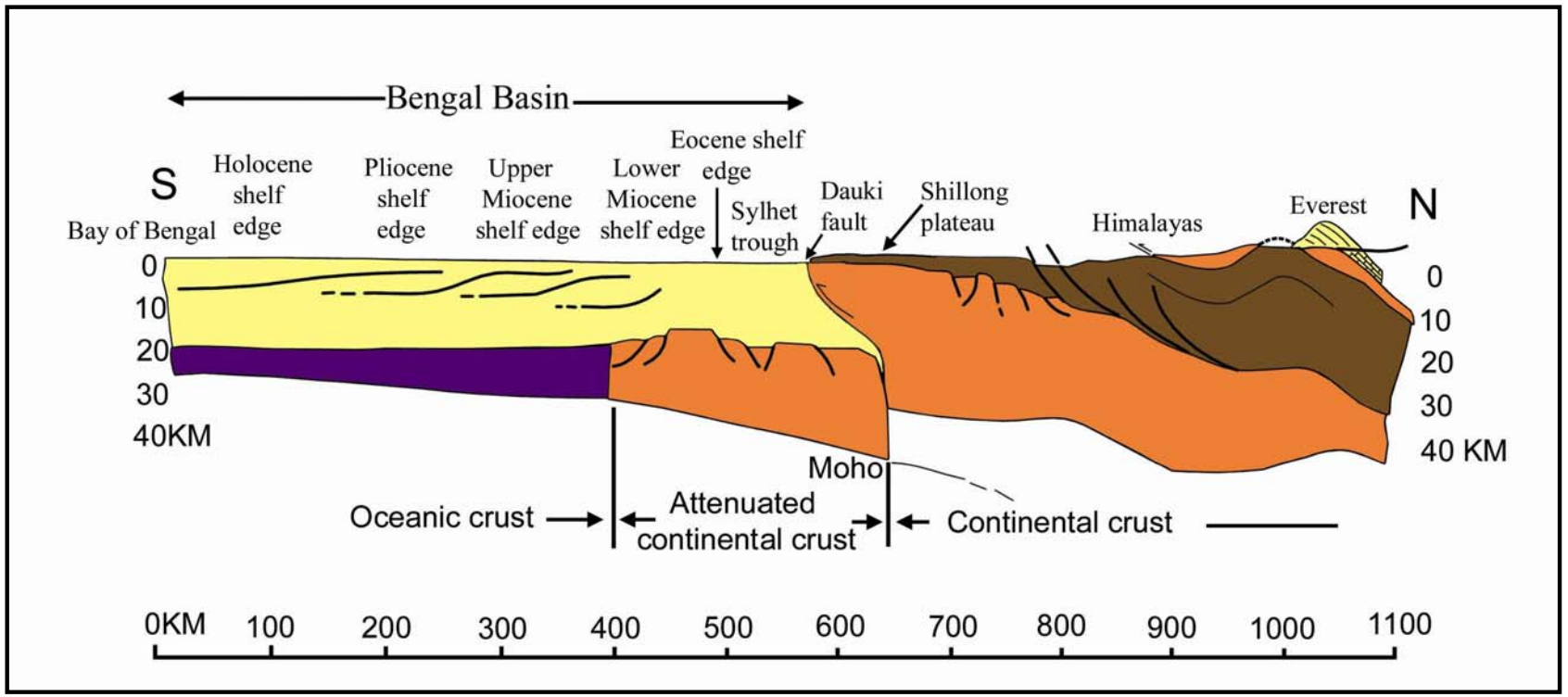

Figure 12. Schematic cross-section of the Bengal Basin (N– S) through the Shillong Plateau. Note the thickening of sediments toward the south (after Uddin and Lundberg, 2004).

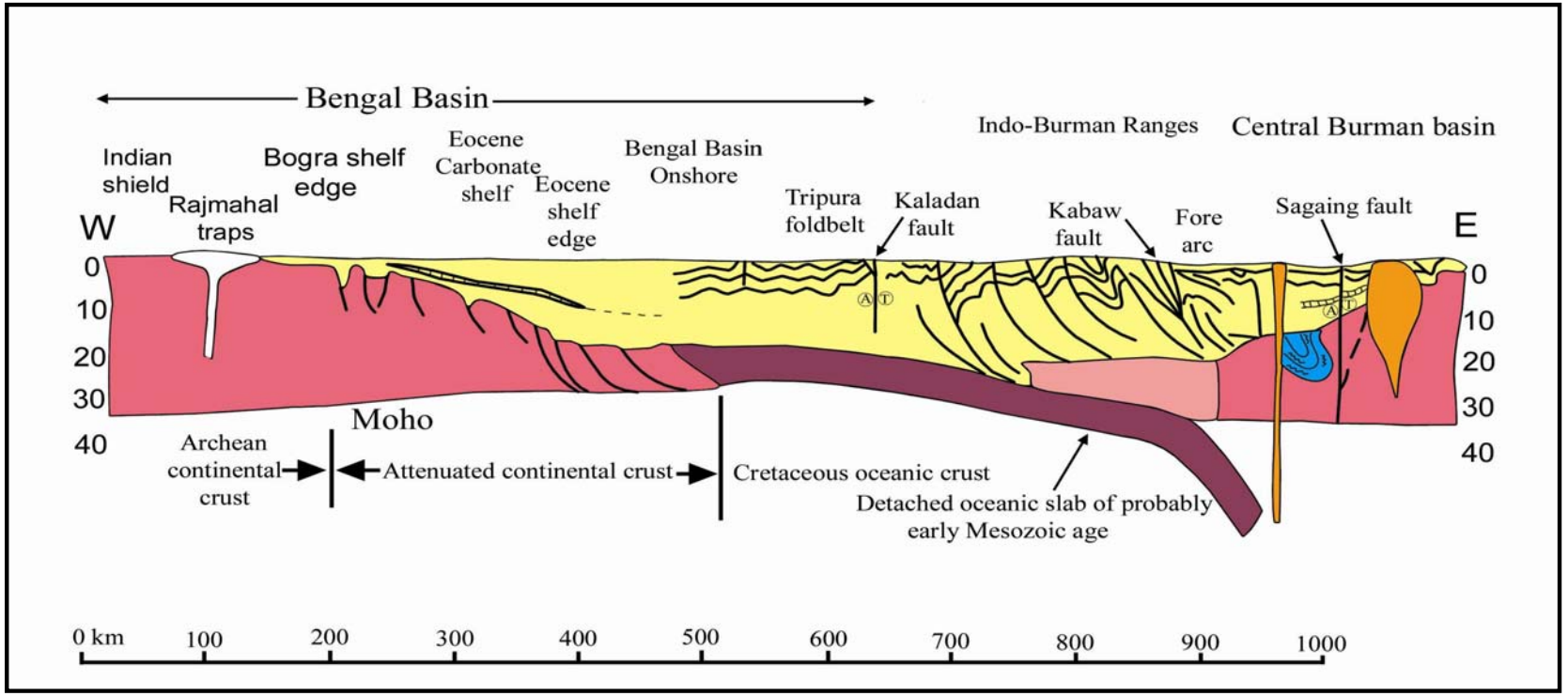

Figure 13. Schematic cross-section of the Bengal Basin (E–W) through the northern Chittagong Hill region. Note the thickening of sediments toward the east (after Uddin and Lundberg, 2004).

The Miocene Surma Group is traditionally divided into two units: the lower Bhuban and the upper Boka Bil formations (Holtrop and Keizer, 1970; Hiller and Elahi, 1984; Khan et al., 1988), both of which extend throughout the Bengal Basin. The Surma Group was deposited in transitional delta front settings and comprises progradational sequences (Alam, 1989). The Surma Group is overlain unconformably by the Upper Miocene to Pliocene Tipam Group. The Tipam Group consists of the Tipam Sandstone and Girujan Clay, which were deposited in bed-load dominated, braided-fluvial, and lacustrine systems (Johnson and Nur Alam, 1991; Reimann, 1993). The Dupi Tila Formation, which caps the sequence, was deposited in meandering river environments (Fig. 14; Johnson and Nur Alam, 1991).

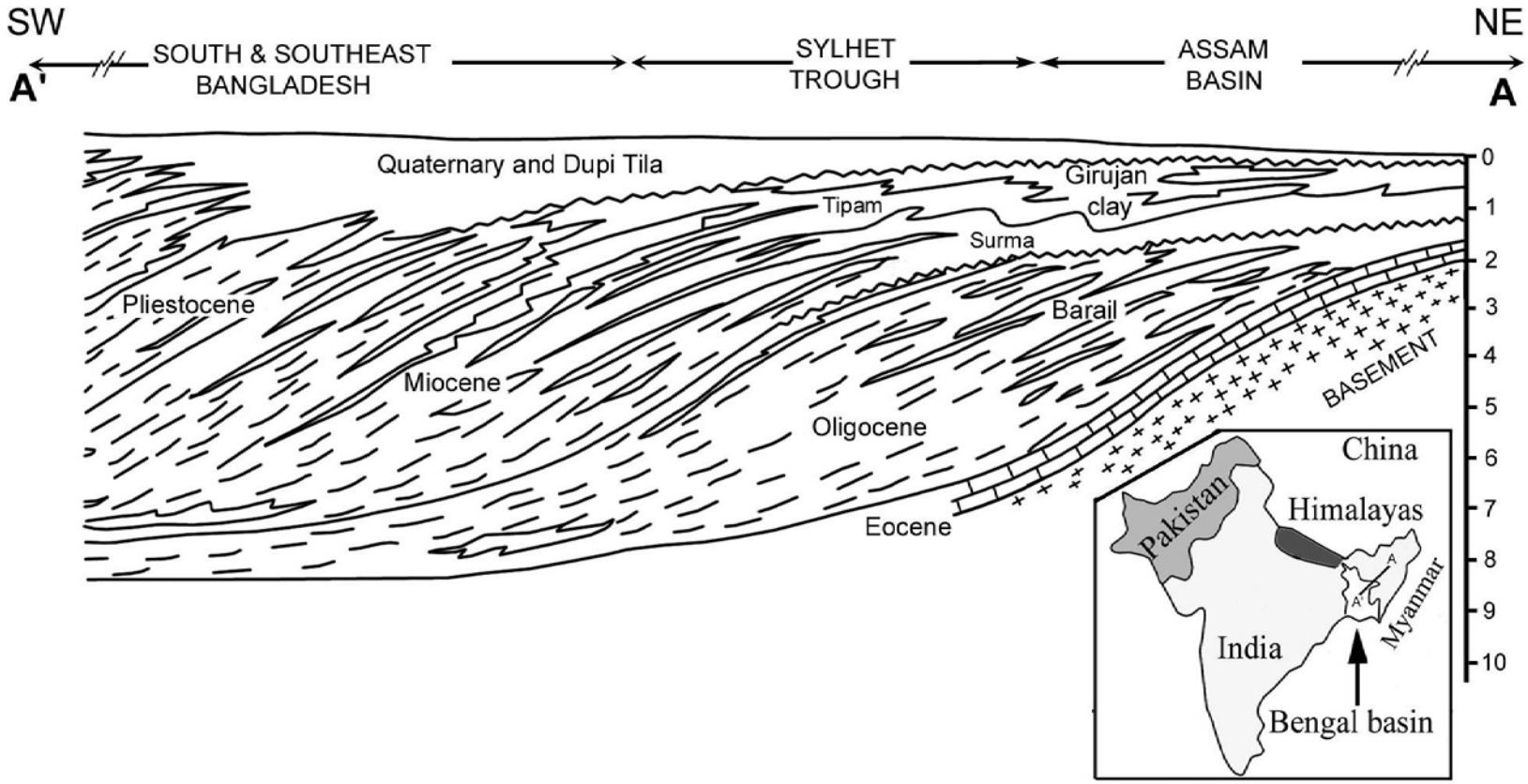

Figure 14. Facies correlation and depositional setting of Cenozoic rocks of Assam-Bengal basins along A' – A in inset (after Petrobangla, 1983).

3.3 ASSAM BASIN

Precambrian rocks of the Shillong Plateau and the Mikir Hills are locally overlain unconformably by a group of younger Proterozoic sediments, called the Shillong Series, and by Cretaceous sediments (Rahman, 1999). Gondwana sediments are present in Assam in block-faulted troughs within basement areas buried under the upper Mesozoic to Recent sediments. These sediments are primarily Permo-Carboniferous and are dominated by coal-shale-sand sequences (Rangarao, 1983). During the early Cretaceous, intense volcanic activity in this region of India resulted in the Rajmahal Trap lava flows, which covered large areas under the Indo-Gangentic plains (Das Gupta and Biswas, 2000) and areas to the south of Assam, and the Sylhet Trap (e.g., Garo Hills in Shillong Plateau). These underlie Upper Cretaceous sediments and are believed to be of Early to Middle Cretaceous in age (110 to 133 m.y.; Rangarao, 1983). The older Disang Group of sediments was deposited in the Eocene time in deep to shallow-water environments. The Disang Group is considered as the deep marine facies equivalent of the Sylhet and Kopili formations of Eocene age (Rangarao, 1983). The Disang Group is overlain by the Oligocene Barail Group (>4 km thick), which comprises three formations: Naogaon, Baragolai, and Tikak Parbat (Table 2). These units represent deposition in shallow marine to tidal settings (Rangarao, 1983). The Miocene Surma Group was deposited in a variety of depositional environments, ranging from deep marine to deltaic. The Mio-Pliocene Tipam Group overlies the Surma Group (~ 500 to 2300 m thick) and was deposited under fluvial conditions (Figs. 9 and 14). The Plio-Pleistocene Moran Group also accumulated in fluvial environments.

CHAPTER 4: SANDSTONE PETROGRAPHY

4.1 INTRODUCTION

Sandstone petrography deals with quantitative detrital modes, calculated from point counts of thin sections to infer the sandstone provenance and tectonic setting (Dickinson and Suczek, 1979; Ingersoll and Suczek, 1979; Dickinson et al., 1982, Dickinson, 1985; Ingersoll et al., 1995; Wanas and Abdel-Maguid, 2006). Proportions of detrital framework grains are plotted on various ternary plots, from which various tectonic settings can be distinguished (Graham et al., 1976; Ingersoll, 1978; Dickinson and Suczek, 1979; Ingersoll et al., 1984; Bernet et al., 2007; Ingersoll and Eastmond, 2007). Composition of detrital sediments is controlled by various factors, including source rocks, modes of transport, depositional environments, climate, and diagenesis. Provenance studies that focus on some key attributes of detrital mineralogy provide important constraints on basin evolution and unroofing history of mountain belts (Dorsey, 1988; Uddin and Lundberg, 1998a, b). Reconstruction of provenance from detailed modal analyses is based on the assumption that modes of transportation, depositional environments, climates, and diagenesis have not significantly altered detrital grain composition (Basu, 1976).

This chapter describes the petrology and modal analysis of Cenozoic sediments deposited in the Assam and Bengal basins in the eastern Himalayas. Petrographic studies describe textural and mineralogical relationships of individual

grains and show variations in framework grains in order to understand tectonic evolution and provenance (Dickinson and Suczek, 1979; Dickinson et al., 1982; Ingersoll et al., 1984; Garzanti et al., 2007).

Sandstone compositional studies involve consideration of both mono- and polycrystalline framework grains in order to understand tectonic evolution and provenance (Dickinson and Suczek, 1979; Ingersoll et al., 1984; Ingersoll et al., 1995; Bernet et al., 2007; Ingersoll and Eastmond., 2007). Monocrystalline grains are counted as mineral grains (monocrystalline quartz, feldspar, etc), and polycrystalline grains are counted as lithic fragments (e.g., polycrystalline quartz grains and sedimentary, metamorphic, or volcanic lithic fragments, etc).

4.2 METHODS

Thirty-five sand(stone) samples of Cenozoic age from the Assam and Bengal basins were analyzed for this study. Bengal Basin samples were collected from well-exposed sequences from the Sylhet trough and Ulahtaung anticline (Figs. 4 and 5). Assam Basin samples were collected from four surface sections in the Digboi-Margherita area of upper Assam (Fig. 6). Petrographic modal analyses were conducted following the Gazzi-Dickinson method, where sand-sized minerals included in lithic fragments are counted as the mineral phase rather than the host lithic fragment in order to normalize for grain-size variation (Table 3; Dickinson, 1970b; Ingersoll et al., 1984). Thin sections were stained for plagioclase and potassium feldspars. A minimum of 300 points were counted from each sample.

Modal sandstone compositions were plotted on standard ternary diagrams (QtFL, QmFLt, QmPK, LsLvLm, $LsLm_1Lm_2$, etc.) and used to assess temporal changes in provenance (Dickinson, 1970a; Dorsey, 1988). The following

compositional parameters were evaluated: Qt = total quartz; Qm = monocrystalline quartzose grains; Qp = polycrystalline quartz grains, including chert grains; F = total feldspar grains; P = plagioclase feldspar grains; K = potassium feldspar grains; L = lithic fragments, excluding Qp; Lt = total lithic fragments, including Qp; Ls = sedimentary lithic fragments; Lv = volcanic lithic fragments; Lm =metamorphic lithic fragments; Lsm = sedimentary and metasedimentary lithic fragments; Lvm = volcanic, hypabyssal, metavolcanic lithic fragments; Lm_1 =very low- to low-grade metamorphic lithic fragments; and Lm_2 = low- to intermediate-grade metamorphic lithic fragments (Table 3).

Table 3. Recalculated modal parameters of sand and sandstones (Uddin and Lundberg, 1998a).

1. Primary parameters
(Dickinson and Suczek, 1979; Dorsey, 1988)

Qt = Qm + Qp, where
Qt = total quartzose grains
Qm = monocrystalline quartz (> 0.625 mm)
Qp = polycrystalline quartz (or chalcedony)

Feldspar Grains (F = P + K)
F = total feldspar grains
P = plagioclase feldspar grains
K = potassium feldspar grains

Unstable Lithic Fragments (Lt = Ls + Lv +Lm)
Lt = total lithic fragments, including Qp
Lv = volcanic/metavolcanic lithic fragments
Ls = sedimentary/metasedimentary lithic fragments
Lm = metamorphic lithic fragments
L = total unstable lithic fragments, excluding Qp

2. Secondary parameters
(Dickinson, 1970a; Uddin and Lundberg, 1998a)

P/F = Plagioclase/ total feldspar
Lm_1 = Very low- to low-grade metamorphic lithic fragments
Lm_2 = Low- to intermediate-grade metamorphic lithic fragments

4.3 PETROGRAPHY

Sandstones from the Oligocene Barail Group of the Bengal Basin are generally quartzolithic, with very low feldspar contents. The Miocene Surma Sandstone, the Mio-Pliocene Tipam Sandstone, and the Pliocene Dupi Tila Formation from Bengal Basin are quartzolithic to quartzofeldspathic. Point-counting data for both Bengal and Assam basins are presented in Tables 4 and 5. Petrographic results for sandstones from Bengal and Assam basins are described below, from oldest to youngest.

4.3.1 Barail Group from the Bengal Basin

Seven sandstones, mostly medium- to fine-grained, from the Oligocene Barail Group of the Bengal Basin were studied. These samples are generally quartzolithic with low feldspar contents. All the samples are dominated by mostly monocrystalline quartz grains with few detrital chert and polycrystalline quartz grains (Fig. 15A). The average composition of Barail Group sandstone is $Qt_{83}F_3L_{14}$. Volcanic rock fragments are absent. Most of the samples contain abundant sedimentary lithic fragments, while some contain low- to medium-grade metamorphic rock fragments (Fig. 15A).

4.3.2 Surma Group from the Bengal Basin

Seven samples of Miocene Surma Group were examined for this study. Feldspar content in these Miocene sandstones is significantly higher than in the Oligocene Barail Group (Fig. 15B). Surma Group sediments are mostly quartzolithic to quartzofeldspathic ($Qt_{59}F_{18}L_{23}$). They are fine- to medium-grained and

Table 4. Normalized modal compositions of sandstones of various Cenozoic units from the Bengal Basin.

Sample ID	Qt	F	L	Qm	F	Lt	Qm	P	K	Ls	Lv	Lm	Ls	Lm1	Lm2
Dupi Tila Fm															
SD 01	58	18	24	48	18	34	73	14	14	61	20	20	75	9	15
SD 02	50	23	27	39	23	38	62	15	22	59	15	26	70	13	17
MEAN	54	21	25	43	21	36	67	15	18	60	17	23	73	11	16
STDEV	6	4	2	7	4	3	7	1	6	1	3	4	4	2	2
Tipam Group															
STM 02	53	21	26	41	21	38	66	11	23	78	0	23	78	15	8
STM 04	61	12	27	47	12	41	80	4	17	89	0	11	89	5	6
STM 06	63	14	23	50	14	36	78	11	11	74	3	23	81	16	4
UTM 03	51	11	39	38	11	52	69	10	21	73	13	14	84	8	8
MEAN	57	14	29	44	14	42	73	9	18	79	4	18	83	11	6
STDEV	6	5	7	6	5	7	7	3	5	7	6	6	5	5	2
Surma Group															
FN 07	63	14	23	56	14	30	80	13	7	91	0	9	91	9	0
FN 26	72	12	16	62	12	26	84	11	6	76	0	24	76	20	4
TBH 01	71	11	17	61	11	28	85	8	7	87	0	13	87	8	6
SBK 02	58	21	20	49	21	29	70	14	16	81	0	19	81	16	4
SBK 01	60	19	21	51	19	30	72	14	14	83	0	17	83	17	0
UTBH 12	43	25	31	38	25	37	60	22	19	70	9	21	77	19	4
UTBH 11	44	25	31	33	25	42	56	25	18	57	14	29	67	19	15
MEAN	59	18	23	50	18	32	72	15	12	78	3	19	80	15	5
STDEV	12	6	6	11	6	6	11	6	6	11	6	6	8	5	5
Barail Group															
SBR 02	90	3	7	82	3	15	97	2	1	96	0	4	100	0	0
SBR 04	79	4	17	72	4	24	95	4	1	62	0	38	62	11	27
SBR 06	92	2	6	84	2	15	98	1	1	84	0	16	84	11	5
SBR 09	79	3	18	72	3	25	96	2	1	82	0	18	82	14	4
SBR 10	79	4	17	75	4	21	96	1	3	89	0	11	89	7	4
SBR 11	77	4	19	69	4	27	95	1	4	80	0	20	80	15	5
SBR 12	85	2	13	77	2	21	97	0	3	62	0	38	62	26	13
MEAN	83	3	14	76	3	21	96	2	2	79	0	21	80	12	8
STDEV	6	1	5	5	1	5	1	1	1	13	0	13	14	8	9

Table 5. Normalized modal compositions of sandstones of various Cenozoic units from the Assam Basin.

Sample ID	Qt	F	L	Qm	F	Lt	Qm	P	K	Ls	Lv	Lm	Ls	Lm1	Lm2
Tipam Group															
ATM 01	47	13	40	43	13	43	76	18	5	78	1	21	79	6	15
ATM 02	58	6	36	46	5	48	89	9	2	89	0	11	89	5	7
ATM 03	54	9	37	46	9	46	84	12	4	81	0	19	81	8	12
MEAN	53	9	38	45	9	46	83	13	4	83	0	17	83	6	11
STDEV	6	4	2	2	4	3	7	5	2	5	0	5	5	2	4
Surma Group															
ASU 01	75	0	25	66	0	34	100	0	0	100	0	0	100	0	0
ASU 02	61	5	33	52	5	42	91	7	2	97	0	3	97	2	2
MEAN	68	3	29	59	3	38	95	4	1	98	0	2	98	1	1
STDEV	10	4	6	10	4	6	7	5	1	2	0	2	2	1	1
Barail Group															
ABR 02	64	7	29	57	7	36	90	8	2	73	2	24	75	12	13
ABR 04	67	3	30	51	3	46	95	4	1	80	0	20	80	10	10
ABR 05	62	5	33	45	5	50	89	9	1	73	0	27	73	9	17
ABR 06	53	8	39	38	8	54	83	16	1	79	2	19	81	7	13
ABR 07	55	11	34	45	11	44	80	19	1	79	1	20	80	10	10
ABR 08	54	10	36	45	10	45	82	10	9	78	4	18	81	7	12
MEAN	59	7	34	47	7	46	86	11	3	77	1	21	78	9	12
STDEV	6	3	4	6	3	6	6	5	3	3	1	3	3	2	3
Disang Group															
AD 01	58	3	40	40	3	58	94	6	0	55	1	44	56	24	20
AD 02	50	4	47	38	4	58	91	8	1	61	0	39	61	27	12
AD 03	56	6	38	50	6	44	90	8	2	57	4	38	60	13	27
AD 04	59	6	34	45	6	49	87	10	3	70	4	26	73	9	19
MEAN	56	5	40	43	5	52	90	8	1	61	2	37	62	18	19
STDEV	4	2	5	5	2	7	3	2	1	6	2	7	7	9	6

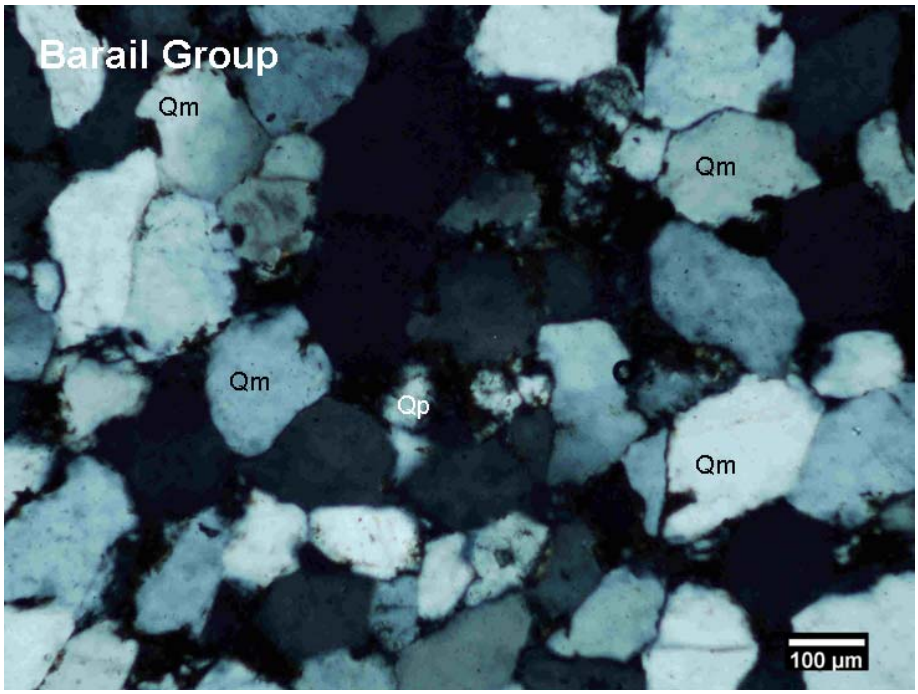

(A)

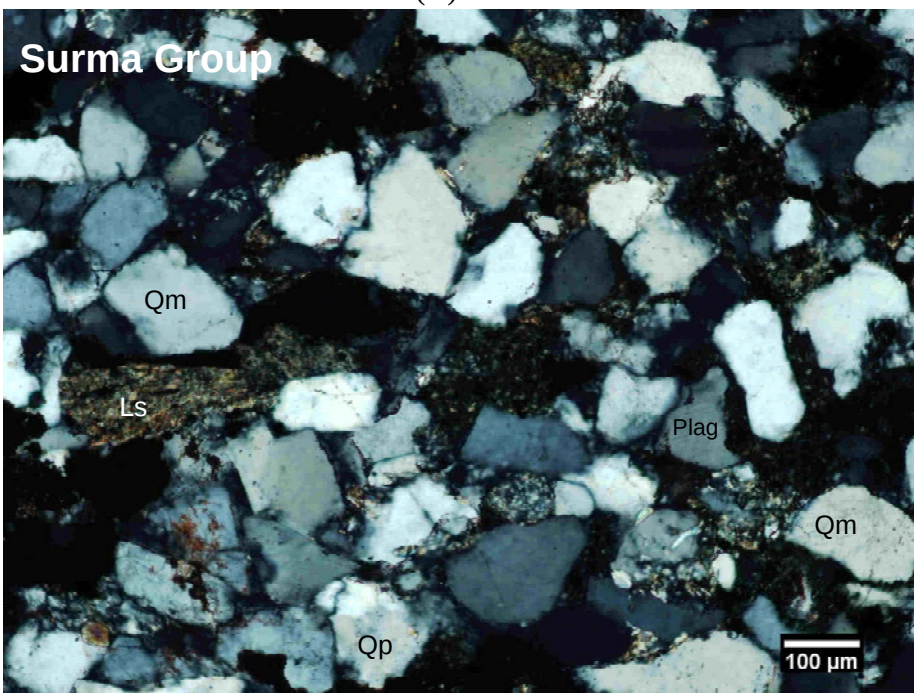

(B)

Figure 15. Representative photomicrographs of sandstone from (A) Oligocene Barail Group (crossed polar), and (B) Miocene Surma Group sandstone (crossed polar) from Bengal Basin.

subangular to subrounded. Quartz grains are mostly monocrystalline and highly undulose. Feldspars occur in significant abundance, and the abundances of plagioclase feldspar and potassium feldspar are approximately equal (Fig. 15B). Most of the feldspars are unaltered and can be easily identified due to staining. These samples are also rich in lithic fragments; sedimentary and low- to medium-grade metamorphic lithic fragments are most common, although a few samples contain high-grade metamorphic rock fragments.

4.3.3 Tipam Group from the Bengal Basin

Four samples of the Mio-Pliocene Tipam Group from the Bengal Basin were analyzed. Sandstones from this group are fine- to medium-grained, quartzolithic to quartzofeldspathic ($Qt_{57}F_{14}L_{29}$), and contain mono- and polycrystalline quartz, abundant feldspar, and lithic grains. Monocrystalline grains are strongly undulose. Some chert and polycrystalline quartz are present (Fig. 16A). These middle Miocene rocks are rich in feldspar, and potassium feldspar dominates over plagioclase feldspar. Lithic fragments are common in these samples. Sedimentary lithic fragments are most abundant, although some volcanic and low-grade metamorphic fragments also are observed.

4.3.4 Dupi Tila Formation from the Bengal Basin

Only two samples of the Pliocene Dupi Tila Formation from the Bengal Basin were studied for this research. Sandstones from the Dupi Tila Formation consist predominantly of quartz, feldspar, and lithic fragments. These sandstones are also

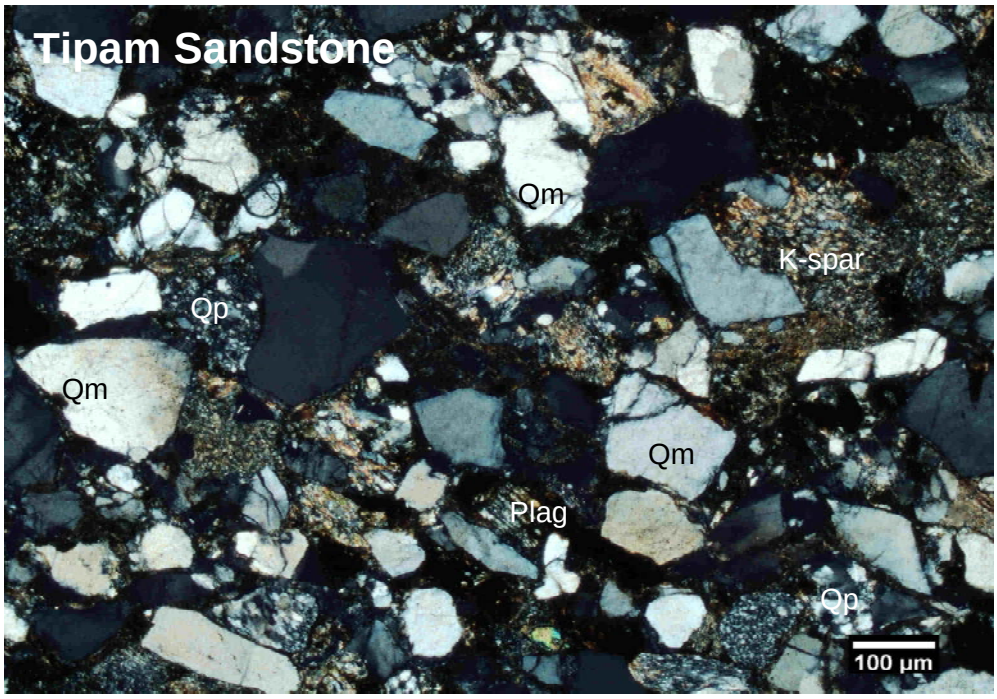

(A)

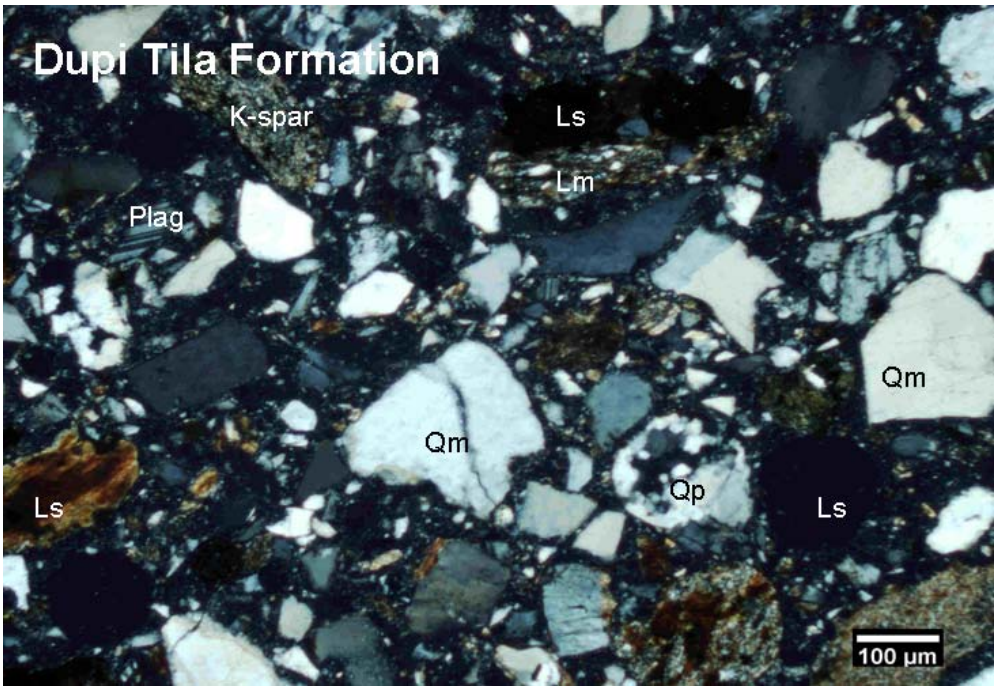

(B)

Figure 16. Representative photomicrographs of sandstone from (A) Mio-Pliocene Tipam Group (crossed polar), and (B) Pliocene Dupi Tila Formation (crossed polar) from Bengal Basin.

quartzolithic to quartzofeldspathic ($Qt_{54}F_{21}L_{25}$). Lithic fragments are clearly visible in thin section (Fig. 16B), and most consist of quartzite, slate, phyllite, siltstone, and argillite. Sedimentary lithic fragments are dominant over metamorphic lithic fragments.

4.3.5 Disang Group from the Assam Basin

Four sandstone samples of the Disang Group from the Assam Basin were analyzed. Most of these are very fine-grained. They are quartzolithic with low feldspar and high lithic contents. The average composition of Disang group sandstone is $Qt_{56}F_5L_{40}$. Monocrystalline quartz grains are dominant and are angular to subrounded (Fig. 17A). Lithic fragments are mainly detrital chert, slate, quartzite, and schist. Volcanic lithic fragments are minor (Table 5).

4.3.6 Barail Group from the Assam Basin

Six samples from of the Barail Group from Assam were studied. The late Eocene-Oligocene Barail Group is characterized by quartzolithic sandstones. The modal composition of sandstone from the Barail Group is $Qt_{59}F_7L_{34}$. Lithic grains mostly consist of sedimentary and metamorphic fragments; volcanic fragments are rare (Fig. 17B). Feldspars are dominated by plagioclase. Lithic fragments consist of chert, schist, phyllite, slate, quartzite, and siltstone.

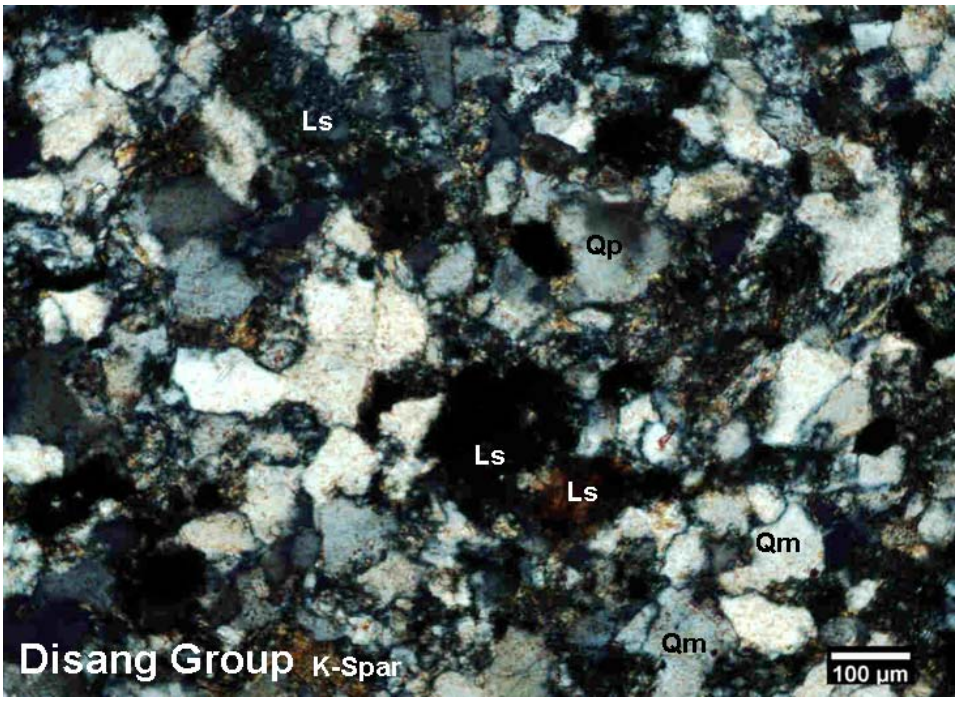

(A)

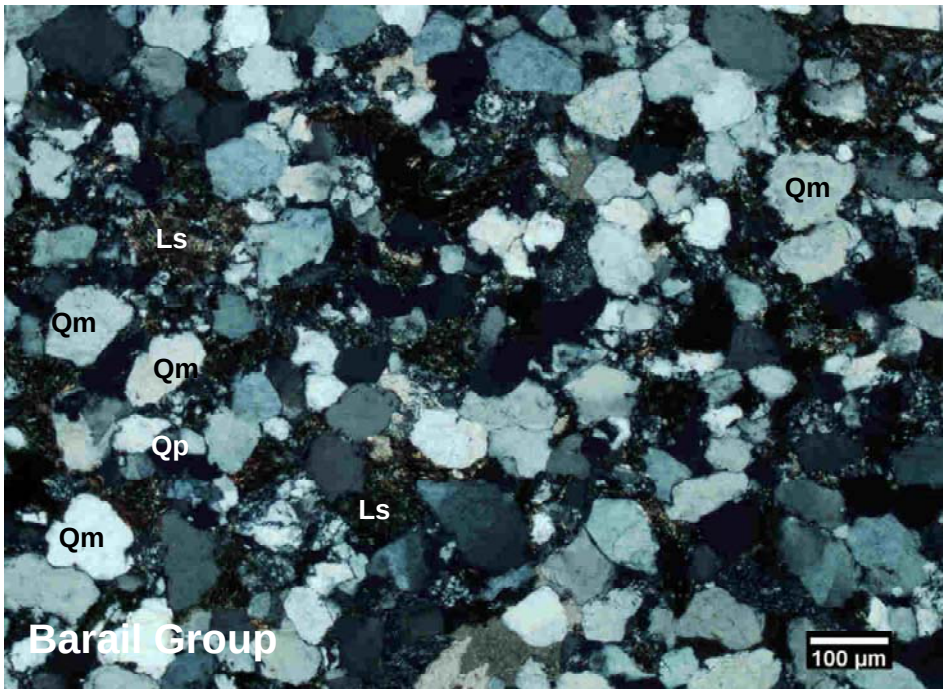

Figure 17. Representative photomicrographs of sandstone from (A) Eocene Disang Group (crossed polar), and (B) Oligocene Barail Group (crossed polar) from Assam Basin.

4.3.7 Surma Group from the Assam Basin

Two Surma Group samples from the Assam Basin were analyzed. The Surma Group was deposited over an unconformity, which marks the Oligocene-Miocene transition in the Assam Basin. The Surma Group sandstones ($Qt_{68}F_3L_{29}$) are quartzolithic with high quartz contents. Quartz grains are angular to subrounded, mainly monocrystalline, and highly undulose (Fig. 18A). The sandstones are rich in lithic fragments consisting of schist, quartzite, slate, detrital chert, phyllite, argillite, and siltstone. Volcanic and metamorphic lithic grains are rare to absent in Surma Group sandstones.

4.3.8 Tipam Group from the Assam Basin

Three samples were analyzed from the Mio-Pliocene Tipam Group (Tipam Sandstone). The Tipam Sandstone is quartzolithic ($Qt_{47}F_{13}L_{40}$) but contains more feldspar than other sandstones in the Assam Basin (Fig. 18B). Feldspars are predominantly plagioclase. Lithic fragments are dominated by sedimentary rock types, but also include low- to intermediate-grade metamorphic rocks.

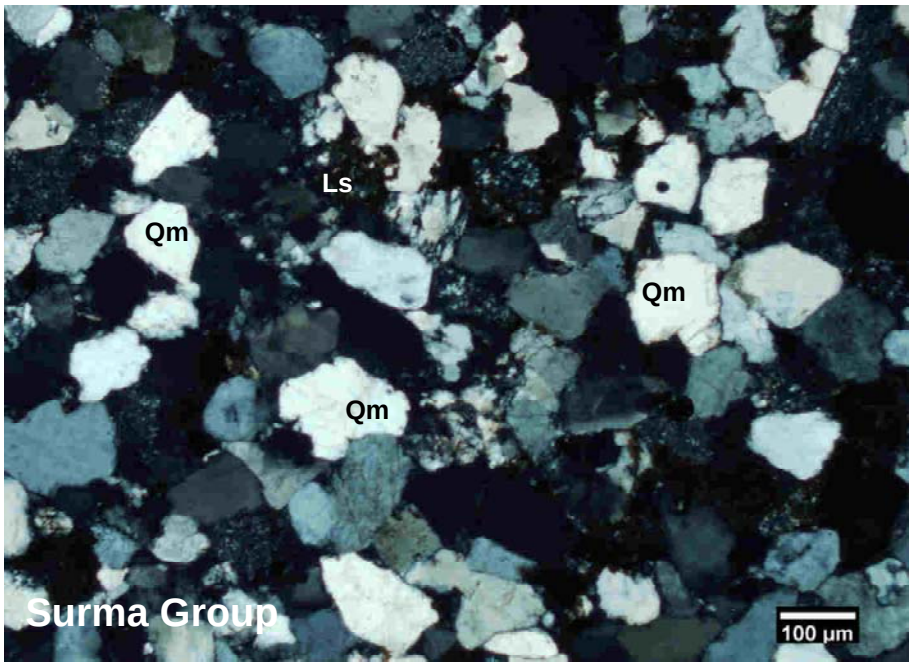

(A)

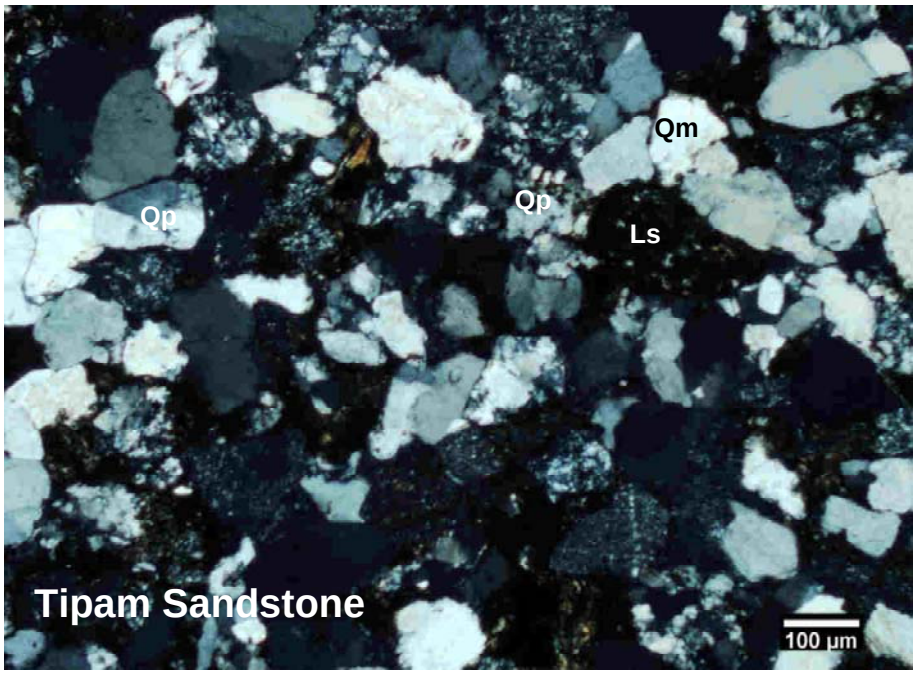

(B)

Figure 18. Representative photomicrographs of sandstone from (A) Miocene Surma Group (crossed polar), and (B) Pliocene Tipam Group (crossed polar) from Assam Basin.

4.4 SANDSTONE MODE AND PETROFACIES EVOLUTION

Ternary diagrams reflecting modal analyses of the major stratigraphic units from the both Bengal and Assam basins are presented in Figures 19 through 28. Cenozoic sands from both basins are dominated by quartz, feldspar, mica, lithic fragments. Most quartz grains are sand to silt-sized, monocrystalline, and angular to subrounded. Lithic fragments are mainly detrital chert and low- to intermediate-grade metamorphic rocks (i.e., slate, quartzite, and schists); volcanic lithic fragments are rare in all samples from both basins. Ternary diagrams of the major components show variations in sand composition throughout the Assam and Bengal basins samples. Plots of different lithic components (sedimentary lithic, Ls; very low- to low-grade metamorphic lithic, Lm_1; and low- to medium-grade metamorphic lithic, Lm_2) reflect the unroofing trend in source area.

The Oligocene Barail Group samples from the Bengal Basin are highly quartz rich and plot in the ‘recycled orogenic’ provenance field on QtFL and QmFLt diagrams (Figs. 19 and 20). High percentages of quartz and rarity of feldspar grains indicate erosion from a low-relief area under strong chemical weathering regimes. Oligocene Barail sediments in the Bengal may have been derived from the Indian craton to the west and deposited on the passive continental margin. The Bengal Basin was positioned further south and distant from the Himalayas during Oligocene. The Himalayas were more than 1500 km north of the Bengal Basin during Eocene and Oligocene time (Le Fort, 1996). Hence, a Himalayan source seems unlikely for the Oligocene sediments in the Bengal Basin. The Indo-Burman Ranges to the east could be a secondary source for the Oligocene Barail sands in the Bengal Basin.

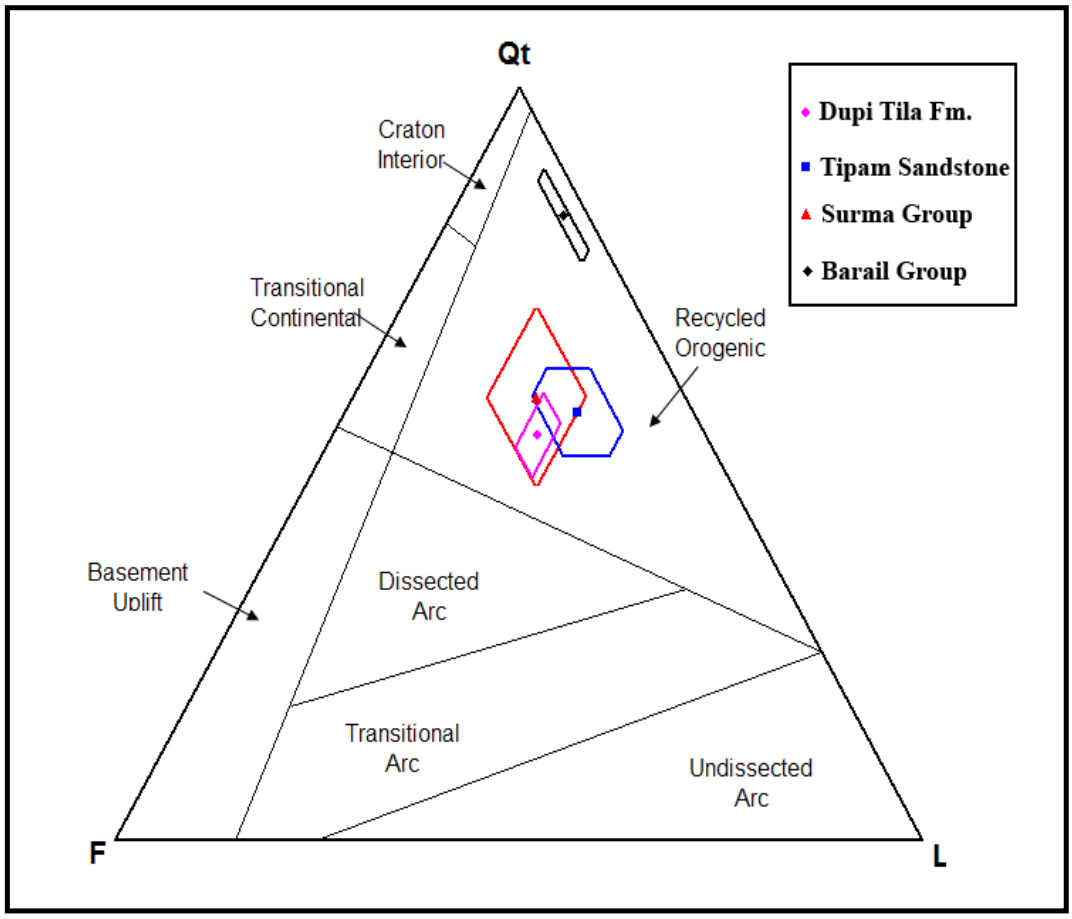

Figure 19. QtFL plot showing composition of Bengal Basin sandstones. Provenance fields are from Dickinson (1985).

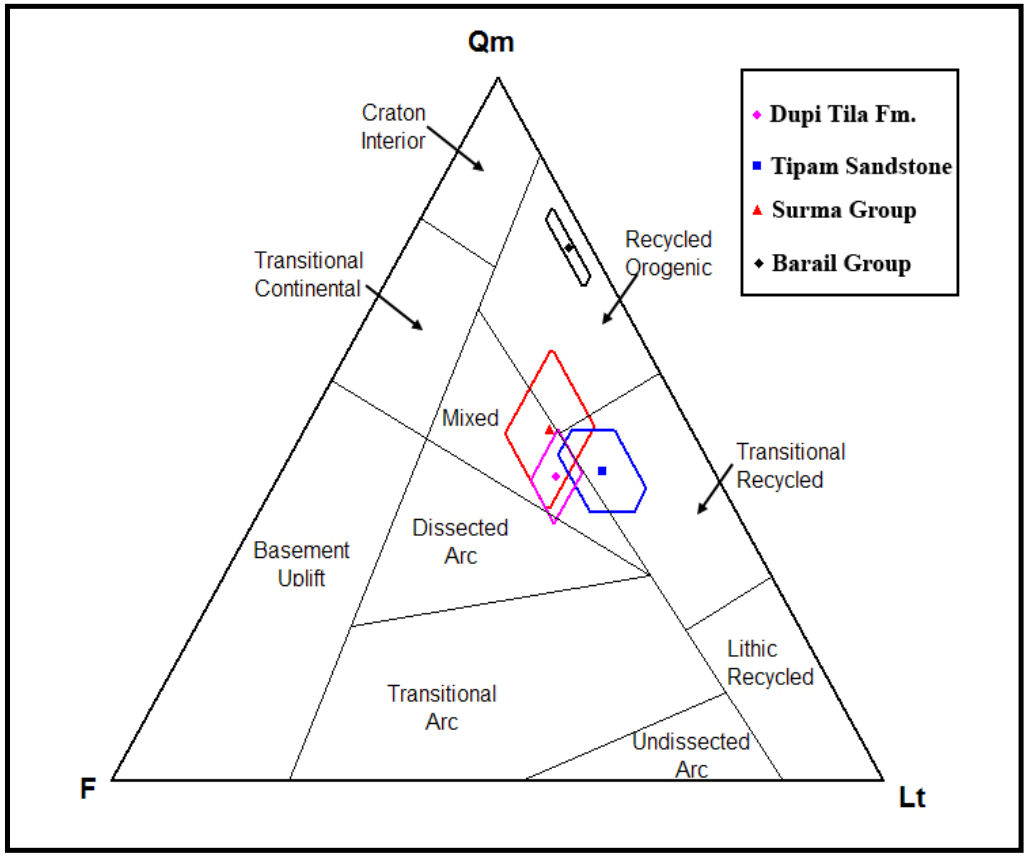

Figure 20. QmFLt plot of Bengal Basin sandstones, showing mean and standard deviation polygons for each stratigraphic unit, along with appropriate provenance fields from Dickinson (1985). Chert and other polycrystalline quartz grains are included in the total lithic counts.

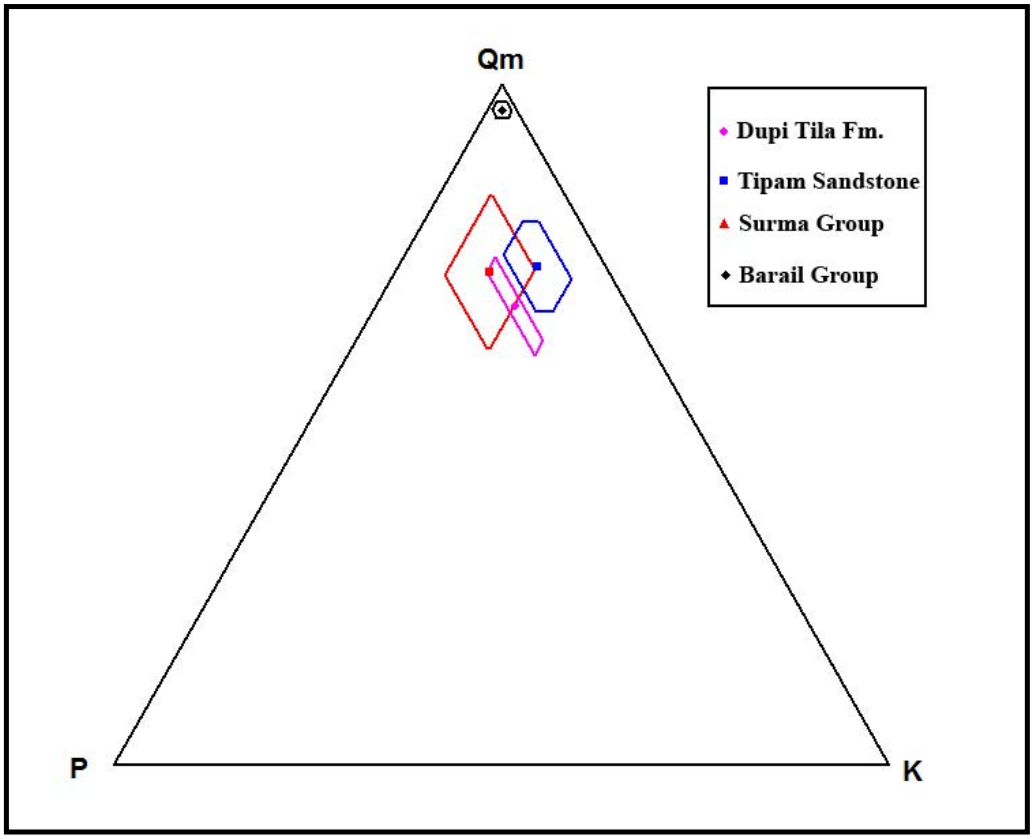

Figure 21. QmPK plot for the Bengal Basin sandstones, showing mean and standard deviation polygons for each stratigraphic unit.

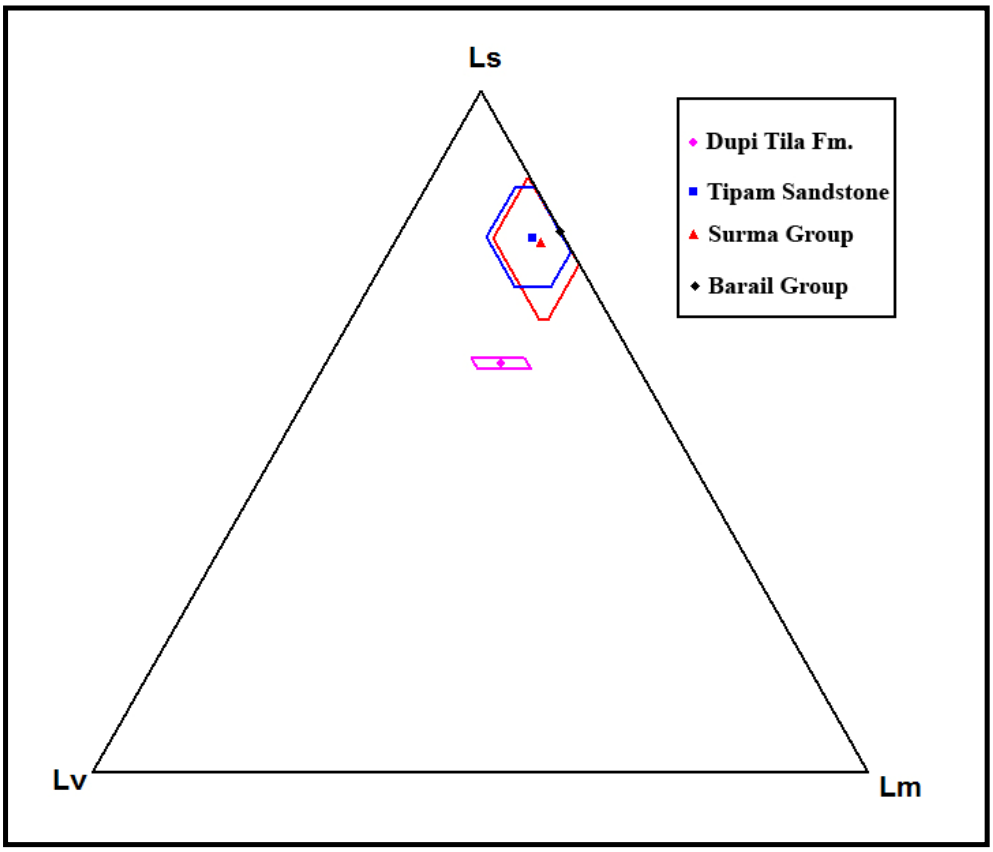

Figure 22. LsLvLm plot showing variations in the composition of lithic fragments in Bengal Basin. Ls = sedimentary lithic fragments, Lv = volcanic lithic fragments, and Lm = low- to intermediate-grade metamorphic rock fragments.

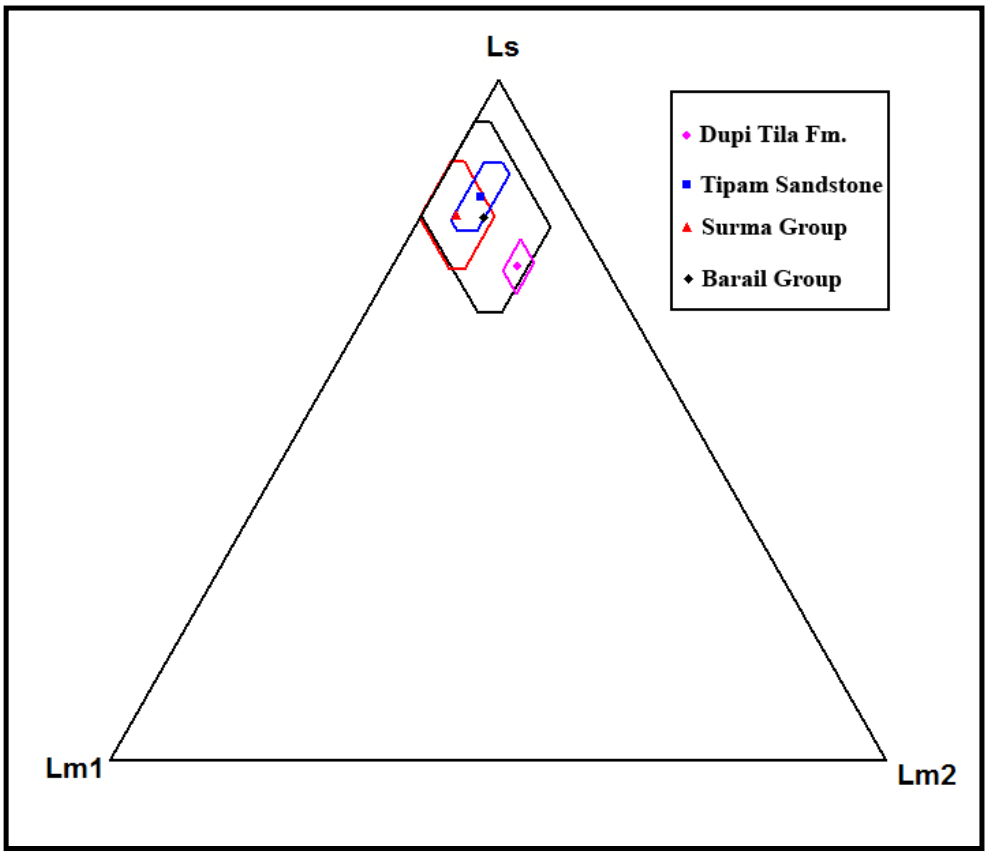

Figure 23. $LsLm_1Lm_2$ plot showing variations in the composition of lithic fragments in Bengal Basin. Ls = sedimentary lithic fragments, Lm_1 = very low- to low-grade metamorphic rock fragments, and Lm_2 = low- to intermediate-grade metamorphic rock fragments.

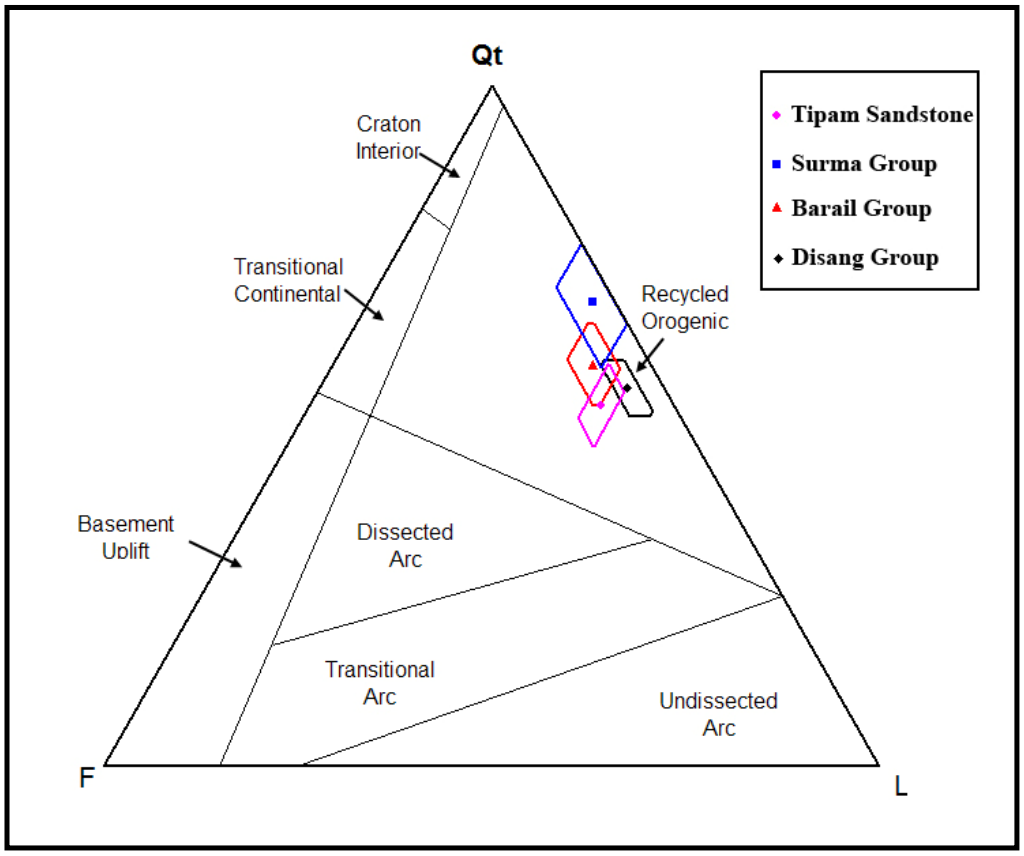

Figure 24. QtFL plot showing composition of Assam Basin sandstones. Provenance fields are from Dickinson (1985).

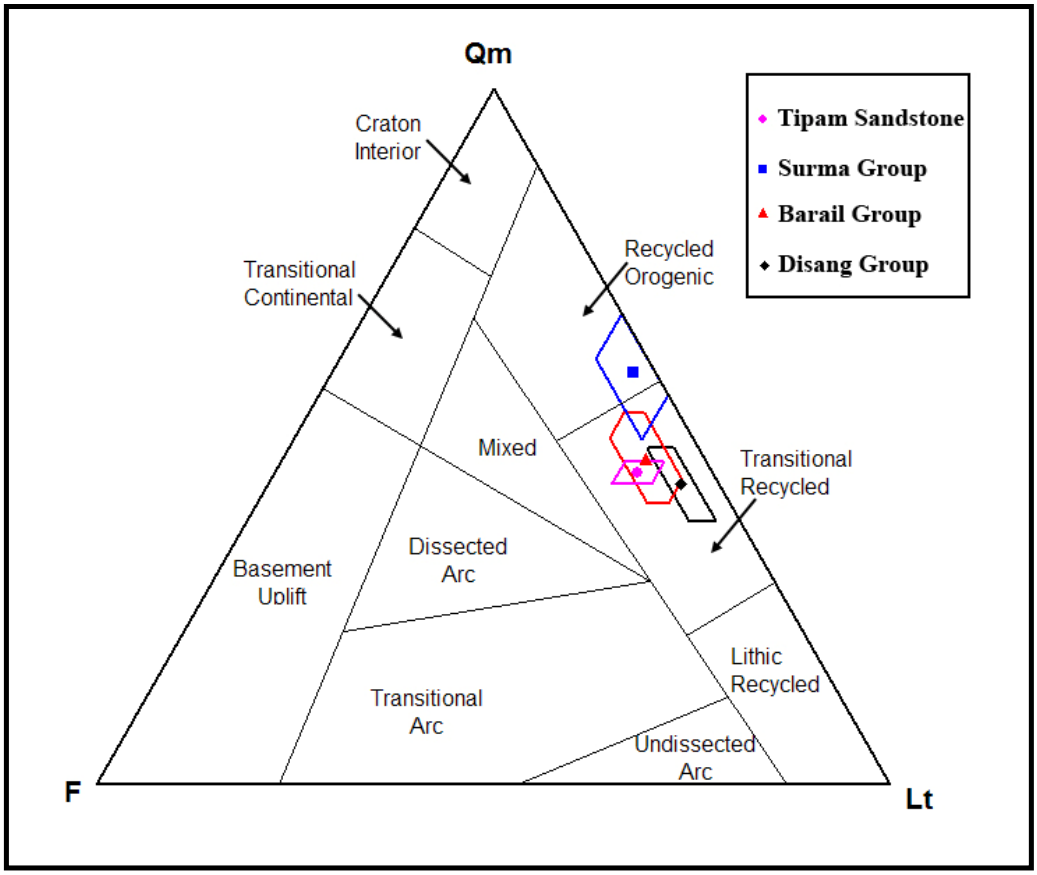

Figure 25. QmFLt plot of Assam Basin sandstones, showing mean and standard deviation polygons for each stratigraphic unit, along with appropriate provenance fields from Dickinson (1985). Cherts and other polycrystalline quartz grains are included in Lt.

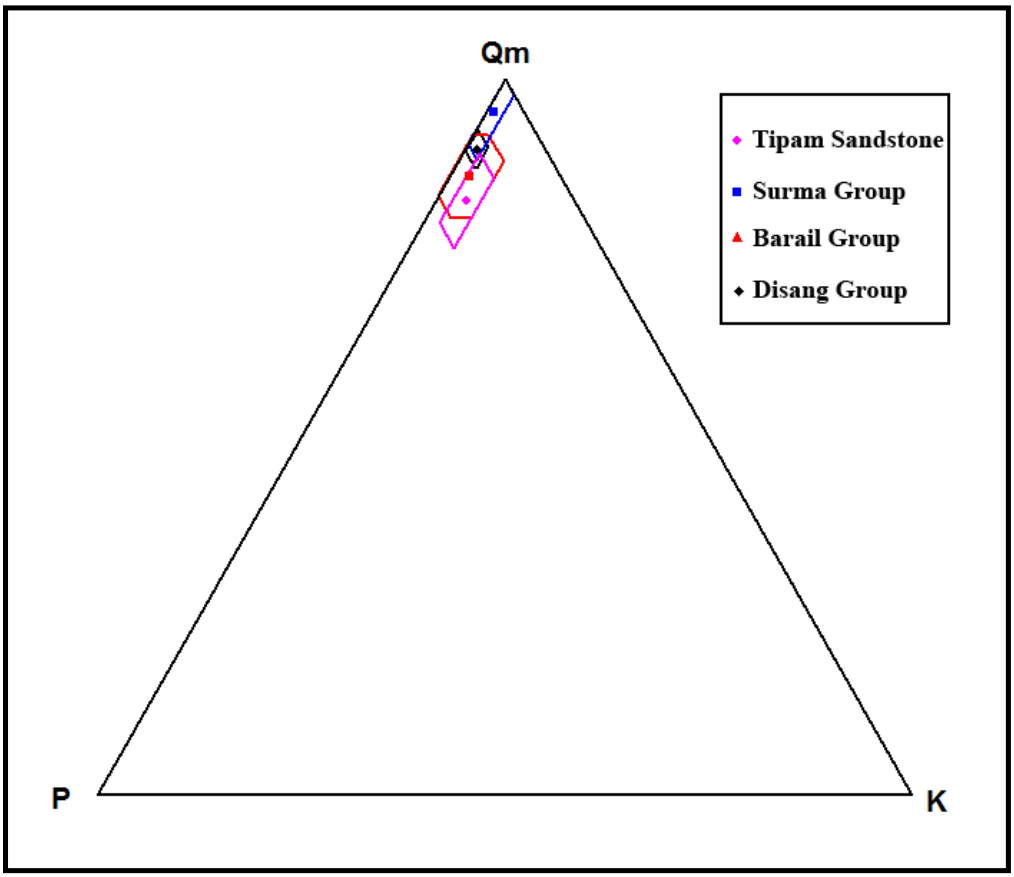

Figure 26. QmPK plot for Assam Basin sandstones, showing mean and standard deviation polygons for each stratigraphic unit.

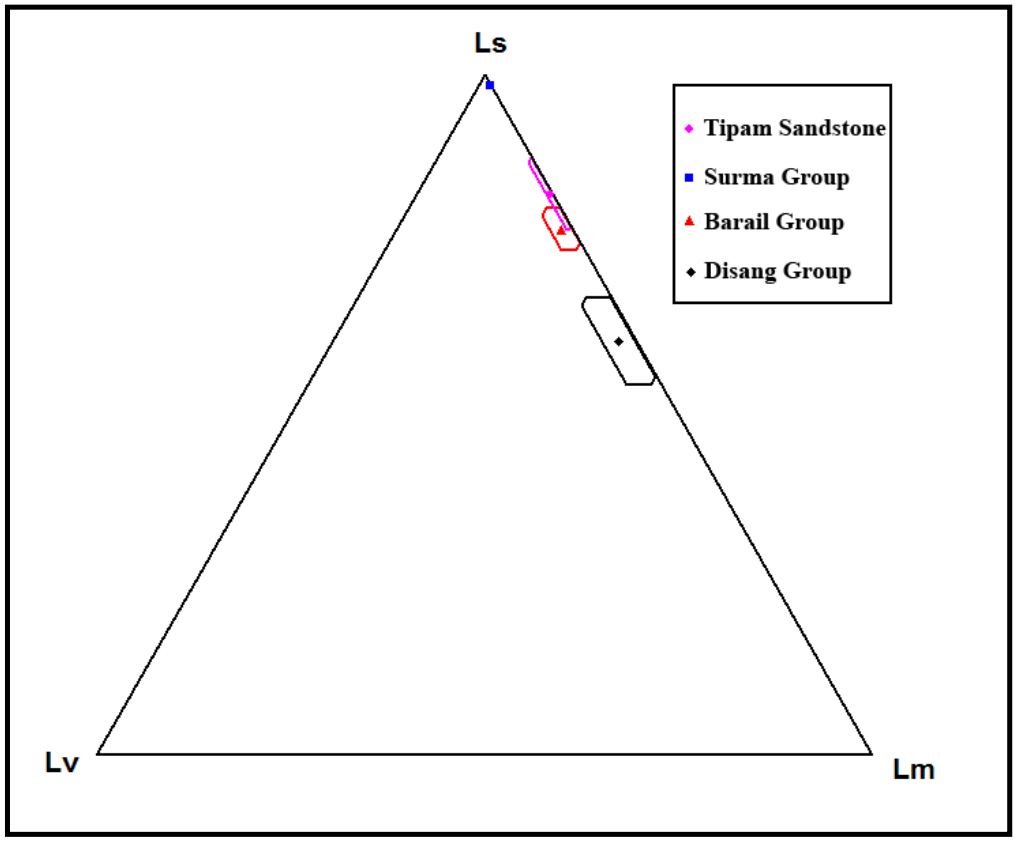

Figure 27. LsLvLm plot showing variations in the composition of lithic fragments in Assam Basin. Ls = sedimentary lithic fragments, Lv = volcanic lithic fragments, and Lm = low- to intermediate-grade metamorphic rock fragments.

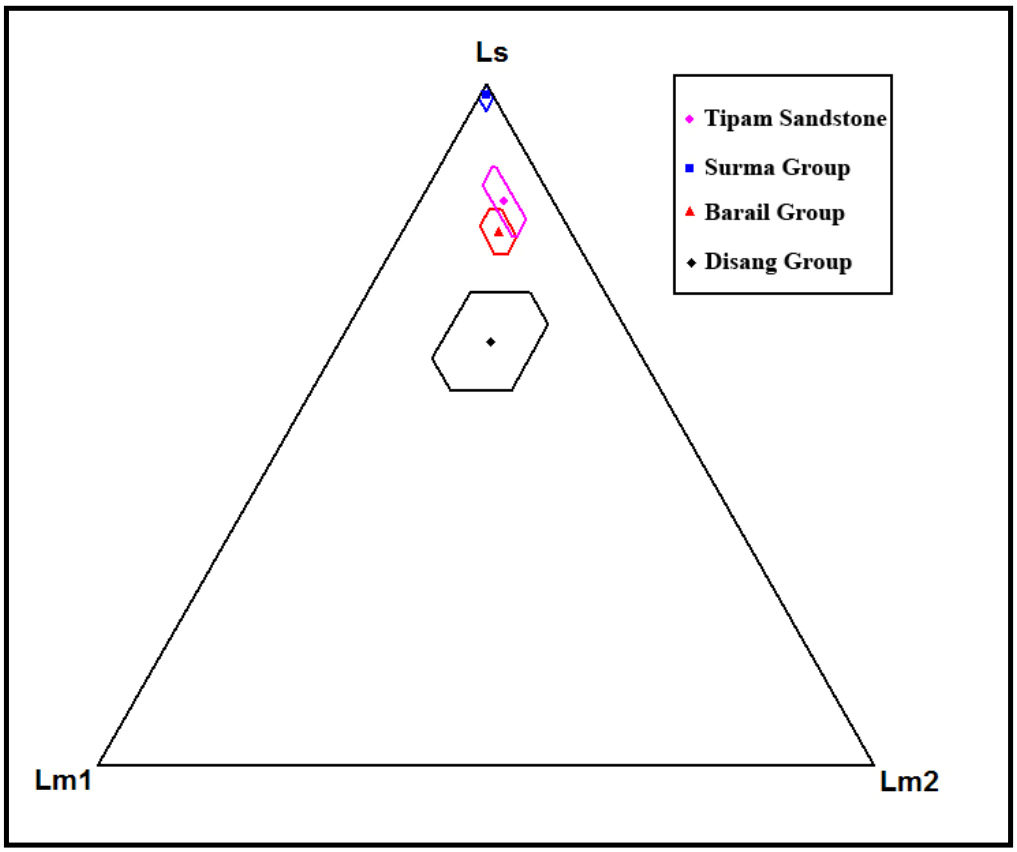

Figure 28. $LsLm_1Lm_2$ plot showing variations in the composition of lithic fragments in Assam Basin. Ls = sedimentary lithic fragments, Lm_1 = very low- to low-grade metamorphic rock fragments, and Lm_2 = low- to intermediate-grade metamorphic rock fragments.

The Miocene, Mio-Pliocene, and Pliocene sediments from Bengal Basin plot in the 'recycled orogenic' field on the QtFL diagram and in both 'recycled orogenic' and 'mixed' fields on the QmFLt diagram (Figs. 19 and 20). Monocrystalline (QmPK) components of sands show that potassium feldspar grains are more abundant than plagioclase and increase upward through the section (Fig. 21). The increase of feldspar grains and lithic fragments in the post-Oligocene indicate the initial input from an orogenic source to the Bengal basin. This is interpreted to be the result of uplift and erosion of the Himalayas. Stream systems probably evolved during Miocene time and cut through the mountain belt to funnel voluminous detritus to the Bengal basin. The Indo-Burman Ranges to the east also may have contributed detritus to the Bengal Basin (Uddin and Lundberg, 1998a).

Modal analyses of Eocene, Oligocene, and younger sandstones of the Disang Group, Barail Group, Surma Group, and Tipam Sandstone from the Assam Basin document compositions that are dominated by monocrystalline and polycrystalline quartz grains. Lithic fragments are most abundant in the Disang Group ($Qt_{56}F_5L_{40}$), while other units have the following QtFL compositions (Barail: $Qt_{59}F_7L_{34}$; Surma: $Qt_{68}F_3L_{29}$, and Tipam: $Qt_{53}F_9L_{38}$). Other ternary diagrams (QmFLt, QmPK, LsLvLm, and $LsLm_1Lm_2$) also indicate that sandstones from the Assam Basin have orogenic provenance signatures (Figs. 24-28). The Eocene Disang sandstones from Assam Basin are quartzolithic in composition with few feldspar grains. This composition strongly suggests that the Disang sandstones are orogenic, as these fall mostly in the 'recycled orogenic' provenance field (Dickinson, 1985), and are derived most likely from nearby eastern Himalayas and/or the Indo-Burman Ranges.

The Oligocene Barail sandstones are quartzolithic, and like the Disang unit, are also orogenic. The increase in monocrystalline quartz in the upper Oligocene may be

attributed to a shift in provenance to recycled orogenic rocks in the Himalayas and the Indo-Burman Ranges, and deposition in deltaic plains. Miocene Surma sequences are also quartzolithic, and are most likely derived from the Himalayas and the Indo-Burman Ranges. Sediments in the Miocene-Pliocene Tipam Group are quartzolithic to quartzofeldspathic. Based on textural and compositional analyses, a nearby source is suggested. Possible sources include the Shillong Plateau to the west, Mishmi thrust to the northeast, and/or the Barail Range in the Kohima and Patkai Hills to the south. During the Miocene, the Himalayan foredeep was formed, indicating major tectonism in the Himalayas to north of the Assam-Arakan basin (Rangarao, 1983; DeCelles et al., 1998). Uplift of the Mishmi thrust, Shillong Plateau, and crystalline basement rocks in the Himalayas (Harrison et al., 1997; DeCelles et al., 1998) possibly could have contributed to the higher feldspar contents in the Tipam Sandstone.

CHAPTER 5: HEAVY MINERAL ANALYSIS

5.1 INTRODUCTION

Detrital heavy minerals can provide important provenance information by complementing overall modal analysis data of sandstones (Morton, 1985; Najman and Garzanti, 2000). In the case of proximal synorogenic sediments, which are transported relatively short distances before rapid deposition, heavy mineral assemblages may closely reflect the petrology of the source area. Heavy minerals generally have specific gravities of 2.9 or more and usually are present in sandstones in proportions of less than 1% (Tucker, 1988). There are over thirty common translucent detrital varieties of heavy minerals that can be used as provenance indicators (Morton, 1985; Mange and Maurer, 1992). Heavy mineral analysis is one of the most widely used techniques in provenance studies, because many heavy minerals are diagnostic of particular source rocks. Furthermore, the processes controlling the distribution of heavy minerals in sandstones are now reasonably well understood (Morton, 1985; Uddin and Lundberg, 1998b; Morton and Hallsworth, 1999) and can be taken into account when reconstructing composition of the source rocks.

Heavy mineral analyses have proven to be effective in provenance reconstruction of sediments in the Himalayan foredeep in the east (Sinha and Sastri, 1973; Uddin and Lundberg, 1998a) and in the west (Chaudhri, 1972; Cerveny et al., 1989), and on deep-sea cores from the Bengal fan (Yokoyama et al., 1990; Amano and Taira, 1992). They have been instrumental in determining the nature of source

rocks, in reconstructing the path of ancestral fluvial systems, and in establishing relationships of source rocks to the unroofing of the Himalayas.

This study reports semi-quantitative analyses of heavy mineral assemblages in representative sandstones from Eocene through Mio-Pliocene strata of the Assam Basin, and compares them with the heavy mineral assemblages in Oligocene through Plio-Pleistocene sandstones from the Bengal Basin in order to help constrain the erosional history of the eastern Himalayas and the Indo-Burman orogens. This was accomplished by determining the relative abundance of all important heavy mineral species preserved in each stratigraphic unit, recognizing dominant members of mineral groups, identifying the first key minerals indicative of certain level of metamorphism, evaluating associations or parageneses of specific heavy minerals, and establishing index minerals from stratigraphic levels in selected sections.

5.2 METHODS

Heavy mineral species have affinities to certain grain-size fractions because of the effect of hydraulic sorting. To remove the sorting effect, coherent samples were disintegrated and dried sieved to select grains in the 0-4 phi range. Concentration of heavy minerals was determined by means of high-density liquids. There is a considerable difference in density between common framework grains and heavy accessory minerals. For this study, a gravity settling method was used with tetrabromoethane ($Br_2CHCHBr_2$, density 2.89-2.96 gm/cc). Dried and weighed samples were added to the heavy liquid in a separating funnel. The mixture was stirred periodically to ensure that the grains were thoroughly wetted. Heavy minerals then gradually accumulated in the bottom of the funnel above the pinch clip. When sinking of the heavy minerals was complete (after 20-24 hours), the stopcock was

opened slowly, and heavy fractions were allowed to pour into filter paper in the lower funnel. The stopcock was then closed immediately to leave a layer of clear liquid below the lighter fraction. The light fraction was then drained into a new funnel. Both fractions were washed thoroughly with acetone and put into an oven for drying.

Magnetic separation of heavy minerals was done using a Frantz magnetometer at the department of Geology and Geography in Auburn University. Four fractions of different magnetic susceptibility were separated (Hess, 1966). These four fractions are: Group-A: Strongly Magnetic (SM); Group-B: Moderately Magnetic (MM); Group-C: Weakly Magnetic (WM); and Group-D: Poorly Magnetic (PM). Strongly magnetic (Group-A) minerals include magnetite, pyrrhotite, hematite, garnet, olivine, chromite, chloritoid, and ilmenite. These were separated using a 0.4-ampere current, a side slope of 20º, and a forward slope of 25º. Group-B minerals including hornblende, hypersthene, augite, actinolite, staurolite, epidote, biotite, chlorite, and tourmaline, were separated from weakly to poorly magnetic minerals using a 0.8-ampere current and a 20º side slope. Finally, Group-C minerals [diopside, tremolite, enstatite, spinel, staurolite (light), muscovite, zoisite, clinozoisite, and tourmaline (light)] were separated using a 1.2-ampere current and a 20º side slope. The rest of the heavy minerals were classified as Group-D (poorly magnetic). This group includes slightly magnetic minerals, such as sphene, leucoxene, apatite, andalusite, monazite, and xenotine, and other non-magnetic minerals like zircon, rutile, pyrite, corundum, fluorite, kyanite, sillimanite and beryl (Hess, 1966). Seventeen polished thin sections of heavy minerals of variable magnetic susceptibility were prepared. Each of the magnetically separated heavy mineral fractions was segregated in different areas of each thin section. Identification of minerals was carried out using a petrographic microscope and a modified Fleet method (Fleet, 1926), in which nearly all grains on

each microscope slide were counted. Grains identified from each magnetically separated fraction were then added together to calculate percentages of heavy minerals present in the 0-4 phi (1-0.063 mm) size fractions of all the slides. Seventeen different heavy mineral species were identified, including opaque minerals as a single group.

5.3 RESULTS

Semi-quantitative point-counting results for heavy minerals in the various stratigraphic units from Bengal and Assam basins are presented in Tables 6 and 7. Total heavy mineral content is low in Oligocene Barail sandstones (0.46-0.62%) compared to those in the Miocene Surma (0.89-1.58%), Mio-Pliocene Tipam (1.10-2.42%), and Plio-Pleistocene Dupi Tila formations (1.43-2.23%) in the Bengal Basin (Fig. 29). In contrast, total heavy mineral percentages in sandstones from Assam Basin (Fig. 30) are as follows: 0.29-0.69% (Eocene Disang), 0.08-0.75% (Oligocene Barail), 0.06% (Miocene Surma), and 1.62-2.45% (Mio-Pliocene Tipam). Heavy mineral assemblages show variations through time in both the Bengal and Assam basins (Figs. 31-35).

Table 6. Normalized abundances of heavy minerals, Bengal Basin, Bangladesh (ZTR – Zircon-Tourmaline-Rutile, and ALS – Aluminosilicates).

	Barail Group (Oligocene) (n=2)	Percentage	Surma Group (Miocene) (n=2)	Percentage	Tipam Group (Mio-Pliocene) (n=2)	Percentage	Dupi Tila Formation Plio-Pleistocene (n=2)	Percentage
		ZTR (%)		ZTR (%)		ZTR (%)		ZTR (%)
Zircon	17		8		6		4	
Tourmaline	22	43.5	11	18.6	5	13.8	9	14.7
Rutile	28		5		10		19	
		ALS (%)		ALS (%)		ALS (%)		ALS (%)
Sillimanite	6		3		10		11	
Kyanite	3	11.0	6	9.3	20	24.3	18	20.2
Andalusite	8		3		7		15	
Chrome Spinel	12	7.8	15	11.6	5	3.3	22	10.1
Epidote	5	3.2	10	7.8	10	6.6	12	5.5
Hornblende	6	3.9	7	5.4	20	13.2	30	13.8
Garnet	13	8.4	18	14.0	20	13.2	30	13.8
Chlorite	7	4.5	6	4.7	2	1.3	7	3.2
Biotite	8	5.2	20	15.5	5	3.3	3	1.4
Pyroxene	8	5.2	8	6.2	5	3.3	7	3.2
Tremolite Actinolite	3	1.9	0	0.0	0	0.0	10	4.6
Apatite	3	1.9	7	5.4	15	9.9	6	2.8
Staurolite	5	3.2	2	1.6	12	7.9	15	6.9
Total grains counted	154		129		152		218	

Table 7. Normalized abundances of heavy minerals, Assam Basin, India (ZTR – Zircon-Tourmaline-Rutile, and ALS – Aluminosilicates).

	Disang Group (Eocene) (n=3)	Percentage	Barail Group (Oligocene) (n=2)	Percentage	Surma Group (Miocene) (n=2)	Percentage	Tipam Group (Mio-Pliocene) (n=2)	Percentage
		ZTR (%)		ZTR (%)		ZTR (%)		ZTR (%)
Zircon	13		11		6		9	
Tourmaline	17	19.5	22	32.1	13	14.8	14	14.0
Rutile	18		27		17		12	
		ALS (%)		ALS (%)		ALS (%)		ALS (%)
Sillimanite	10		3		3		6	
Kyanite	13	15.9	7	8.0	7	5.8	12	9.2
Andalusite	16		5		4		5	
Chrome Spinel	24	9.8	6	3.2	6	2.5	7	2.8
Epidote	7	2.8	5	2.7	12	4.9	9	3.6
Hornblende	12	4.9	6	3.2	23	9.5	9	3.6
Garnet	41	16.7	43	23.0	42	17.3	68	27.2
Chlorite	32	13.0	3	1.6	38	15.6	43	17.2
Biotite	12	4.9	6	3.2	13	5.3	8	3.2
Pyroxene	8	3.3	8	4.3	14	5.8	18	7.2
Tremolite Actinolite	3	1.2	7	3.7	17	7.0	6	2.4
Apatite	12	4.9	11	5.9	16	6.6	5	2.0
Staurolite	8	3.3	17	9.1	12	4.9	19	7.6
Total grains counted	246		187		243		250	

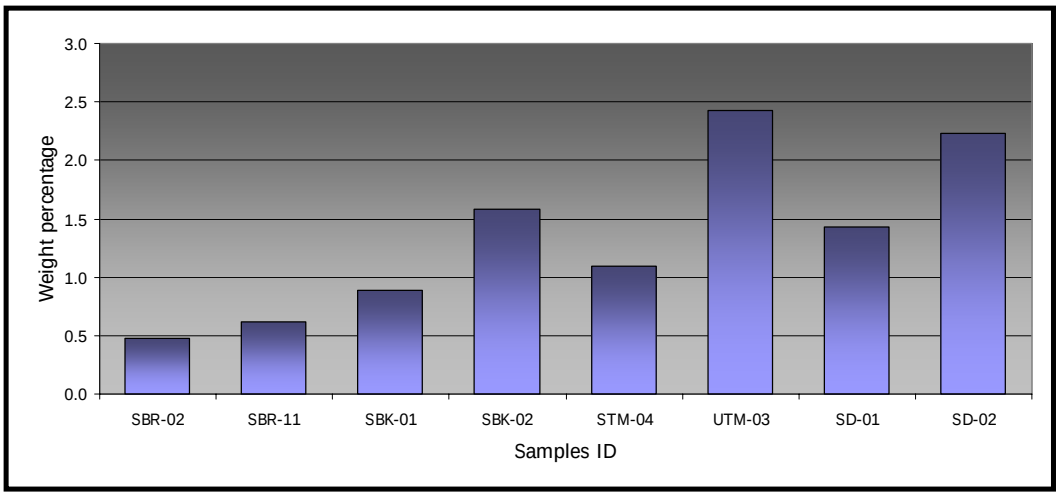

Figure 29. Heavy mineral percentages in sandstones from various stratigraphic units in the Bengal Basin (SBR- Barail: Oligocene, SBK-Surma: Miocene, STM/UTM-Tipam: Mio-Pliocene, and SD- Dupi Tila: PLiocene units).

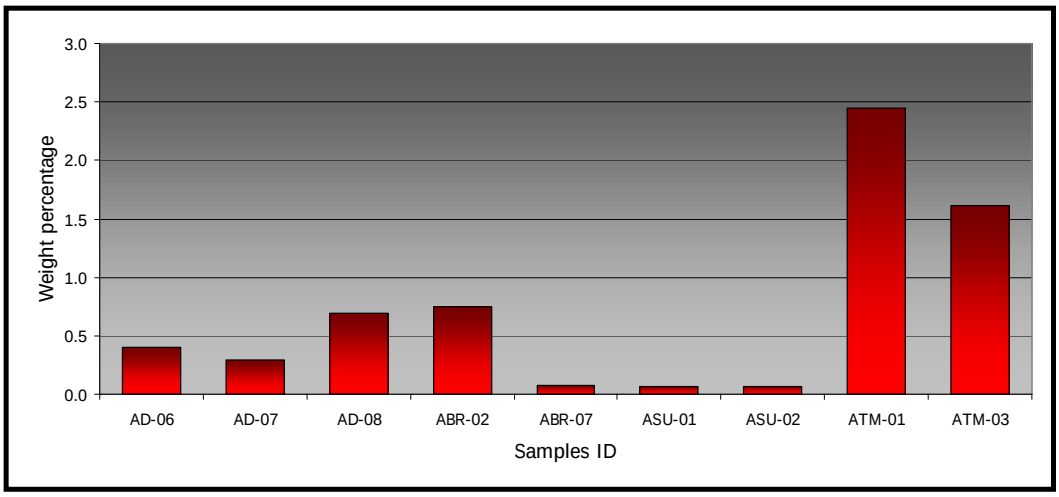

Figure 30. Heavy mineral percentages in sandstones from various stratigraphic units in the Assam Basin (AD- Disang: Eocene, ABR-Barail: Oligocene, ASU-Surma: Miocene, and ATM-Tipam: Mio-Pliocene units).

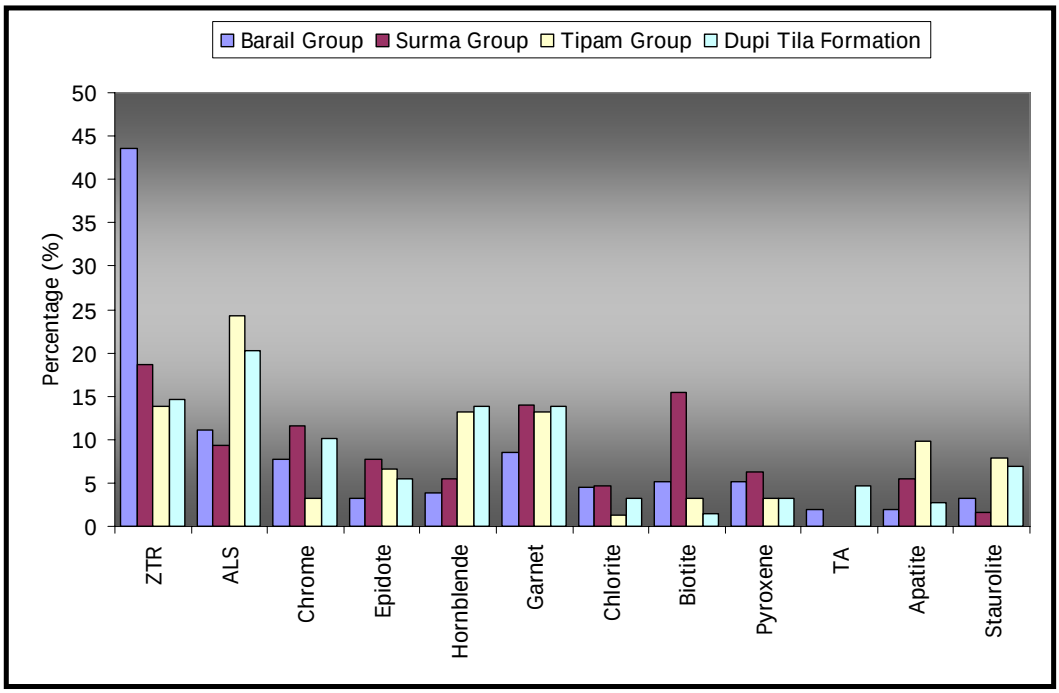

(A)

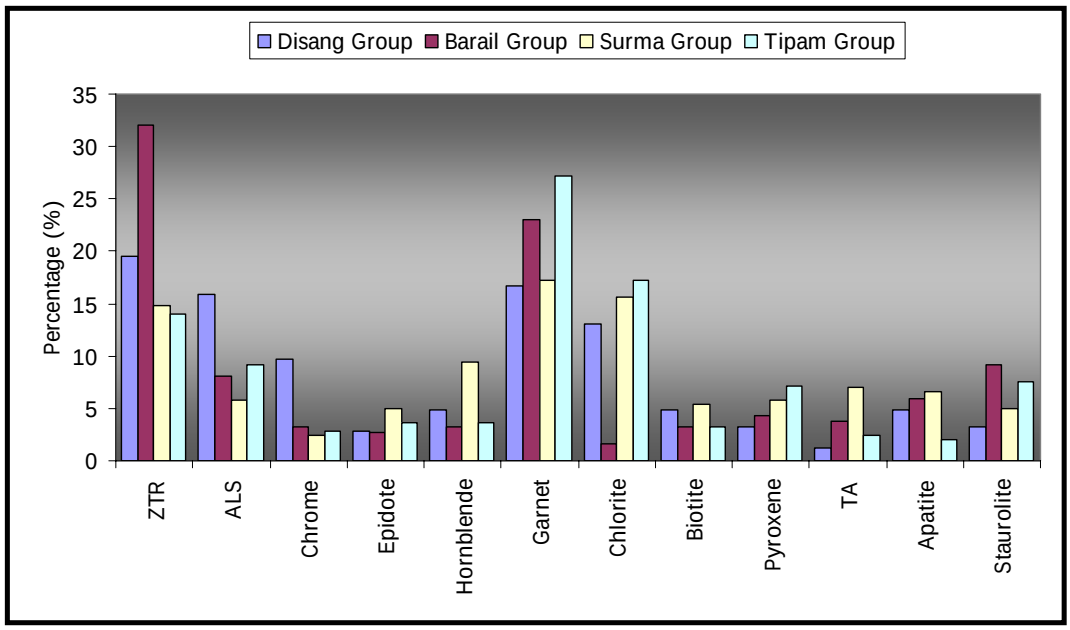

(B)

Figure 31. Heavy mineral distribution in sandstones from various stratigraphic units from Bengal (A) and Assam (B) basins (ZTR=Zircon, Tourmaline, and Rutile; ALS=Alumino-silicates; TA=Tremolite and Actinolite).

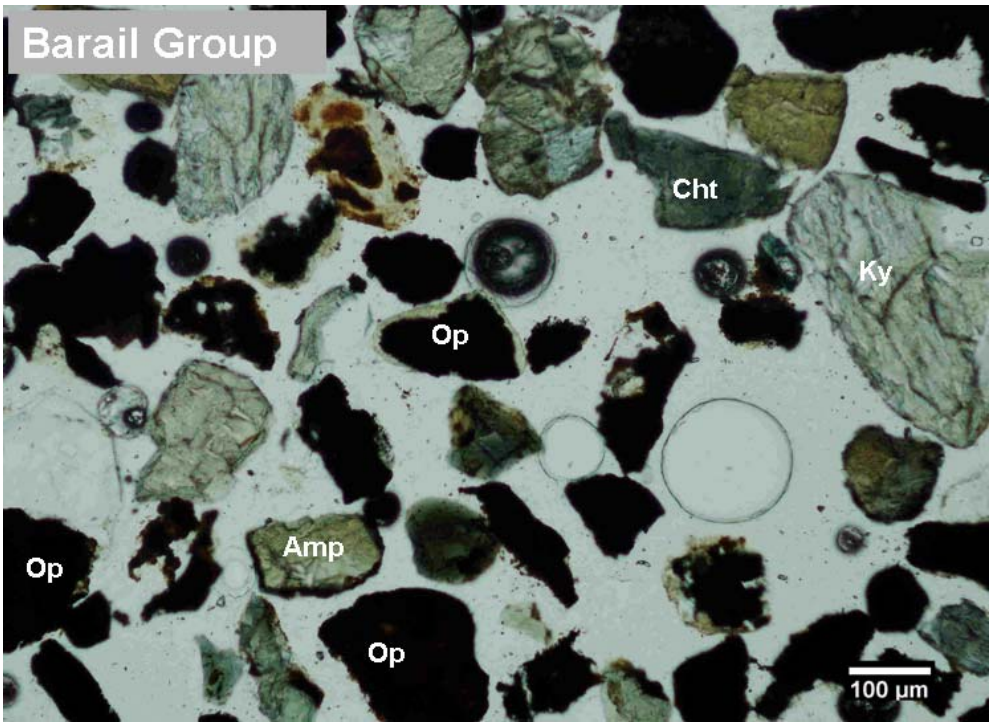

(A)

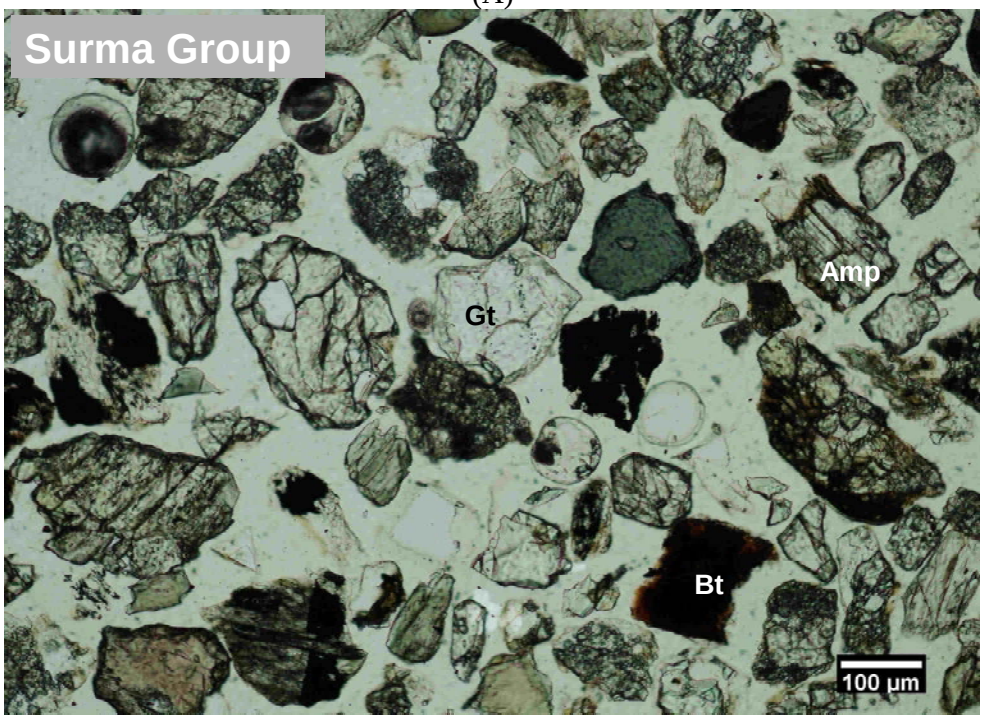

(B)

Figure 32. Representative photomicrographs of heavy minerals from Bengal Basin. (A) Barail Group and (B) Surma Group. Mineral keys: Cht-Chlorite, Gt-Garnet, Ky-Kyanite, Bt-Biotite, Amp-Amphibole, Op- Opaque.

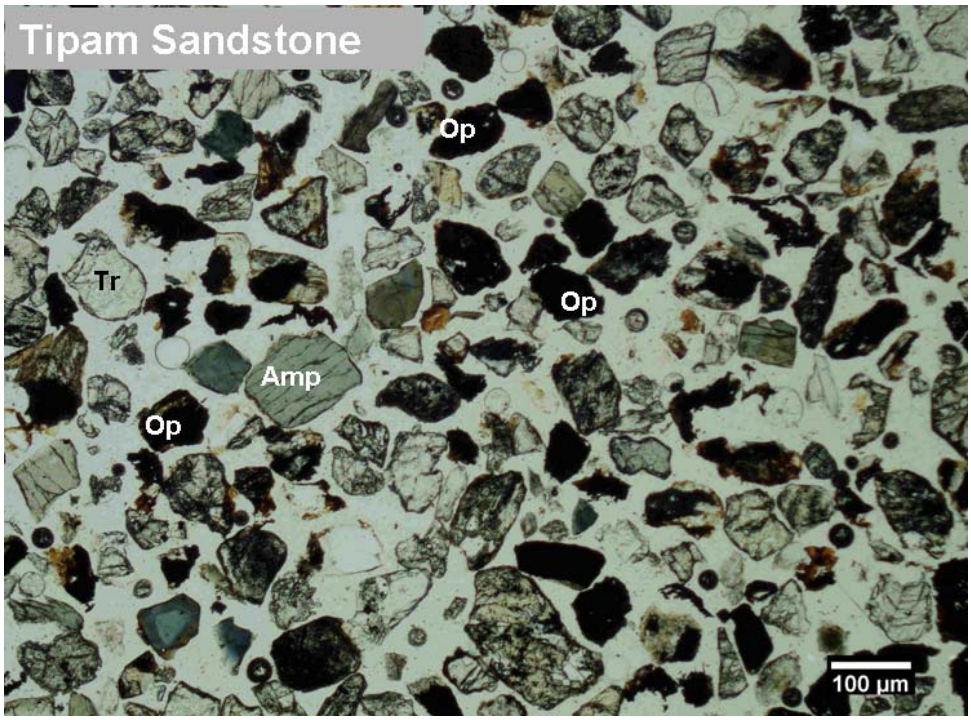

(A)

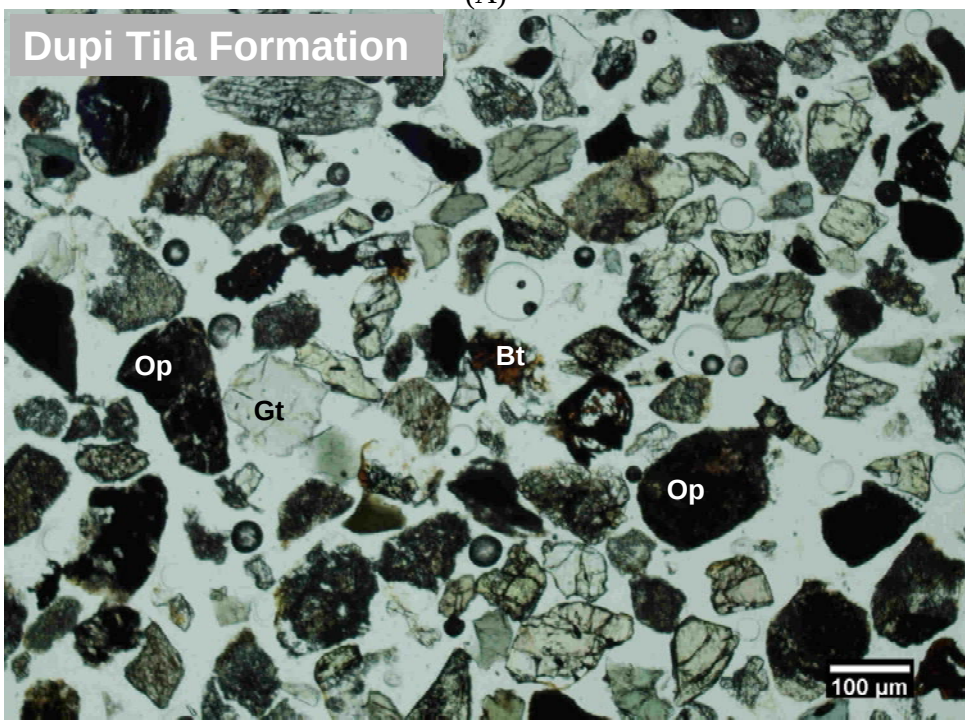

(B)

Figure 33. Representative photomicrographs of heavy minerals from Bengal Basin. (A) Tipam Group and (B) Dupi Tila Formation. Mineral keys: Gt-Garnet, Bt-Biotite, Amp-Amphibole, Tr- tourmaline, Op- Opaque.

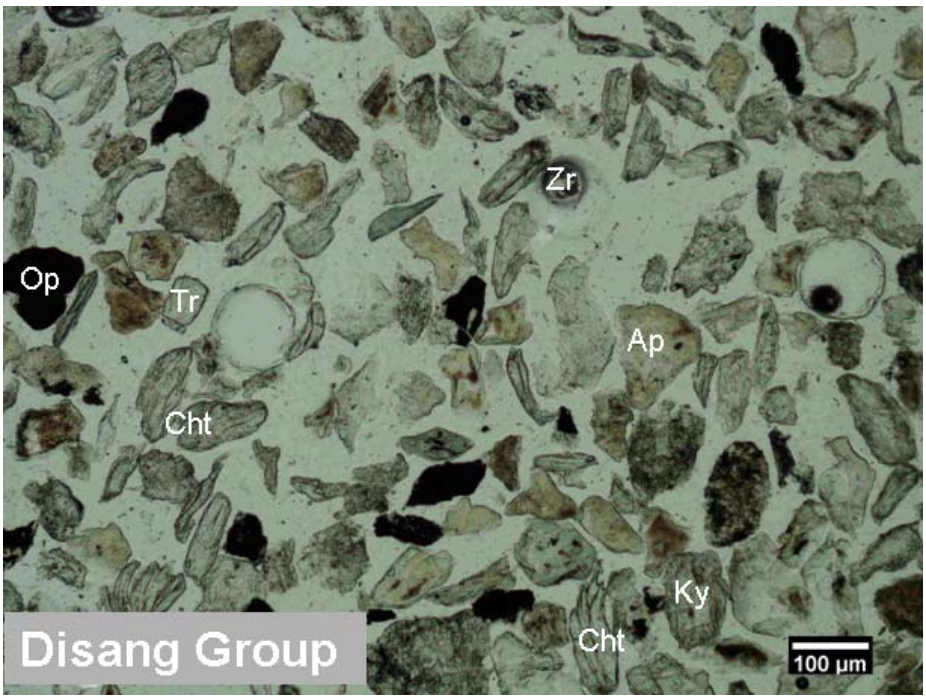

(A)

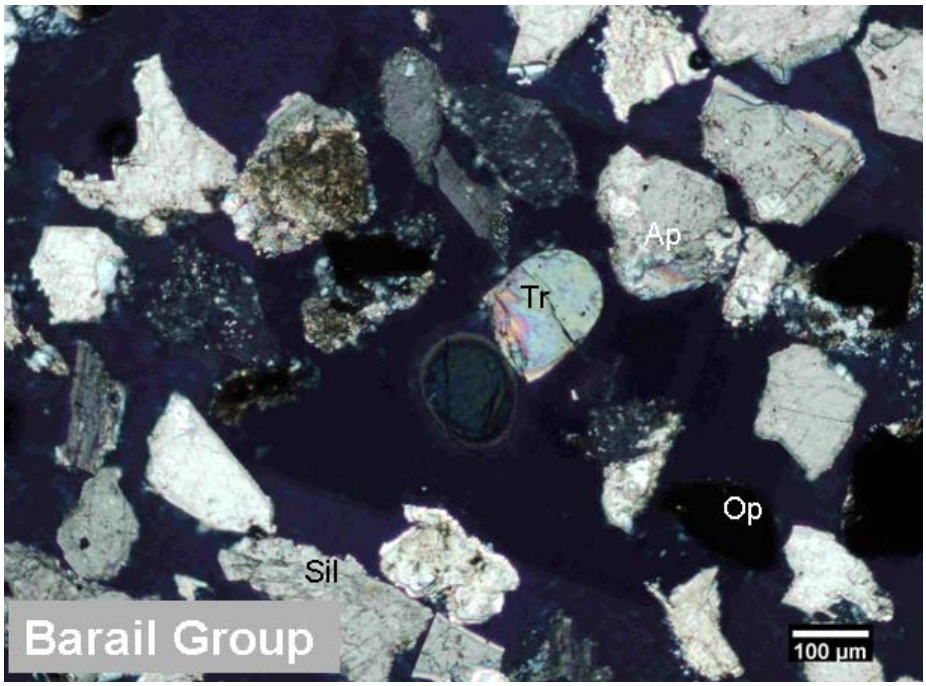

(B)

Figure 34. Representative photomicrographs of heavy minerals from Assam Basin. (A) Disang Group and (B) Barail Group (crossed polars). Mineral keys: Cht-Chlorite, Ky-Kyanite, Sil-Sillimanite, Zr-Zircon, Ap-Apatite, Tr- tourmaline, Op- Opaque.

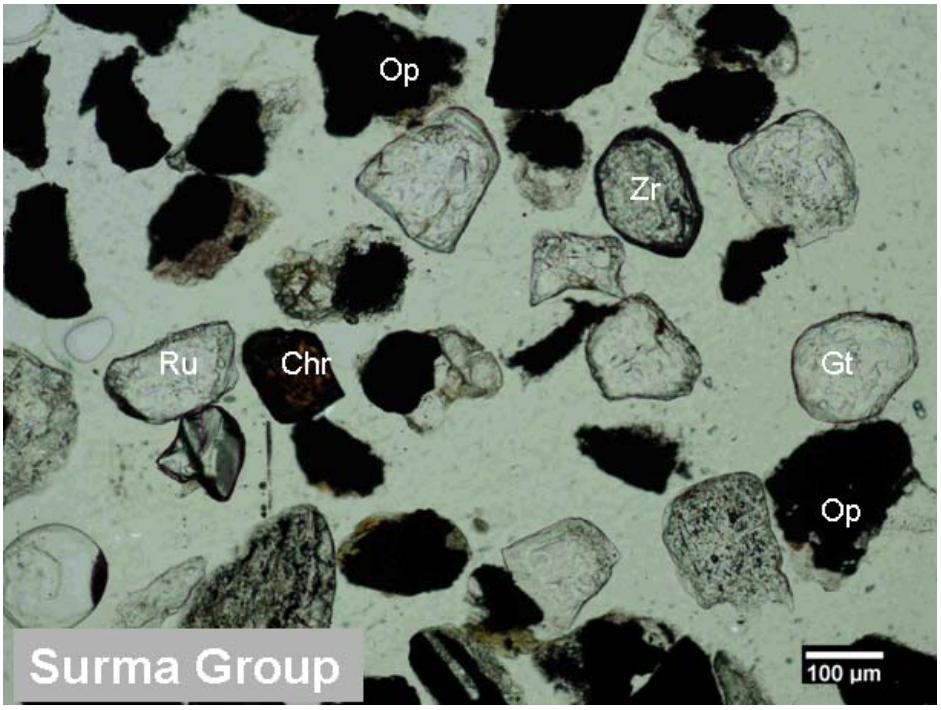

(A)

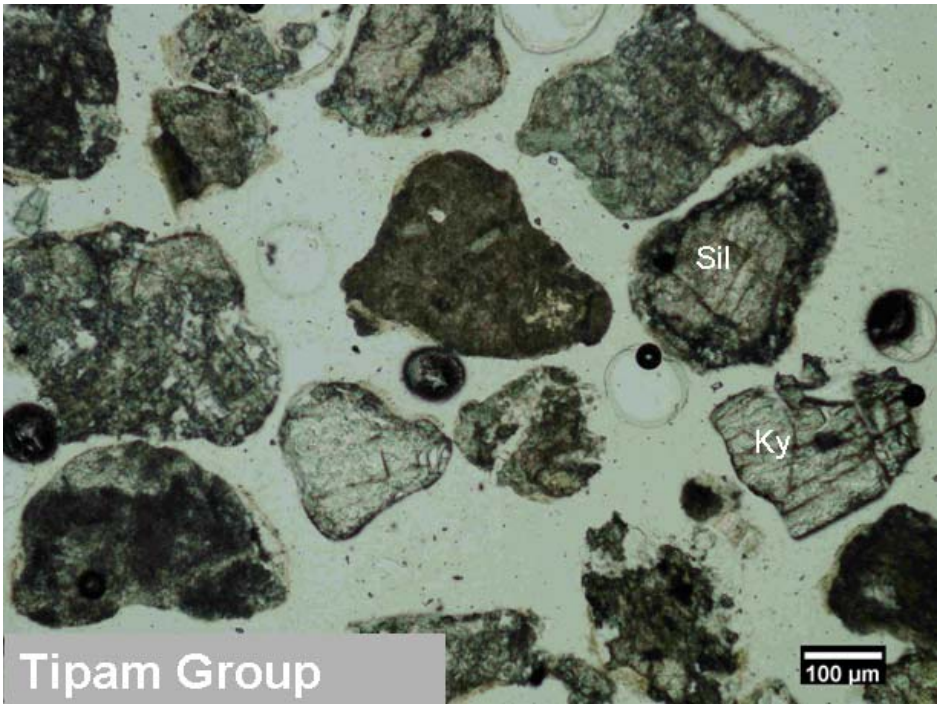

(B)

Figure 35. Representative photomicrographs of heavy minerals from Assam Basin (A) Surma Group and (B) Tipam Group. Mineral keys: Chr- Chrome Spinel, Gt-Garnet, Ky-Kyanite, Sil-Sillimanite, Zr-Zircon, Op- Opaque.

Opaque minerals are dominant in sandstones from both the Bengal and Assam basins. Most of the opaque minerals are unidentifiable using transmitted-light polarizing microscopy. However, these minerals were easier to identify using reflected light microscopy and an electron microprobe equipped with an energy dispersion spectrometer (EDS). Among non-opaque heavy mineral assemblages, stable minerals (ZTR: zircon-rutile-tourmaline; Table 6) are dominant in the Oligocene Barail sands (Fig. 32) in the Bengal Basin. The ZTR index decreases from 43.5% in Oligocene sequences through 14.5% in Plio-Pleistocene units. Rutile is most abundant in Bengal and Assam basins (Tables 6 and 7). Garnet percentages are low in the Oligocene Barail of the Bengal Basin compared to other units. Bengal Basin heavy minerals include garnet, tourmaline, rutile, zircon, chlorite, chrome spinel, kyanite, sillimanite, andalusite, pyroxene, amphibole, biotite, staurolite, apatite, actinolite/tremolite, and epidote. Aluminosilicate heavy minerals become more common in the younger sequences of the Bengal Basin. Amphibole percentages increase in the younger units of the Bengal Basin. Minerals of the epidote family, (e.g., epidote, zoisite, and clinozoisite) are common in sandstones of all stratigraphic units of the Bengal Basin. Heavy mineral assemblages of sands and sandstones of the Mio-Pliocene and Plio-Pleistocene units are similar to those of the underlying Miocene sandstone, but they contain more abundant high-grade heavy minerals.

Eocene Disang Group sandstones in the Assam Basin contain fewer ZTR minerals (19.5%) than the Oligocene Barail Group (32.2%). Disang Group sandstones have more chlorite/chloritoid than those of the Barail Group. Heavy mineral distributions in Miocene and post-Miocene sands and sandstones from the Assam Basin are more or less similar to those of comparable age in the Bengal Basin. The common heavy minerals in sandstones from the Assam Basin are zircon, tourmaline,

rutile, aluminosilicates (sillimanite, kyanite, and andalusite), chlorite, chloritoid, garnet, epidote, actinolite, tremolite, chrome spinel, pyroxene, and amphiboles. Miocene and younger units in the Assam Basin contain fewer opaque minerals than the older Disang and Barail units. Among the ultra-stable heavy minerals, tourmaline and rutile are very abundant in the Assam Basin. Garnets are common in all sandstones sequences from the Assam Basin.

5.4 PROVENANCE HISTORY

Heavy mineral studies aid in deciphering sediment provenance and stratigraphic correlation, as they include a much wider spectrum of silicate, sulfate, sulfide, oxide, and phosphate minerals (Mange and Maurer, 1992; Mange and Morton, 2007; Milliken, 2007; Uddin et al., 2007). Semi-quantitative point counts of heavy mineral assemblages from the Bengal and Assam basins sediments provide information on the source rocks from which they derived. Oligocene sediments in the Bengal Basin are overwhelmingly quartzose and contain only small amounts of heavy minerals, most of which are opaque varieties (Fig. 32) (Uddin and Lundberg, 1998b). Low diversity of heavy minerals indicates intense weathering during deposition of Palaeogene sands in the Bengal Basin. This may reflect the basin's position close to the equator (Lindsay et al., 1991). Compared to the Oligocene, Miocene sediments from the Bengal Basin contain abundant and diverse heavy mineral assemblages (Fig. 32), suggesting derivation from orogenic fronts that may have moved closer to the Bengal Basin. The younger stratigraphic units, the Tipam Group and sandstone of the Dupi Tila Formation, contain heavy mineral assemblages that are even more abundant and more diverse than those of the older units (Fig. 33). These observations suggest the emergence of additional source terranes with complex lithologies, ranging from high-grade contact metamorphic rocks to various igneous bodies. Changes in the abundance of aluminosilicates and related minerals upward through Bengal Basin stratigraphic units reflect systematic unroofing of progressively deeper crustal levels in the eastern Himalayas (Uddin and Lundberg, 1998b). Presence of chrome spinels in stratigraphic units from the Bengal Basin indicate exhumation of arc and ophiolitic rocks from suture zones of the Himalayas and/or the Indo-Burman Ranges (Figs. 1 and 3).

Heavy minerals of the Eocene Disang Group of the Assam Basin show a suite of minerals dominated by abundant opaque minerals, ultra-stable ZTR minerals, chlorites, chrome spinel, and monazite. Although low in ZTR percentages, the Eocene Disang Group contains heavy mineral assemblages that are similar to those in the Oligocene Barail Group. This finding also is supported by Sinha and Sastri (1973) and Kumar (2004). The Disang Group consists of shale, siltstone, and fine-grained sandstone, whereas the Barail Group is mostly represented by very fine- to fine-grained sandstones. The Miocene Surma Group that unconformably overlies the Oligocene Barail Group has diverse heavy mineral assemblages. These assemblages contain abundant chlorite, chloritoid, hornblende, and epidote, as well as common ZTR and garnets, indicating derivation from low- to medium-grade metamorphic terranes. The Tipam Group heavy mineral suite is very diverse in Assam Basin. It contains almost all mineral species found in the underlying Surma Group, but also includes enstatite, hypersthene, and higher percentages of aluminosilicates. These heavy mineral assemblages suggest orogenic source terranes with input from low- to high-grade metamorphic rocks.

CHAPTER 6: MICROPROBE ANALYSES

6.1 INTRODUCTION

Chemical analysis of individual mineral species has recently become an integral part of provenance studies. A large number of detrital heavy mineral species can be used to narrow down the provenance of any sedimentary basin, like the Assam and Bengal basin system in the eastern Himalayas. The chemical composition of number of heavy mineral species ranges broadly, reflecting conditions of formation and derivation from different igneous and metamorphic source rocks. Although the chemistry of such minerals varies enough to be of petrogenetic significance, density and stability remain relatively homogeneous within each mineral species.

The prime objective of this chapter is to employ heavy mineral chemistry to evaluate the temporal evolution of provenance for Tertiary sediments of Assam and Bengal basins. The Bengal and Assam basins are located close to two major mountain systems, the Himalayas and the Indo-Burman Ranges. It is important to establish the relative contribution of sediments from these two orogenic belts through time. Geochemical analysis, using a variety of microbeam techniques, was applied in this study to garnets, chrome spinel, and tourmaline.

6.2 MINERAL CHEMISTRY

Garnet, chrome spinel, and tourmaline were chosen for mineral chemistry analysis for this research. Except for garnets, all are common in sediments of both basins. Each of these minerals can be subdivided into compositional varieties that are used as an indicator of the source rocks from which they were derived. Several workers have studied provenance based on chemistry of these minerals (Henry and Guidotti, 1985; Morton, 1985; Henry and Dutrow, 1990; Morton and Taylor, 1991; Nanayama, 1997; Mange and Morton, 2007).

Garnet [$(Mg, Fe^{2+}, Mn, Ca)_3(Al, Cr, Ti, Fe^{3+})_2(SiO_4)_3$] or [$X_3Y_2(SiO_3)_4$] geochemistry is the most widely used mineral chemical tool for determination of sediment provenance, as garnets are very common in metamorphic rocks and certain igneous rocks. Garnet, a relatively stable mineral under both weathering and diagenetic conditions, has been used to evaluate provenance in a number of regions (Morton and Taylor, 1991, Morton and Hallsworth, 2007), the most relevant to this study being the offshore Bengal fan (Yokoyama et al., 1990). Increasing metamorphic grade is reflected by an increase in the ratio $(Fe^{2+} + Mg^{2+})/ (Ca^{2+} + Mn^{2+})$ in the cubic-coordination (X) site, as noted by Sturt (1962) and Nandi (1967). In pelitic schists, as well as mafic protoliths, Mg concentration increases with respect to Fe^{2+} with increasing metamorphism (Spear, 1993). Significant occupation of the octahedral site by cations other than Al^{3+} (i.e., Cr^{3+}, Fe^{3+}) also may be useful in constraining the chemical conditions of crystallization.

Chrome spinel [$(Mg,Fe^{2+})(Cr,Al,Fe^{3+})_2O_4$] or [$A_8B_{16}O_{32}$] is a ubiquitous accessory mineral in mafic and ultramafic rocks (Irvine, 1973, 1977; Dick and Bullen, 1984, Nixon et al., 1990; Mange and Morton, 2007). The composition of chrome

spinel [$A_8B_{16}O_{32}$] is a sensitive indicator of parental melt conditions and, hence, of the source rock. There are 32 oxygen ions and 24 cations in the unit cell; eight of the cations are in four-fold coordination (the A positions), and 16 are in six-fold coordination (the B positions) (Deer et al., 1992). Two structural types, known as normal and inverse spinels, differ in their distribution of cations among the A and B positions. $FeAl_2O_4$ (hercynite), $ZnAl_2O_4$ (gahnite), and $MnAl_2O_4$ (galaxite) are normal spinels, while $MgFe_2^{3+}O_4$ (magnesioferrite) and $Fe^{2+}Fe_2^{3+}O_4$ (magnetite) have inverse structure. In nature, pure end-members are rare. Spinels occur mostly as solid-solution series, and varieties are designated by the most dominant cations (Deer et. al., 1992).

Tourmaline [$XY_3Z_6(BO_3)_3Si_6O_{18}(OH)_4$] is a complex borosilicate with a considerable range of potential compositions. This wide compositional range makes tourmaline an ideal mineral for use in geochemical discrimination of provenance (Henry and Guidotti, 1985; Henry and Dutrow, 1992). Tourmaline crystallizes under a wide variety of igneous and metamorphic conditions. The omnipresence of tourmalines probably accounts for its traditional neglect in provenance studies; the simple presence of tourmaline does not place many constraints on the source rock type. However, when chemistry is considered, tourmaline becomes a particularly valuable petrogenetic indicator. Ternary plots of AL-Fe(tot)-Mg and Ca-Fe(tot)-Mg can differentiate between tourmalines from a variety of rock types (Henry and Guidotti, 1985; Henry and Dutrow, 1992).

6.3 METHODS

Seventeen samples were sieved into whole-phi fractions; the 2-3 and 3-4 phi fractions were used for the analysis. Highly magnetic fractions were removed from the heavy-mineral separates using hand-held magnets and a Franz magnetic separator.

The remaining "heavy" fraction was divided further into three to four groups using a Franz magnetic separator, with the aim of concentrating the mineral species for electron microprobe analyses. Slides were prepared by drilling 1/8" holes in 1.5" X 0.75" plexiglas sheets, pouring grains from each magnetic subfraction into different holes (from low, medium to high magnetic susceptibility), and then setting them with epoxy. The plexiglas sheets were then mounted on glass slides, ground to standard optical thickness of 30 micrometers, and polished for microprobe analysis. Before the samples were put into the microprobe sample chamber, non-conductive samples were carbon-coated to ensure conduction. Standards and samples were coated to the same thickness. Carbon coating was carried out by carbon evaporation under vacuum. A polished brass block was used to monitor the thickness of the carbon coat. As the thickness of coat increases on the brass, it changes color from orange (150 Å) to indigo red (200 Å), then to blue (250 Å), and then to bluish green (300 Å).

The electron microprobe provides a complete micro-scale quantitative chemical analysis of inorganic solids such as minerals. The method is nondestructive and utilizes the characteristic x-rays stimulated by an electron beam incident on a flat surface of the sample. X-rays are emitted by the sample in response to a finely focused electron beam incident on the sample at a right angle. Some of the beam electrons are scattered backward. The backscattered electrons, as well as the characteristic x-rays of the elements, carry information about chemical composition. These electrons are called backscattered electrons because they come back out of the sample. Because they are moving so fast, they travel in straight lines. In order to form an image with BSE (backscattered electrons), a detector is placed in their path. When they hit the detector, a signal is produced and used to form a TV image. Because energies of backscattered, characteristic X-rays, and secondary electrons differ,

different detector setups are required for the detection of the three types of electron signal.

The electron microprobe serves two main objectives: (1) complete quantitative chemical analysis of microscopic volumes of solid materials through x-ray emission spectral analysis; and (2) high-resolution scanning electron and scanning x-ray image production. There are two types of scanning electron images: backscattered electron (BSE) images, which show compositional contrast; and secondary electron (SE) images, which show enhanced surface and topographic features. Scanning-cathodoluminescence images form by light emission in response to the interaction between the scanning electron beam and the sample. In this study, the backscatter technique mainly was used for imaging minerals.

Samples were analyzed with the University of Georgia JEOL 8600 electron microprobe using a 15 KeV accelerating voltage and 15 nA beam current. Mineral grains were qualitatively identified using a Noran Microtrace energy dispersive spectrometer (EDS) equipped with a SiLi detector and controlled by a PGT Avalon 4000 multichannel analyzer running eXcalibur software. Attempts were made to do some quantitative analyses that were performed with wavelength dispersive spectrometers (WDS) automated with Geller Microanalytical Laboratory's dQANT software, using natural and synthetic mineral standards. Analyses were calculated using Armstrong's (1988) Phi-Rho-Z matrix correction model. Backscattered electron imagery (BEI) was acquired using Geller Microanalytical Laboratory's dPICT imaging software.

Table 8 lists the standards that were used for the current study. Most of them come from the C. M. Taylor Corporation. The USNM standards come from the National Museum of Natural History, a branch of the Smithsonian Institution. This

study used two synthetic standards obtained from the University of Oregon microprobe lab, and an almandine standard obtained from the Harvard Mineral Museum. Calibration for each analytical session was checked using the Kakanui Hornblende (USNM) and Pryope #39 (C. M. Taylor) standards.

Table 8. Electron microprobe standards used in this study.

Electron Microprobe Standards			
Element	**Standard**	**Source**	**Comment**
Cr	Chromite #5	C M Taylor Corp	
Mn	Spessartine #4b	C M Taylor Corp	
TiO2	Rutile	C M Taylor Corp	
Ca	Sphene #1A	C M Taylor Corp	
Fe	Hematite #2	C M Taylor Corp	Used for oxide (spinel) analyses
Fe	Syn. Fayalite Ol-11	Univ. of Oregon	Used for silicate analyses
Ni	Ni metal	C M Taylor Corp	
Si	Diopside 5A	C M Taylor Corp	Si standard for all phases except garnet
Mg	Olivine #1	C M Taylor Corp	
Al	Syn. Spinel	C M Taylor Corp	
K	Orthoclase MAD-10	C M Taylor Corp	
Na	Ameila Albite	USNM	This is a ubiquitous Na standard
Si	Almandine	Harvard Mineral Museum oxygen standard # 112140	Si standard for garnet analyses
F	Syn. Fluoro-Phlogopite	University of Oregon M-6	
Cl	Scapolite	USNM R 6600-1	

6.4 RESULTS

Microprobe analyses were done on a total of 51 grains (17 garnets, 16 chrome spinel, and 18 tourmalines) in the University of Georgia Microprobe Lab with assistance from Mr. Chris Fleisher. Some previously generated data for garnet grains (6 garnets) were taken from Kumar (2004) and Zahid (2005) to maintain equal homogeneity among the stratigraphic units from both Assam and Bengal basins and because time did not permit analysis of more grains. Calculations of various weight percentages for analyzed garnet, chrome spinel, and tourmaline grains are presented in appendices A, B, and C, respectively.

6.4.1 Garnet

Garnets are rare to absent in Eocene and Oligocene sequences from both the Assam and the Bengal basins as reported by Kumar (2004) and Zahid (2005). Variations in different end components (pyrope, almandine, grossular, and spessartine) in garnets are plotted in figures 36, 37, 38, 39, and 40. Most of detrital garnets analyzed from various stratigraphic units within the Bengal and Assam basins are almandine rich (average 66%, maximum 80% from the Bengal Basin; average 60%, maximum 80% from the Assam Basin). Pyrope content is generally low (average 11%, maximum 33% from Bengal Basin; average 12%, maximum 41% from Assam Basin), and the grossular component is subordinate (average 16% and 18% from Bengal and Assam basins, respectively). The average spessartine component generally does not exceed 8% in samples from both basins.

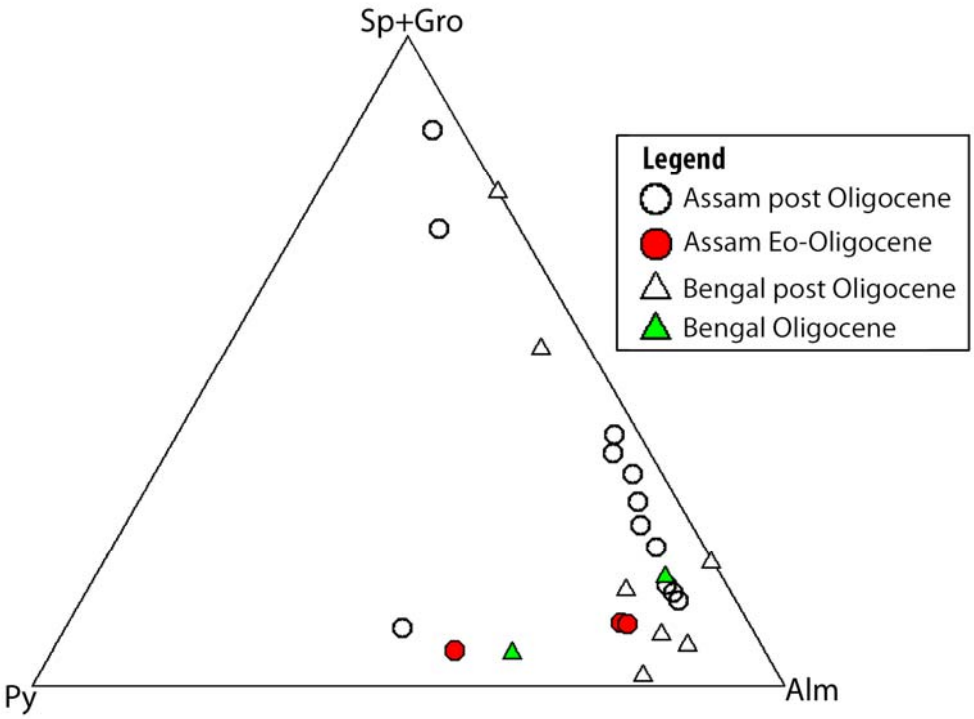

Figure 36. Chemical composition of garnets from Bengal Basin and Assam Basin sediments plotted on (Sp + Gro)- Py- Alm. Sp = spessartine; Gro = grossular; Alm = almandine; Py = pyrope (adapted after Nanayama, 1997). Most garnets plot closest to the Almandine pole.

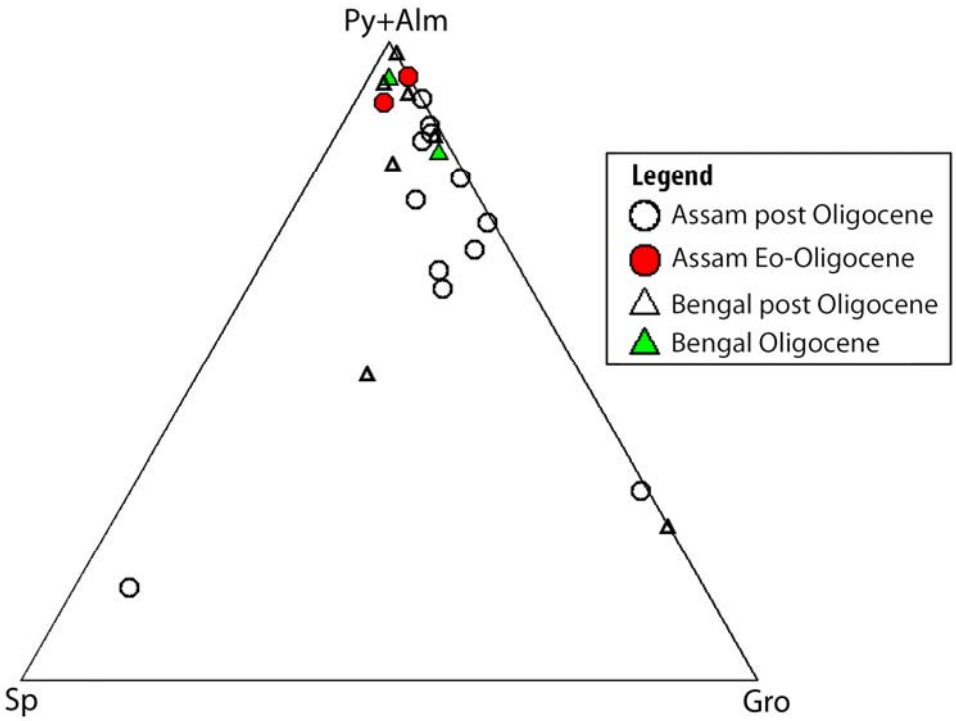

Figure 37. Chemical composition of garnet from Bengal Basin and Assam Basin sediments plotted on (Py + Alm)- Sp- Gro. Sp = spessartine; Gro = grossular; Alm = almandine; Py = pyrope (adapted after Nanayama, 1997).

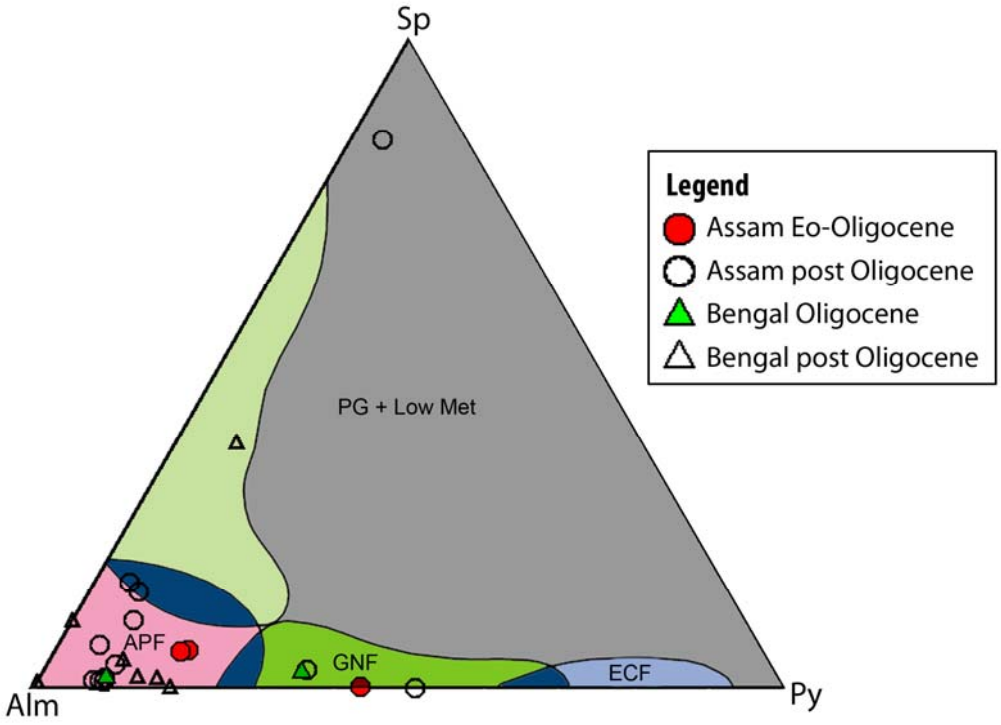

Figure 38. Chemical composition of garnets from Bengal Basin and Assam Basin sediments. Sp = spessartine; Alm = almandine; Py = pyrope; APF = amphibolite facies; GNF = granulite facies; ECF = eclogite facies; PG = pegmatite; Low Met = low metamorphic rock (adapted after Nanayama, 1997).

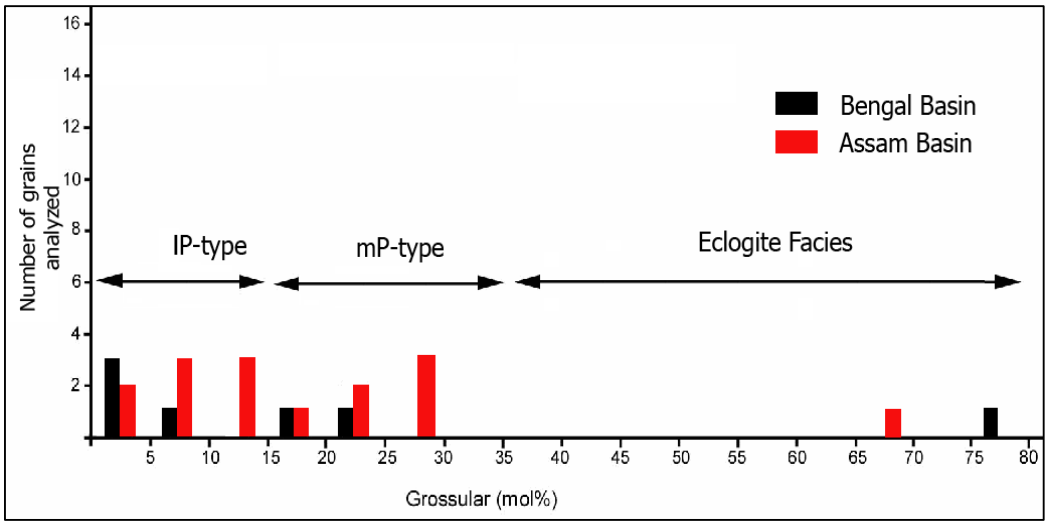

Figure 39. Grossular content (mol. %) of garnets from Bengal Basin and Assam Basin in relation to lP-type (low pressure), mP–type (medium pressure), and eclogite facies (adapted from Nanayama, 1997). Garnets from both basins are mostly of low- to medium-pressure type.

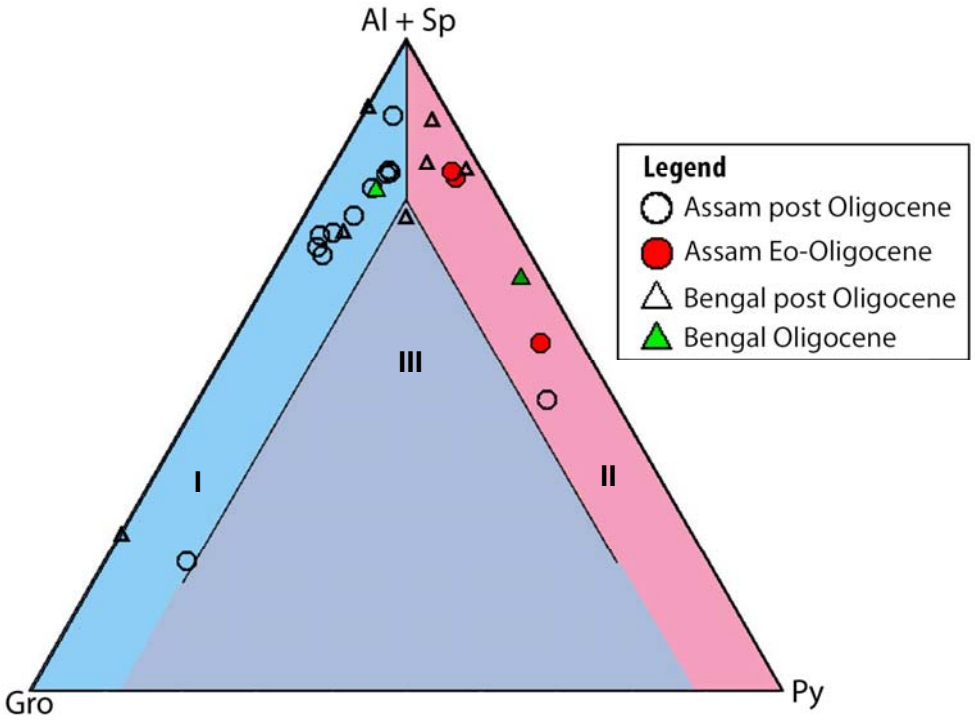

Figure 40. Chemical composition of garnets from Bengal and Assam basins sediments and relationships to three fields. I = garnets with almandine and grossular with < 10% pyrope; II = garnets with almandine and pyrope with < 10% grossular; and III = garnets with pyrope and grossular both with > 10% (Al-Almandine; Sp-Spessartine; Gr-Grossular; Py-Pyrope; adapted after Morton, 1992).

In the (Sp+Gro)-Py-Alm plot (Fig. 36), most of the garnet grains fall close to the almandine pole and show low pyrope contents. Two of the Mio-Pliocene (Tipam Group) garnets show high spessartine and grossular contents. All post-Oligocene garnets show a trend towards the Sp+ Gro apex. However, on the (Py+Alm)-Sp-Gro plot (Fig. 37), all the grains plot close to Py+Alm pole and along the Py+Alm–Gro line with one exception from the Mio-Pliocene Tipam Sandstone from Assam. This reflects very low spessartine content. Plotted on the Sp-Alm-Py ternary diagram (Fig. 38), grains plot close to the almandine pole with a few in granulite facies field (GNF).

The grossular content (mol. %) of garnet grains indicate that most of the garnets from both basins are derived from low- to medium-grade metamorphic pressure regimes. Only one sample from each basin has grossular contents indicative of eclogite metamorphic rocks (Fig. 39). Most garnet grains in the (Al+Sp)-Gro-Py ternary diagram (Morton, 1992) from both basins fall in the almandine-grossular and almandine-pyrope fields (Fig. 40). Eo-Oligocene garnets from the Assam Basin plot in the almandine-pyrope field. Some of the garnet grains of the various sequences of the Assam and Bengal basins are high in pyrope but low in grossular content, suggesting that they are derived from high-grade metamorphic facies. Others contain low pyrope, indicating low- to medium-grade metamorphic sources. Hence, there are at least two different provenances for the garnets for the both basins. One could be from granulite facies rocks and the other could be from low- to medium-grade regionally metamorphosed garnet-mica schists (Le Fort, 1996; DeCelles, et al., 2001) of the Himalayas and Indo-Burman Ranges.

6.4.2 Chrome Spinel

A total of 16 chrome spinels grains were analyzed from both Bengal and Assam basins. The elemental percentage of chromium in the spinels from both basins is high, ranging from 30% to 57% (average 46%) in the Bengal Basin and from 16% to 54% (average 42%) in the Assam Basin. Other trivalent cations that are very common in these spinels are Al and Fe^{3+} and divalent Mg and Fe^{2+}.

Several plots have been prepared to assess the provenance signature of the chrome spinels (Figs. 41-43). A ternary plot of Fe^{3+} -Cr^{3+}-Al^{3+} (Fig. 41) from both Assam and Bengal basins indicates Alpine-type peridotites (e.g., associated with ophiolites) and stratiform peridotite complexes (e.g., those associated with layered igneous complexes) (Dick and Bullen, 1984). Alpine-type peridotites consist of over 95% harzburgite and originate as depleted residues of partial melting. In these peridotites, Cr increases with increasing Fe^{3+}, but Fe^{3+} concentrations overall remain quite low. Spinels from stratiform complexes generally have much higher concentrations of Fe^{3+} than Alpine-type peridotites, and greater scatter of Fe^{3+} relative to Cr concentrations. Spinels analyzed for this study show an overlap between Alpine-type and stratiform complexes, although Alpine-type spinels predominate (Figs. 41, 42, and 43; Appendix B; Dick and Bullen, 1984).

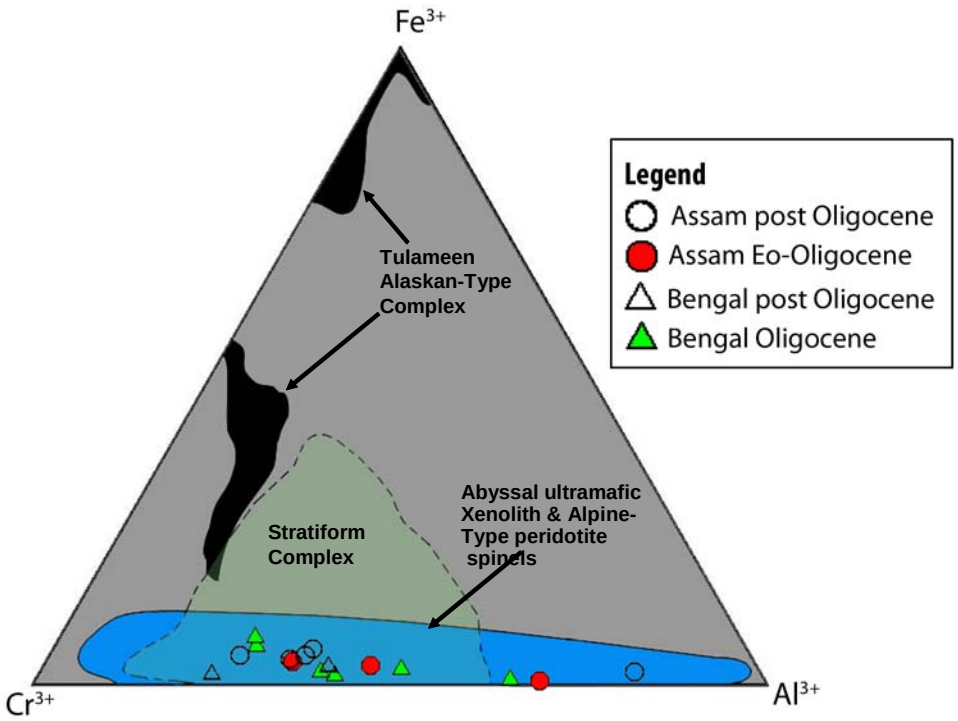

Figure 41. Ternary plot of major trivalent cations in chrome spinels of Bengal and Assam basins. Three major provenance fields have been drawn. Note that the abyssal ultramafic xenolith and Alpine-type peridotites overlap with stratiform complexes (after Nixon et al., 1990).

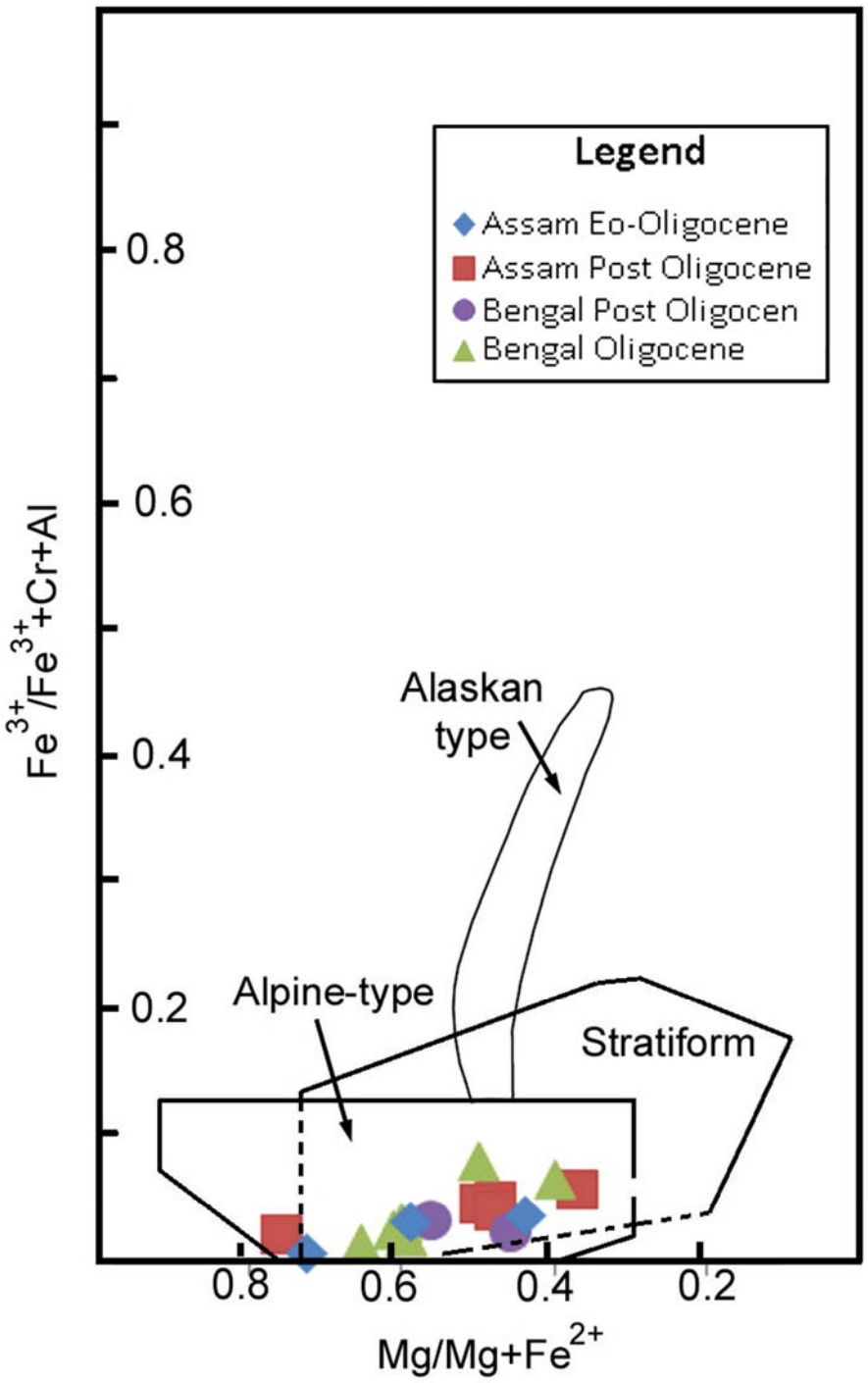

Figure 42. Plot of $Mg/(Mg+Fe^{2+})$ versus the ratio of trivalent cations $Fe3+/(Fe^{3+}+Al+Cr)$ for detrital spinels. Note the overlap in Alpine and stratiform peridotite fields (Irving, 1974).

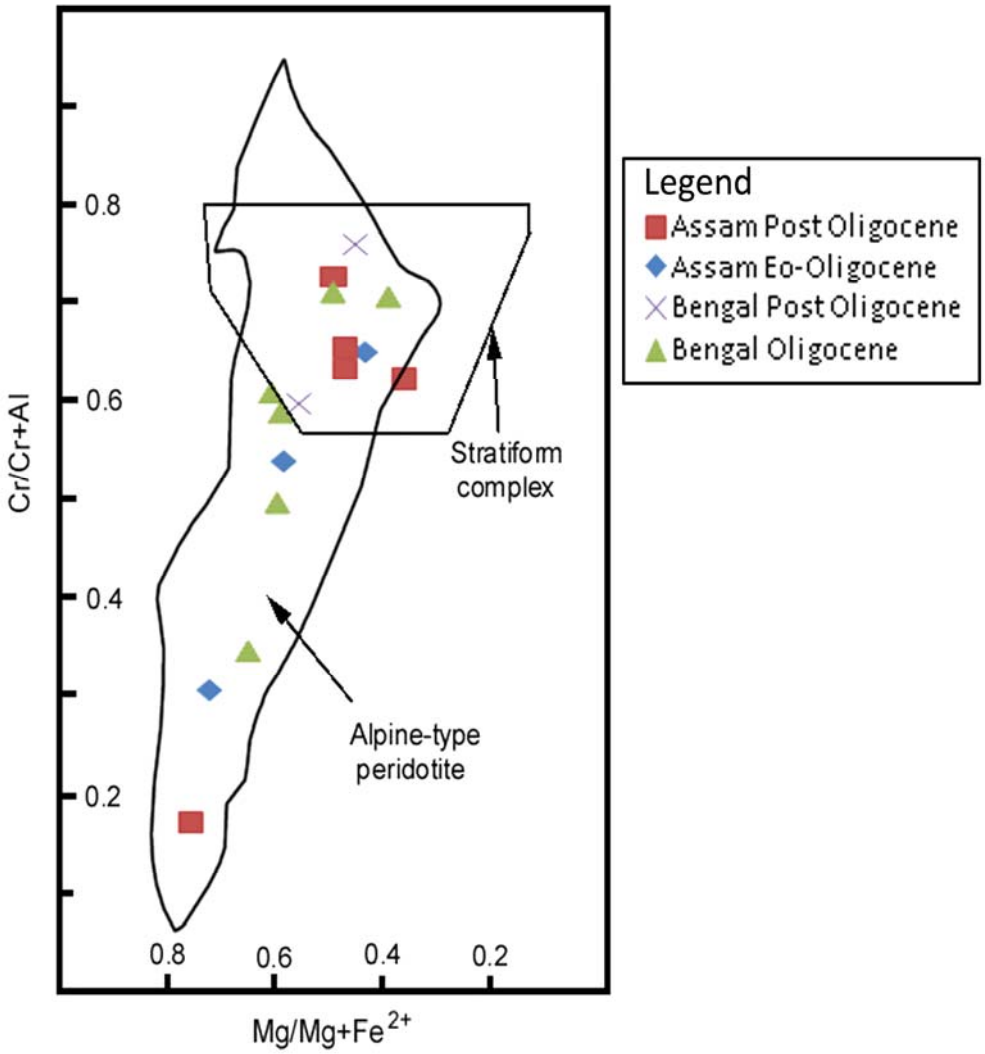

Figure 43. $Mg/(Mg+Fe^{2+})$ versus $Cr/(Cr+Al)$ for detrital chrome spinels. Note that, although some data points fall in the overlap between stratiform field complex (layers rich in chromite in a layered igneous complex) and Alpine-type peridotite (ophiolites), data on the whole reflect an Alpine-type peridotite provenance (after Dick and Bullen, 1984).

A plot of $Mg/(Mg+Fe^{2+})$ against $Fe^{3+}/(Fe^{3+}+Al+Cr)$ shows the importance of Fe-rich spinel in ultramafic bodies formed by fractional crystallization in the crust (Alaskan-type peridotites and stratiform complexes; Fig. 42). The data for this study plot entirely within the field of Alpine-type peridotites (Irving, 1974). The field for Alaskan-type complexes is entirely outside the range of sampled grains and can be excluded as a probable provenance. The stratiform field partly overlaps the Alpine-type peridotite field (Figs. 42 and 43). However, none of the grains show a high Fe^{3+} composition that would distinguish at least some stratiform complex chrome spinels. Based on co-interpretation of the $Mg/Mg+Fe^{2+}$ versus $Fe^{3+}/(Fe^{3+}+Al+Cr)$ and Cr-Al-Fe^{3+} plots (Figs. 42 and 43), the detrital chrome spinels from the Bengal and Assam basins likely were derived mainly from Alpine-type peridotites.

6.4.3 Tourmaline

Tourmaline is usually considered in terms of its common end-member components because there is a large potential for substitution. In most cases, natural tourmalines belong to two completely miscible solid-solution series: schorl-dravite and schorl-elbaite. There is a miscibility gap that exits between dravite and elbaite (Deer et al., 1992). Therefore, tourmalines are typically described in terms of their position in the schorl-elbaite series or in the schorl-dravite series.

Al-Fe(tot)-Mg and Ca-Fe(tot)-Mg plots for tourmalines from both basins are shown in figures 44 and 45. According to the Al-Fe(tot)-Mg plot (Fig. 44), most of the tourmalines were sourced from metapelites and metapsammites. Only a few grains from Oligocene samples from the Bengal Basin appear to have derived from Li-poor granitoid and associated pegmatites.

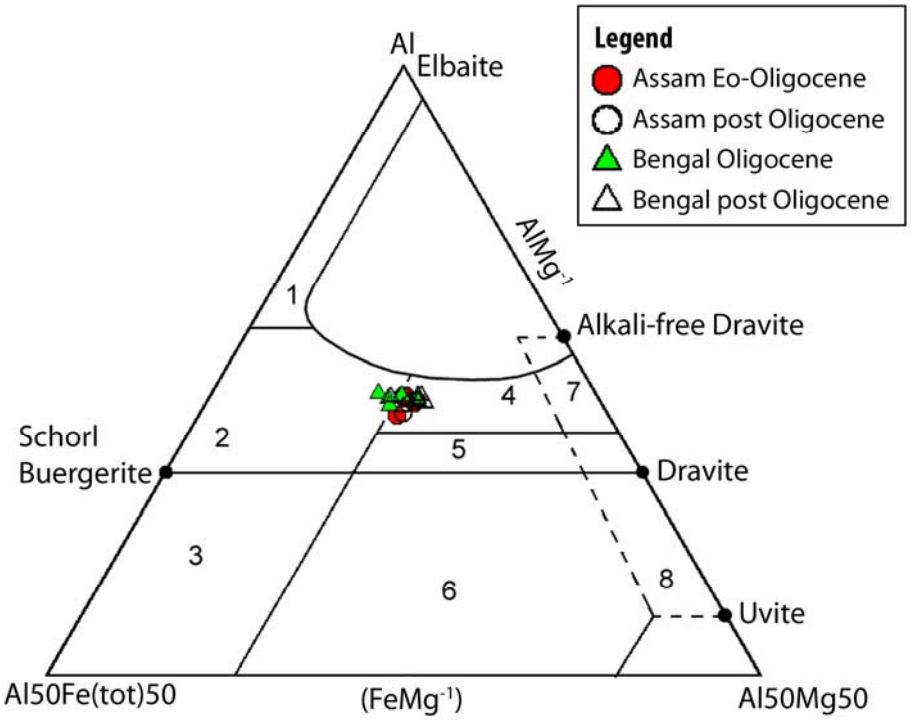

Figure 44. Al-Fe(tot)-Mg plot (in molecular proportion) for tourmalines from the Bengal and Assam basins. Fe(tot) represents the total iron in the tourmaline. Several end members are plotted for reference. Different rocks types are: (1) Li-rich granitoid pegmatites and aplites, (2) Li-poor granitoids and associated pegmatites and aplites, (3) Fe^{3+}-rich quartz-tourmaline rocks, (4) metapelites and metapsammites (aluminous), (5) metapelites and metapsammites (Al-poor), (6) Fe^{3+}-rich quartz-tourmaline rocks, calc-silicate rocks, and metapelites, (7) low-Ca metaultramafics and Cr, V-rich metasediments, and (8) metacarbonate and meta-pyroxinites (after Henry and Guidotti, 1985).

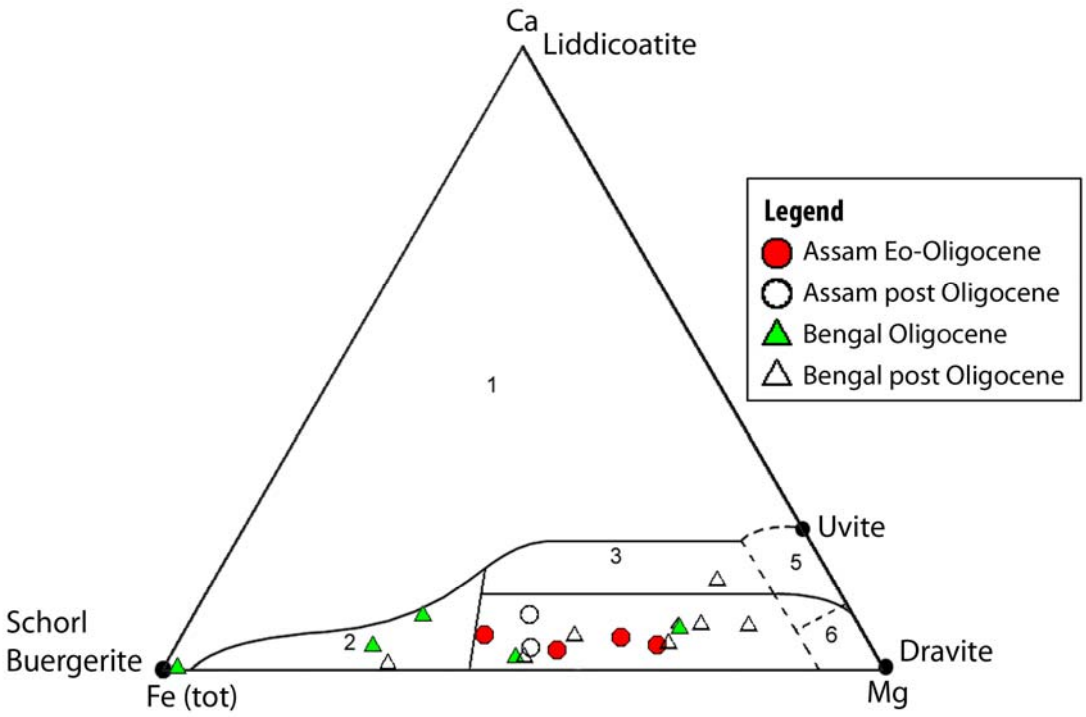

Figure 45. Ca-Fe(tot)-Mg plot (in molecular proportion) for tourmalines from the Bengal and Assam basins. Several end members are plotted for reference. Different rocks types are: (1) Li-rich granitiod pegmatites and aplites, (2) Li-poor granitoid and associated pegmatites and aplites, (3) Ca-rich metapelites, metapsammites, and calc-silicate rocks, (4) Ca-poor metapelites, metapsammites, and quartz-tourmaline rocks, (5) metacarbonates, and (6) meta-ultramafics (after Henry and Guidotti, 1985).

On the Ca- Fe(tot)-Mg plot (Fig. 45), tourmalines from the Bengal and Assam basins fall mostly in the fields for Ca-poor metapelites, metapsammites, and quartz-tourmaline rocks. A few tourmaline grains from the Oligocene of Bengal Basin fall in the Li-poor granitoid and associated pegmatite field. Hence, there are at least two distinct sources for the tourmalines, one of which could be recycled metasedimentary rocks from adjacent orogenic belts (Himalayas and the Indo-Burman Ranges), and the other one could be from plutonic rocks of the orogenic belts and the crystalline rocks of the Indian craton.

6.5 DISCUSSION

6.5.1 Garnets

Provenance has been constrained successfully using the compositions of detrital garnet populations. Since variations in garnet composition are dependent on paragenesis, they have proved very useful in identifying and characterizing different provenances (Morton, 1985). Garnets from Bengal and Assam basins have been classified into three groups (after Morton et al., 1992): (1) type-I garnet reflects a solid solution between almandine and grossular with <10% pyrope; (2) type-II garnets reflects a solid solution between almandine and pyrope with <10% grossular; and (3) type-III garnets are those wherein both pyrope and grossular are >10%. All but one of the garnets of Bengal and Assam basins are type-I and type-II grains. The majority of these garnets reflect derivation from low- to medium-grade metamorphic sources (Fig. 39). These garnets are rich in almandine, with some being rich in pyrope, but all of them are low in spessartine content. Almandine garnets could have derived from garnetiferous schists formed by regional metamorphism of argillaceous sediments.

These garnets probably derived from the Higher Himalayas to the north of Bengal Basin (Upreti, 1999) and the Indo-Burman Ranges to southeast of Assam Basin.

Further downstream, garnets in Bengal Fan sediments are mostly almandine-rich with very low pyrope content and likely were derived from the Himalayas to the north (Yokoyama et al., 1990).

6.5.2 Chrome Spinel

Chrome spinels have been widely used as provenance indicators for mafic and ultramafic rocks, especially of Alpine type peridotites (Press, 1986; Cookenboo et al., 1997; Zhu et al., 2005). The origin of Alpine-type peridotites can be constrained by Cr# and Mg#. Chrome spinels from peridotites and basalts of mid-ocean ridges have Cr# less then 0.06, and typically have high Mg# (0.7 to 8.5; Dick and Bullen, 1984). In contrast, spinels derived from back-arc basin basalts usually have lower Mg# for a given Cr#, and associated island-arc spinels show Cr# in excess of 0.60 (Dick and Bullen, 1984). A plot of Cr# versus TiO_2 % (Fig. 46) indicates that some spinels are from mid-oceanic and island arc basaltic sources. The detrital spinels of this study show a much greater range of Cr# compositions than oceanic spinels (Fig. 46).

Peridotites from ophiolite complexes are classified as Type I if their spinel populations are similar chemically to spinels from mid-oceanic ridge basalts. They are referred to as Type III if the spinel populations are largely similar in chemistry to the spinels from arc-settings and oceanic plateaus (Dick and Bullen, 1984). Ophiolites with spinels showing the range of compositions as found in Type I and Type III ophiolites are classified as transitional or Type II (Dick and Bullen, 1984).

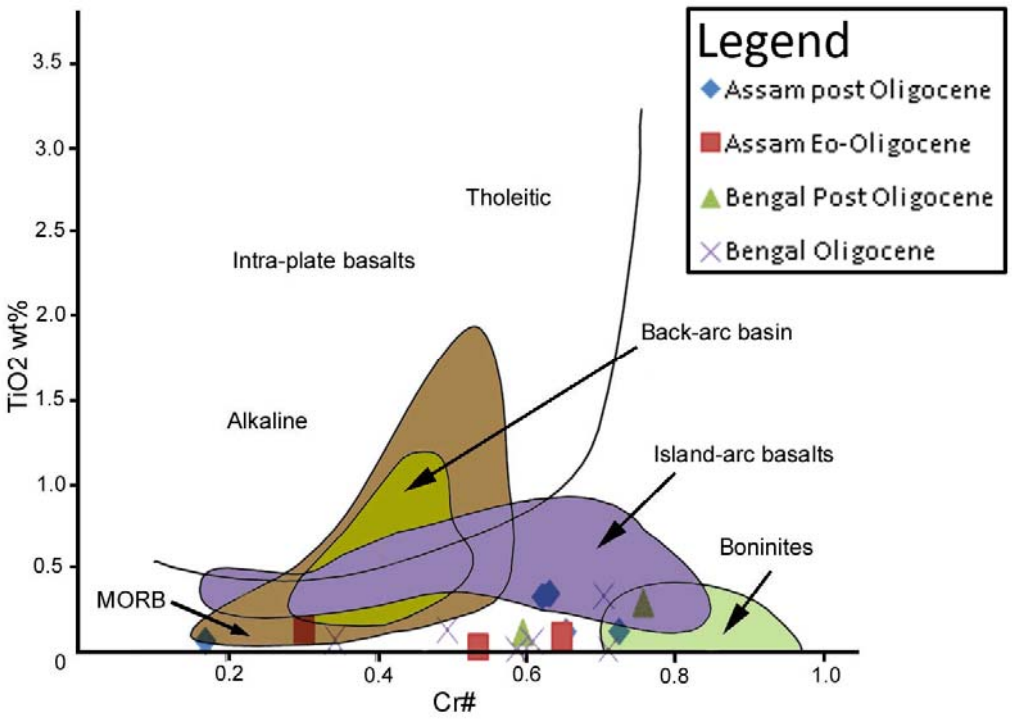

Figure 46. Plot of TiO_2 versus Cr# in Bengal and Assam basin detrital spinel relative to spinels from various potential source rocks. MORB = Mid-oceanic ridge basalt (after Arai, 1992).

The composition of spinels from Bengal and Assam basins may be a mixture of mid-ocean ridge-derived basalts (type I) with more depleted marginal-basin and island-arc suites (type III; Figs. 46 and 47). Spinels with high Al (Cr # = 0.10-0.30) and high Mg (Mg # 0.70-0.85) content are common constituents of abyssal peridotites, dunites, and basalts (Dick and Bullen, 1984). Most chrome spinels show low Al but high Cr content (Cr# 0.35 to 0.78). The lack of both high-Al and high-Mg spinels, which are indicative of mid-ocean-ridge origin, strongly suggests that with few exceptions, the detrital chrome spinels from the study area did not originate from a mid-ocean-ridge source.

Spinels from the Bengal and Assam basin likely were derived either from Himalayan arc material or ophiolites (Type III ophiolites or associated rocks with depleted mantle composition of Type II ophiolite), the continental flood basalt of the Rajmahal Traps, and/or the Indo-Burmese ophiolites (Type III or Type II setting). Based on tectonic location of the Bengal and Assam basins, paleogeographic considerations, and provenance work on chrome spinels from the Tianba Formation of the northern zone of Tethyan Himalayas (Zhu et al., 2005), the Rajmahal Trap (Fig. 3) and the Indo-Burman Ranges are more logical sources of spinels in the Bengal Basin. In contrast, chrome spinel in the Assam Basin could have been derived from Alpine-type ophiolites present in the Indo-Burman Ranges or in the Himalayas. Detailed tectonic reconstructions of the Assam Basin area suggest that the thrust slices of the Schuppen belt have traveled ~300 km to the northwest during Oligocene–Pliocene time (Rangarao, 1983). The ophiolites in the Indo-Burman Ranges consist of podiform chromite, cumulates, and harzburgite (Venkataraman et al., 1986). The spinels from the Assam and Bengal basins are mostly type I and II, suggesting derivation from Indo-Burman Range ophiolites.

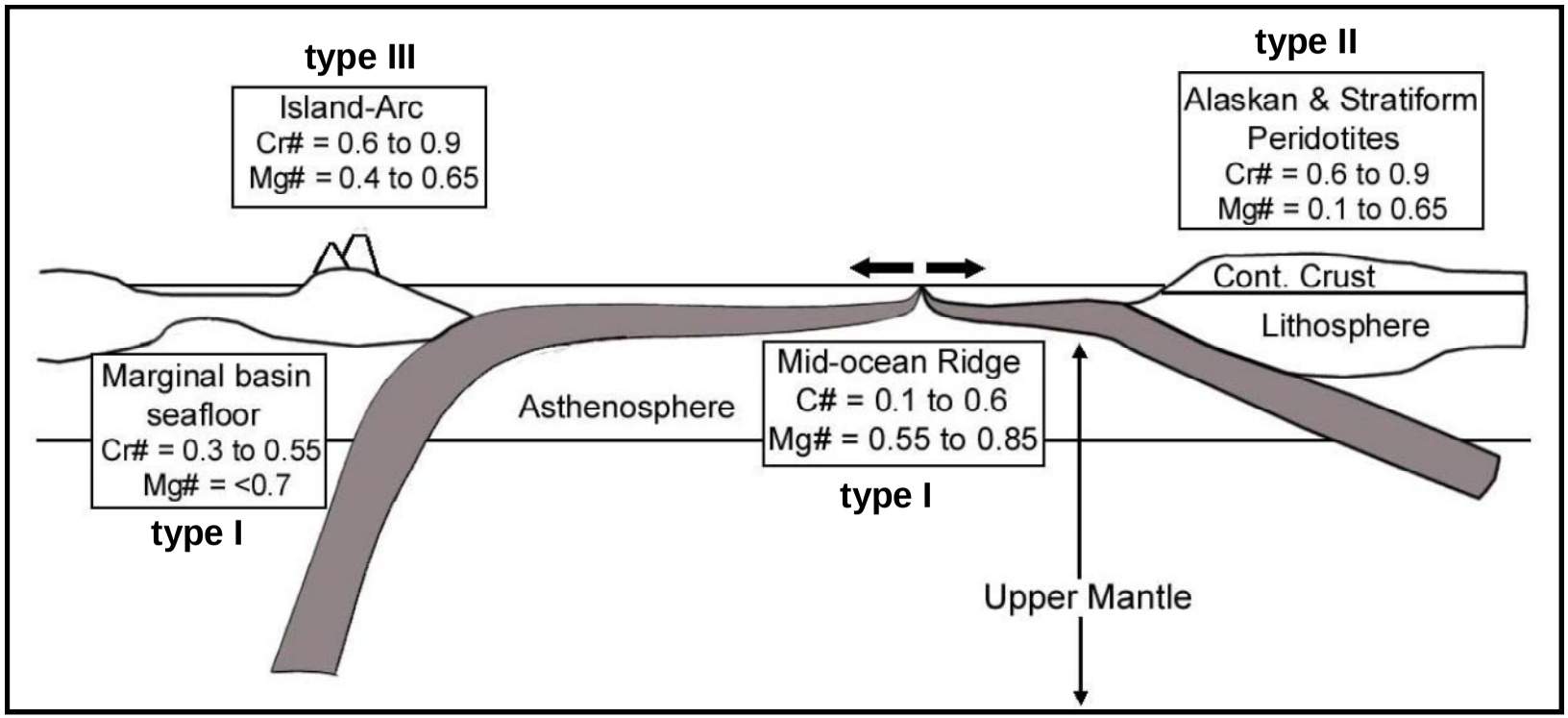

Figure 47. Schematic diagram (not to scale) showing spinel composition from different tectonic settings including those of sea-floor and continental crust origins (modified from Cookenboo et al., 1997).

Based on low Al and low Mg (Mg# 0.30 to 0.76) contents, the sources of the spinels of the Assam Basin were from the east, probably the ophiolites of the Indo-Burman Ranges. The chrome spinels from the Oligocene of Bengal Basin may have been derived from both Alpine-type ophiolites present in the Indo-Burman ranges and the Rajmahal Trap.

6.5.3 Tourmaline

Microprobe data show that tourmalines from the Assam and Bengal basins were derived from metapelites, metapsammites, and quartz-tourmaline rocks. Only a few grains correspond to the Li-poor granitoid and associated pegmatite occurrences (Figs. 44 and 45). Although there are at least two different sources for the tourmalines, it can be argued that the Assam and Bengal basins sediments have a predominant metasedimentary provenance, with minor contributions from granitoid and pegmatitic rocks.

CHAPTER 7: WHOLE ROCK CHEMISTRY

7.1 INTRODUCTION

Major element geochemistry of sedimentary rocks has implications for understanding the earth and the processes that shape it. Among other things, is has been used to discriminate tectonic settings of sandstones. The composition of sediments preserves a record of their provenance (Bhatia, 1983; Roser and Korsch, 1988; McLennan et al., 1993; Wanus and Abdel-Maguid, 2006). Geochemical analysis of sedimentary rocks is a valuable tool for identifying the tectonic settings of matrix-rich sandstones that have not been strongly affected by diagenesis, metamorphism, or other processes (McLennan et al., 1993). The use of geochemistry for provenance discrimination is now becoming more commonplace (Bhatia, 1983; Bhatia and Crook, 1986; Roser and Korsch, 1988; Taylor and McLennan, 1995; Wanus and Abdel-Maguid, 2006). Changes in the chemical composition of sediments also may be potentially useful for evaluating paleoclimatic conditions and maturity of the sediments (Nesbitt and Young, 1984; McLennan et al., 1993; Taylor and McLennan, 1995; Rieu et al., 2007).

7.2 METHODS

A total of 21 samples were selected from different Tertiary stratigraphic units in both the Bengal and Assam basins. Samples were dried in an oven at 50°C for approximately 24 hours. Approximately 20 gm of dried sediment for each sample was crushed with a mortar and pestle. Five grams of powdered sediment for each sample was sent to the ACME Laboratories Ltd., Vancouver, BC, Canada, for analysis. In the lab, a split of 1.0 gm for each sample was leached in hot (95°C) Aqua Regia (HNO3 + HCL of 1:3). Compositions of sandstone samples were analyzed by Inductively Coupled Plasma-Mass Spectrometry (ICP-MS) and Inductively Coupled Plasma-Emission Spectrometry (ICP-ES) methods. Geochemical analysis includes the following 11 oxides (SiO_2, Al_2O_3, Fe_2O_3, MgO, CaO, Na_2O, K_2O, TiO_2, P_2O_5, MnO, and Cr_2O_3) and 7 trace elements (Ba, Ni, Sr, Zr, Y, Nb, and Sc).

7.3 RESULTS

Major element and trace element data set are presented in appendix D. Silica is abundant in all samples, ranging from 61-88% in the samples from both Bengal and Assam basins (Figs. 48-49). Oligocene sandstones from the Bengal Basin have high silica contents. Chemical Index Alteration (CIA = $[(Al_2O_3/(Al_2O_3+K_2O+Na_2O+CaO)]*100$) is high for most samples, but is highest for the Oligocene samples from the Bengal Basin (Appendix D). Al_2O_3 is the second highest abundant major element in both Bengal and Assam basins. Several diagrams, including a ternary plot, were prepared to interpret the whole rock chemistry data of the samples for this study (Figs. 50-52).

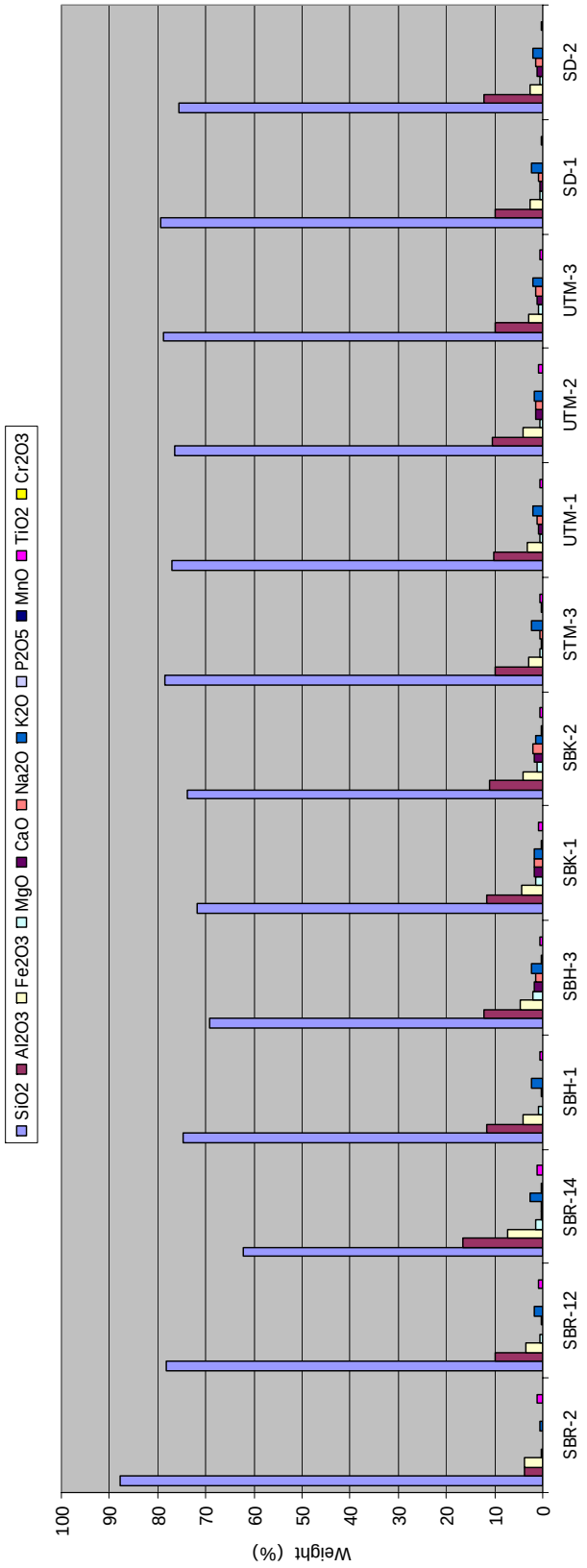

Figure 48. Weight percentages of major oxides from the Bengal Basin.

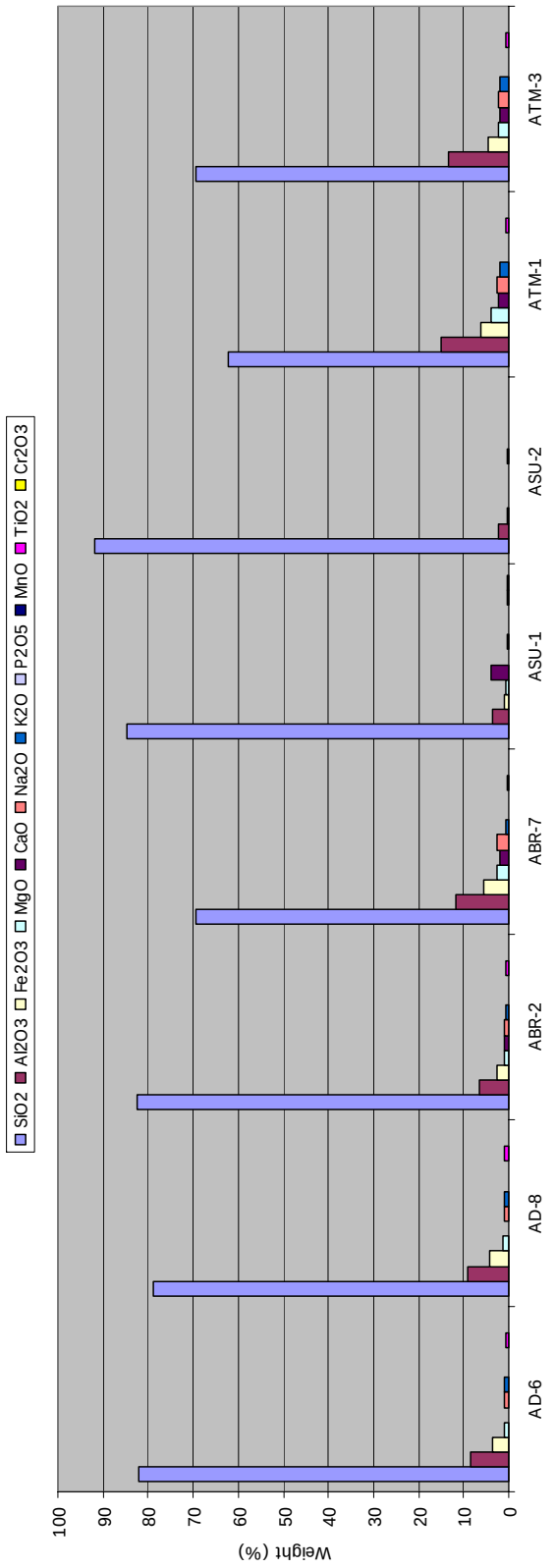

Figure 49. Weight percentages of major oxides from the Assam Basin.

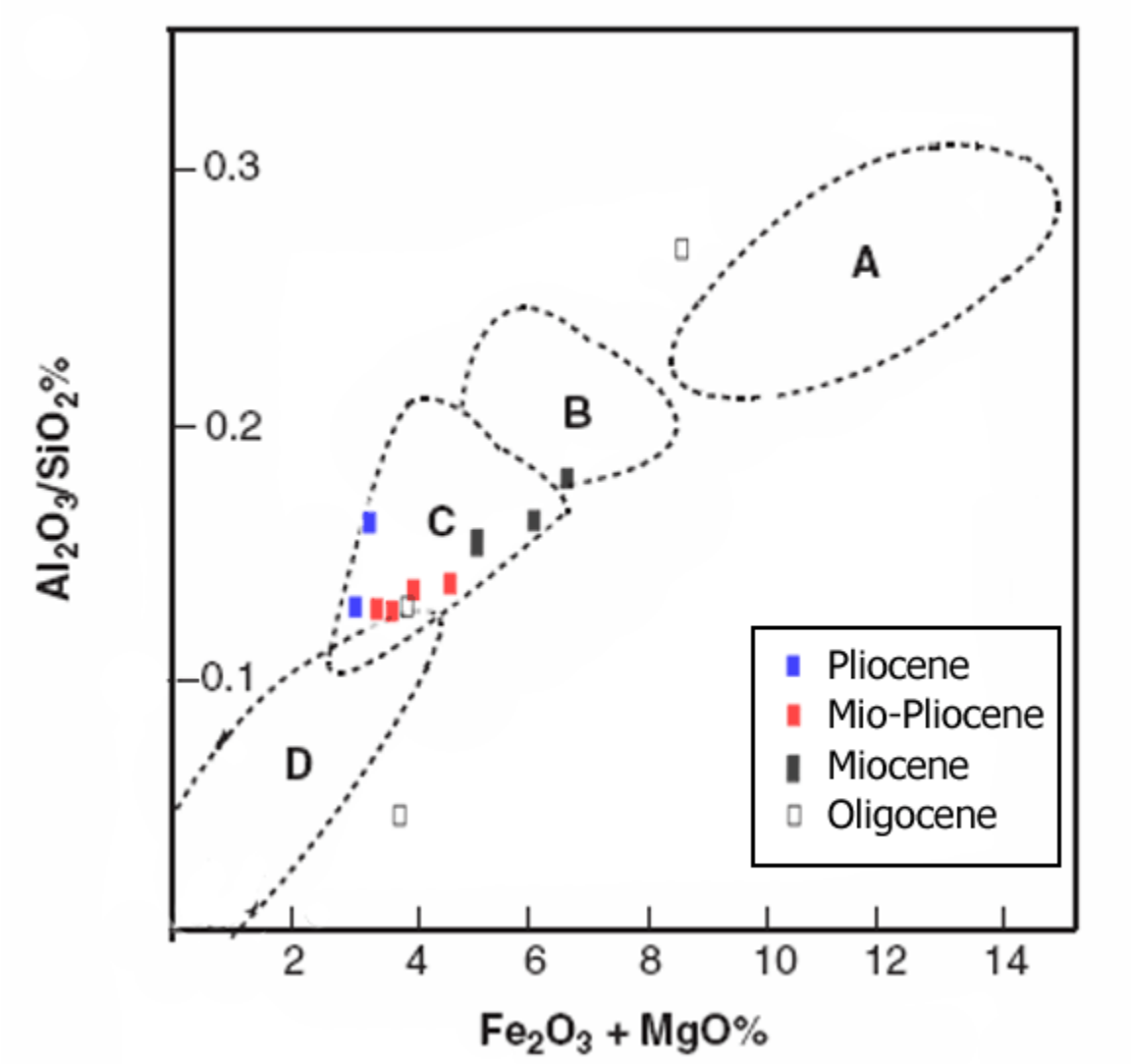

Figure 50. (Fe_2O_3+MgO) % versus Al_2O_3/SiO_2 % for sandstones of various stratigraphic units from Bengal Basin. (A) Oceanic island Arc, (B) Continental island Arc, (C) Active continental margin, and (D) Passive margin. Most samples from the Bengal Basin fall within the "active continental margin" field (adopted from Bhatia, 1983).

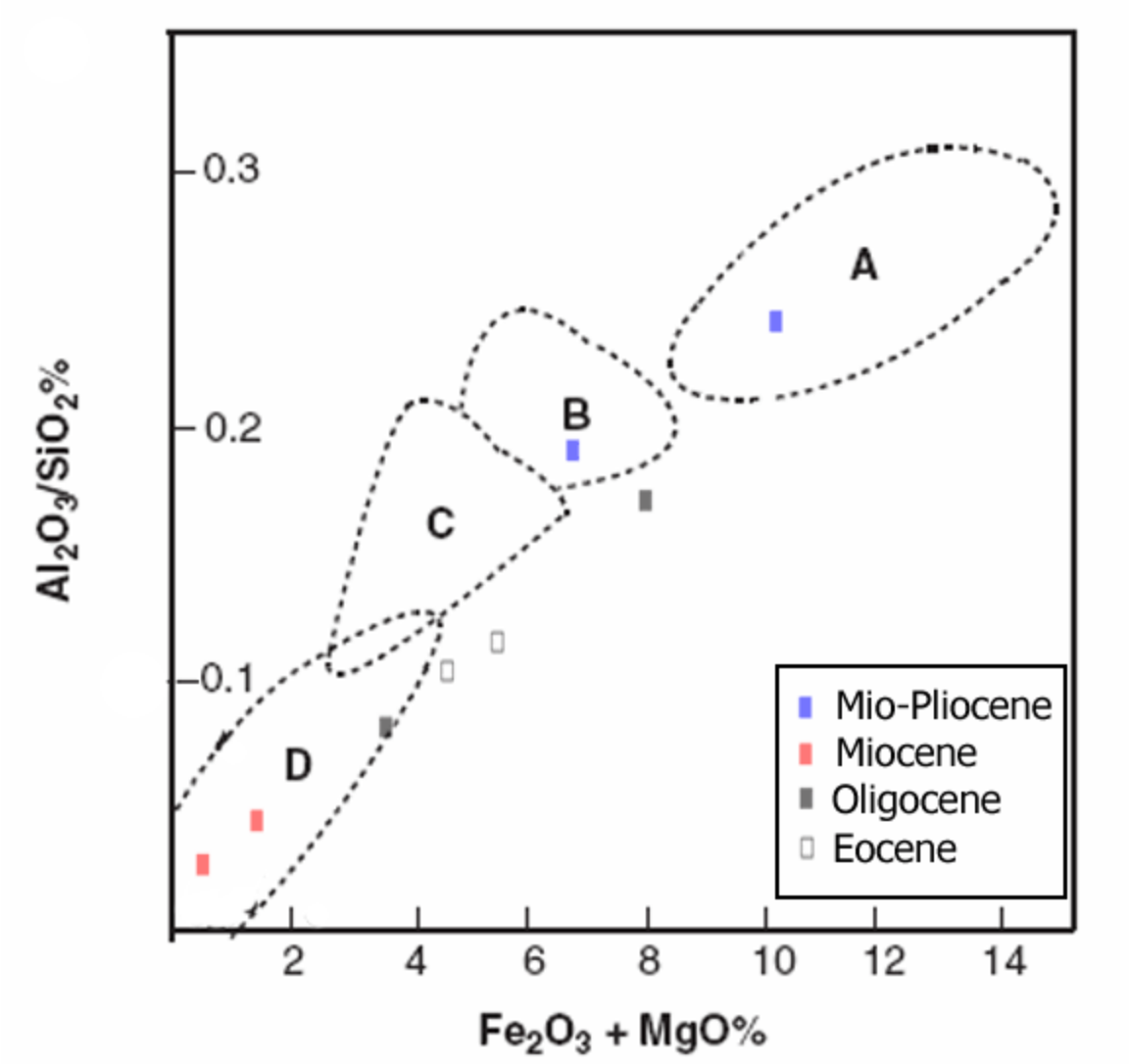

Figure 51. (Fe_2O_3+MgO) % versus Al_2O_3/SiO_2 % for sandstones of various stratigraphic units from Assam Basin. (A) Oceanic island Arc, (B) Continental island Arc, (C) Active continental margin, and (D) Passive margin. Data from Assam do not show an obvious pattern like the Bengal Basin. Samples plot in almost all tectonic fields, with some falling outside of designated tectonic boundaries (adopted from Bhatia, 1983).

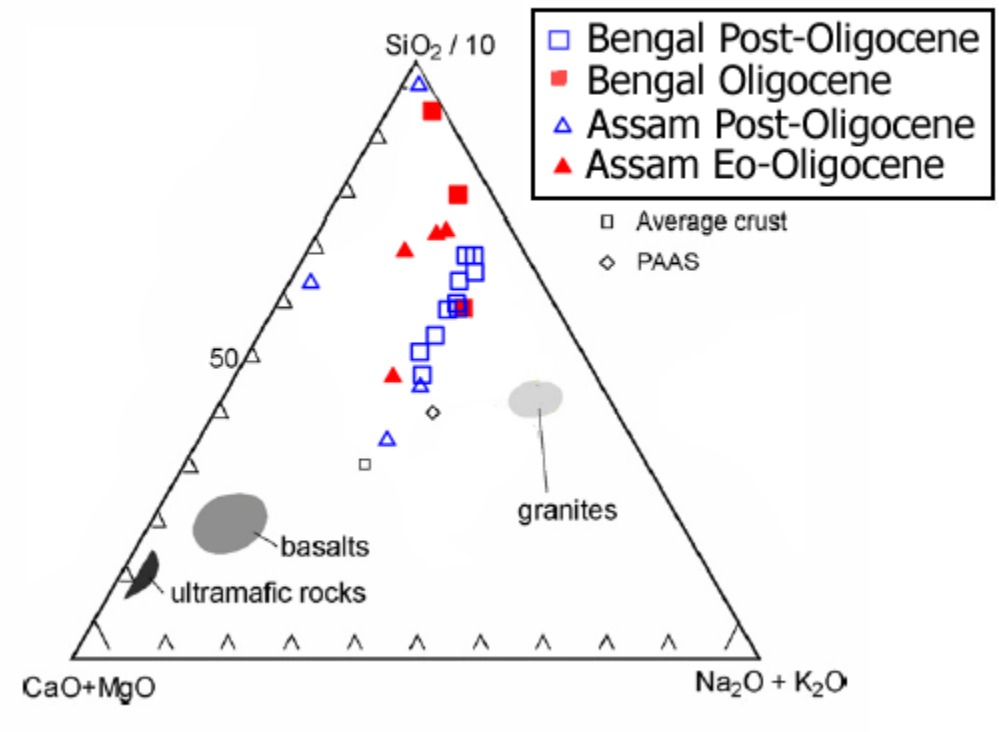

Figure 52. Possible source-rock affinities of sandstone samples from Bengal and Assam basins illustrated in a Si-Ca+Mg-Na+K triangular diagram (after Taylor and McLennan, 1985). Post-Archean Average Shale (PAAS) and average crust after Taylor and McLennan (1985). Studied samples are silica-rich and have closest affinities to granites compared to basalts and ultramafic rocks.

A plot of (Fe_2O_3+MgO) versus Al_2O_3/SiO_2 (Fig. 50) indicates that, after the Oligocene, sediments from the Bengal Basin were deposited in active continental margin settings. In contrast, the same plot for Assam Basin sediments indicates a range of tectonic settings (Fig. 51). A plot of Si-(Ca+Mg)-(Na+K) (Fig. 52) shows that almost all the sandstone samples from the Bengal and Assam basins are high in silica and plot closer to the granite field than to basaltic and ultramafic provenance fields.

7.4 PROVENANCE HISTORY

Major element chemistry of sandstones has been used to discriminate the tectonic settings and the provenance of the Assam and Bengal foreland basins. Results of whole-rock analysis suggest that the post-Oligocene sandstones in the Bengal Basin were deposited in active continental margin settings (Fig. 50). Based on sandstone composition, Uddin and Lundberg (1998a) suggested that the Bengal Basin was located close to the equator, where chemical weathering was intense, and received detritus most likely from the passive Indian craton margin. During the Miocene, however, the Bengal Basin was receiving orogenic detritus from the uplifted Himalayan and Indo-Burman Ranges at an active continental margin (Uddin and Lundberg, 1998a). Whole-rock chemistry data reveal that most sandstones from the Assam Basin and post-Oligocene samples from the Bengal Basin were derived from granitic source terranes. Higher CIA values for Oligocene samples from the Bengal Basin are suggestive of intense chemical weathering and consequent alteration of weaker minerals such as potassium feldspars. The Bengal Basin was further south, closer to the equator, at that time. The Assam Basin was very close to the Himalayan Mountains and the Indo-Burman Ranges, both of which

contain several granitic bodies. Other sources could be the Gangdese batholith in Tibet, Mishmi hills, Shillong Plateau, and the Mogok Metamorphic Belt (MMB) of Myanmar (Fig. 1; Rangarao, 1983; Khin, 1990; DeCelles et al., 1998; Mitchell et al., 2007).

CHAPTER 8: $^{40}Ar/^{39}Ar$ DETRITAL MUSCOVITE AGES

8.1 INTRODUCTION

Argon is a noble gas, which occurs naturally in the atmosphere, and potassium is a common a very element in many rock-forming minerals. Various isotopes of these elements are relevant to the K/Ar and $^{40}Ar/^{39}Ar$ radiometric dating techniques (Fig. 53). ^{40}Ar is a naturally occurring isotope and is produced by the radioactive-decay of ^{40}K, due to electron-capture and positron-emission pathways (Faure, 1986). ^{39}Ar originates by the decay of ^{39}K and ^{42}Ca; ^{38}Ar occurs naturally and forms by the radioactive decay of ^{38}Cl, ^{37}Ar forms by decay of ^{40}Ca, and ^{36}Ar occurs naturally and forms by the radioactive decay of ^{40}Ca (Dickin, 1995). The ratio of the naturally occurring $^{40}Ar/^{36}Ar$ in the atmosphere is 295.5, facilitating the correction for atmospheric ^{40}Ar (Faure, 1986). The age equation for $^{40}Ar/^{39}Ar$ dating (e.g., McDougall and Harrison, 1999) is as follows: $t = (1/\lambda)\ln(^{40}Ar^{*}/^{39}Ar_{K}(J)+1)$, where λ is the decay constant for $^{40}K \rightarrow ^{40}Ar$, which is $5.543*10^{-10}$/year. $^{40}Ar^{*}$ is the ^{40}Ar formed due to the radioactive decay in the phase of interest. $^{39}Ar_{K}$ is the ^{39}Ar formed artificially by bombardment with fast, high-energy neutrons in a nuclear reactor (Merrihue and Turner, 1966; McDougall and Harrison, 1999) and is used as a proxy for measurement of the parent potassium.

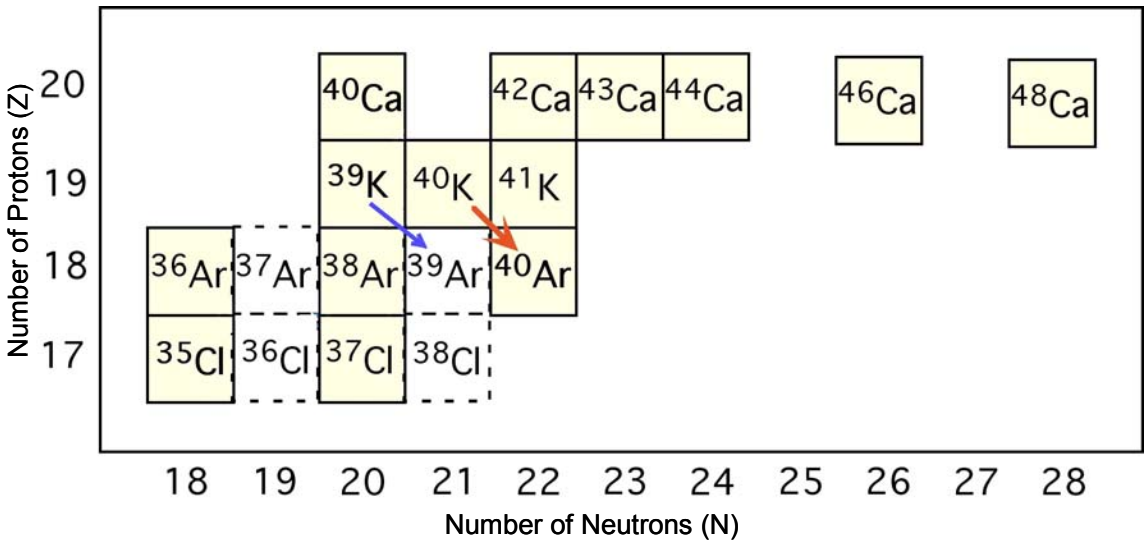

Figure 53. Decay scheme of isotopes relevant to the $^{40}Ar/^{39}Ar$ dating method. Yellow-filled boxes indicate naturally-occurring isotopes. Red arrow denotes the natural $^{40}K \rightarrow {}^{40}Ar^{*}$ decay reaction and the blue arrow indicates the $^{39}K(n,p)^{39}Ar_K$ reaction that occurs in a nuclear reactor.

If a grain of muscovite is weathered from uplifted bedrock, transported, and deposited in a sedimentary basin, the $^{40}Ar/^{39}Ar$ age of that grain should provide a measure of the time of cooling of its source through the closure temperature interval (typically 300-400°C; Hames and Bowring, 1994), provided that no additional radiogenic ^{40}Ar is lost during transport or after deposition (Hodges et al., 2005). The difference in age between isotopic closure and deposition reflects the time required to remove 10-20 km of sediment (range depends on geothermal gradient and uncertainty in the closer temperature). Sediment thickness and thermal gradients are moderate in eastern Himalayan basins, and $^{40}Ar/^{39}Ar$ studies in foreland basins deposits and distal Bengal fan have not been compromised by thermal resetting (Copeland and Harrison, 1990).

Detrital mineral populations from individual sedimentary samples typically show a range of $^{40}Ar/^{39}Ar$ mineral ages, reflecting mixed provenance with multiple age 'modes.' In such samples, the youngest mode has particular sedimentological significance: the difference between its age and the depositional age of the sample represents the maximum duration of the transport from source to depocenter. To the extent that rapid transport is related to high relief in the source region, this phenomenon may indicate that a well-developed Himalayan orogenic 'front' existed, and uplifted and unroofing ages may come close to be the depositional age of the clastic wedge (Hodges et al., 2005).

The Himalayan mountain chain is a relatively young geological feature. The Bengal and Assam foreland basins (Fig. 1) in the eastern part of the Himalayas represent one of the world's largest orogenic depositional systems. Although much of these orogenic wedges remain buried, marginal uplifts expose stratigraphic sequences that

provide information on Eocene through the Pleistocene depositional history. To understand the provenance of these huge sediment sequences in Himalayan foreland basins, muscovites from various stratigraphic horizons of the Assam Basin were analyzed for $^{40}Ar/^{39}Ar$ cooling ages. Data were then compared with regional detrital geochronological data to trace the source terranes that contributed clastic sediments to the Himalayan-Assam-Bengal system through time.

8.2 METHODS

Three sandstone samples from the exposed Naga-Disang thrust area of the upper Assam area were analyzed. Rock samples containing muscovite were prepared for laser analyses as follows: (1) samples were crushed, cleaned, and sieved; (2) uncontaminated muscovites were separated under a binocular microscope; and (3) grains were packed into an irradiation disc and sent to McMaster University Research Reactor in Hamilton, Ontario, Canada. $^{40}Ar/^{39}Ar$ isotopic analyses were performed at the Auburn Noble Isotope Mass Analysis Laboratory (ANIMAL) at Auburn University. ANIMAL is equipped with a low-volume, high-sensitivity, 10-cm radius sector mass spectrometer and automated sample extraction system (based on CO_2 laser) for analysis of single crystals. Analyses are typically made using a filament current of 2.240 A, and potentials for the source and multiplier of 2000 V and –1300 V, respectively. The high sensitivity and low blank of the instrument permits measurement of 10^{-14} mole samples to within 0.2% precision. The Fish Canyon sanidine (28.03 ± 0.09 Ma; Renne et al., 1998) was used as a flux monitor for this study. Approximately 50 irradiated muscovite grains from each sample were placed in a copper holding disc and analyzed by fusing single muscovite crystals with a CO_2 laser. The data were reduced using Isoplot 3 (Ludwig, 2003). All samples were corrected for background measurements of atmospheric argon contamination; ^{36}Cl, ^{37}Ar, and ^{39}Ar, K and Ca isotope fluctuation. Corrections also were made for irradiation gradient fluctuation; mass discrimination; and mass spectrometer sensitivity through blank and air corrections every five and ten samples, respectively.

8.3 $^{40}Ar/^{39}Ar$ RESULTS

Age population distributions were constructed through probability plots for each sample (Figs. 54). Data are provided in Appendix E. Oligocene samples from the Assam Basin (Fig. 54) show a polymodal distribution with one consistent peak muscovite cooling age of 75 Ma. Miocene samples show a distinct bimodal distribution of muscovite cooling ages (Fig. 54). The Miocene sample from the Assam Basin contains muscovite grains having cooling ages ranging from 28 Ma to 81 Ma, with two noticeable modes at 28 Ma to 50 Ma and 65 Ma to 80 Ma (Fig. 54). The younger Oligocene samples from the Assam Basin yield cooling ages ranging from 35 Ma to 197 Ma, with a strong mode at 70 Ma to 80 Ma, and 5 smaller peaks of higher ages. The older Oligocene samples from the Assam Basin show age distributions from 62 Ma to 205 Ma with a conspicuous peak at 76 Ma, and 6 other peaks of higher ages. The Oligocene and Miocene samples differ in age distribution, although both have conspicuous age modes between 65 Ma to 80 Ma.

8.4 PROVENANCE INTERPRETATION

Rocks of southern Tibet have yielded detrital ages ranging from Cretaceous to Tertiary in previous studies (Harrison et al., 1988; Copeland et al., 1995). The southern margin of Tibet was marked by an Andean-type arc, known as the Gangdese or Transhimalayan batholith, even before the early Tertiary onset of the collision between India and Asia (Copeland et al., 1995). Plutonic rocks of the Gangdese batholith, which include granite, granodiorite, and tonalite, have crystallization ages from ~120 to 40 Ma (Harris et al., 1988). The batholith also shows two distinct periods of plutonism centered

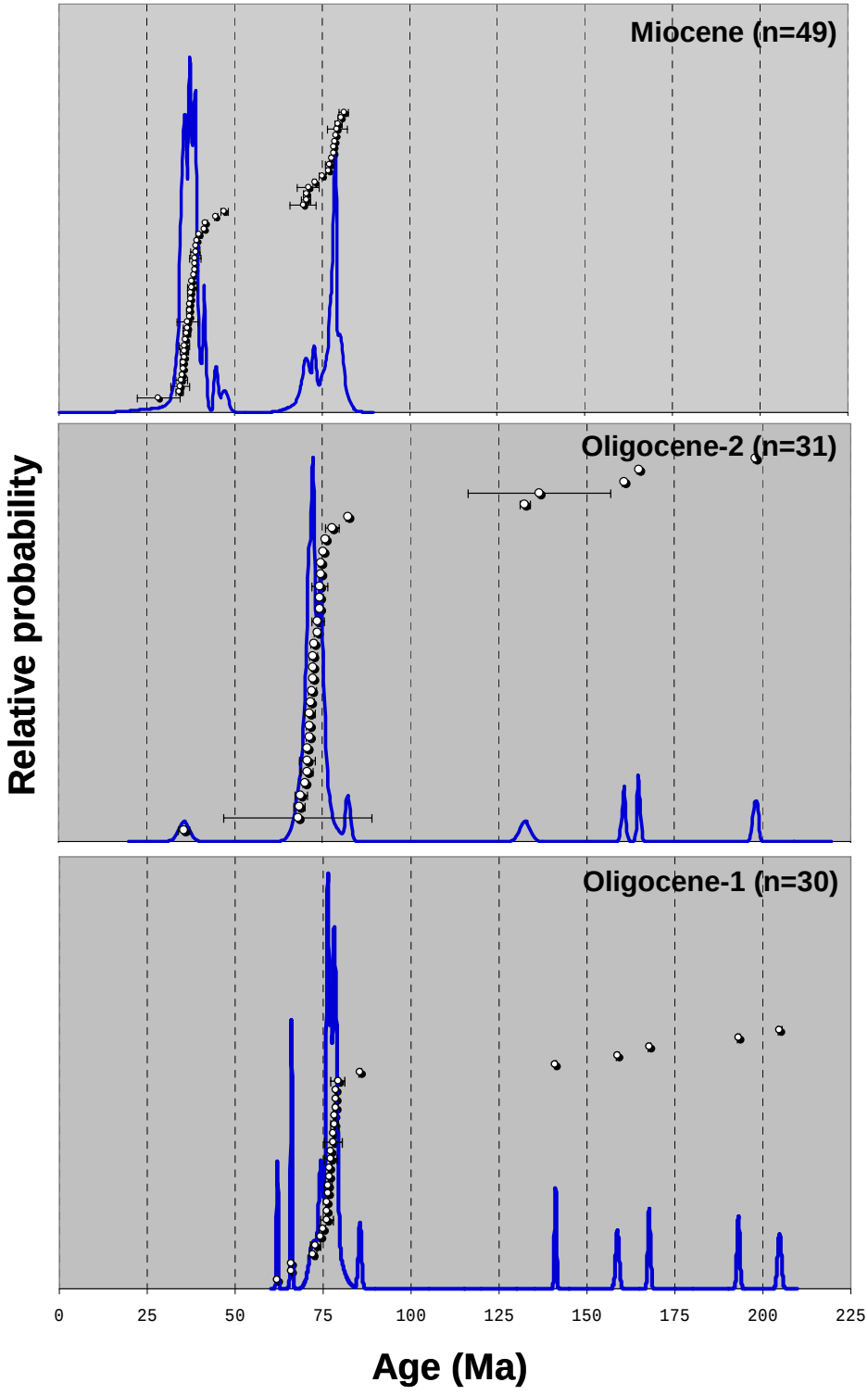

Figure 54. Probability plots for $^{40}Ar/^{39}Ar$ ages of single muscovite crystals from Assam Basin. Error bars represent one standard deviation.

broadly between 120 to 90 Ma and 70 to 40 Ma (Harris et al., 1988).Copeland and others (1995) found that cooling ages of the Gangdese batholith plutons in the vicinity of Lasha were younger than ~94 Ma and concentrated between 40 and 70 Ma. The Burmese Mogok Metamorphic Belt (MMB), which consists of regionally metamorphic rocks such as gneisses and schists, and granites, extends along the western margin of the Shan Plateau in the central Myanmar (Fig. 1). The MMB extends northward along the eastern Himalayan syntaxis. This belt also contains exposures of Paleozoic meta-sedimentary, early Mesozoic meta-igneous, and late Mesozoic intrusive rocks (Mitchell et al., 2007). Barley et al. (2003) reported SHRIMP zircon ages of 170 Ma from the deformed granite orthogneiss in this belt. Brook and Snelling (1976) reported K/Ar ages of 185 Ma on hornblende and 55 Ma on biotite crystals from the gneiss of the MMB. Najman et al. (1997)'s work on Oligocene and Miocene sequences in Western Himalayas reveal detrital average ages ranging from 28 Ma and 22 Ma. Rahman and Faupl (2005) studied Miocene samples from the Bengal basin that revealed an age range of 25 Ma to 35 Ma. Miocene samples from both north and southern Bengal Basin show a considerable range of muscovite cooling ages from 12 Ma to 516 Ma with conspicuous modes of 17 Ma and 26 Ma (Uddin et al., 2005; in pers. comm., 2008). Farther south, in the downstream sections in the Bengal Fan turbidites, Copeland and Harrison (1990) found an average age for muscovite grains of ca. 30 Ma (range from 23.4 to 88.2 Ma) in stratigraphic sequences of about 13 Ma. This study suggested rapid uplift and denudation in the Himalayas during the Neogene (Copeland and Harrison, 1990). The Main Central Thrust (MCT) was active by 24-21 Ma, as the MCT hanging wall was deforming at ~ 22 Ma (Hubbard and Harrison, 1995). Harrison et al. (1997), however, suggest a much later (late Miocene)

date of deformation. Monazite from graphite schists in the Lesser Himalayas reveals a range of early to middle Miocene ages (15.8-11 Ma; Catlos et al., 2001).

Muscovites from Oligocene strata from Assam yield a cooling ages that range from 35 to 204 Ma. Provenances of these muscovite grains are uncertain, but could include the Gangdese batholith and the MMB, both of which are located near the Assam Basin.

Muscovite cooling ages of 28 Ma to 50 Ma from Miocene sediments in Assam Basin suggest derivation from the Eocene-Oligocene 'Eohimalayan' metamorphic event (Hodges et al., 1994), Tibetan Plateau, and possibly the Indo-Burman Ranges. Based on Harris et al (1988)'s data from the Tibetan Plateau, Miocene muscovite grains from Assam yielding ages from 65 Ma to 80 Ma indicate derivation most likely from the Gangdese batholiths of southern Tibet. The study by Uddin et al. (2005) of muscovite grains (12 Ma to 516 Ma) from the Miocene sediments of the Bengal Basin indicates derivation from a combination of sources; from the Himalayas, Tibetan Plateau, and Indo-Burman Ranges.

Data from this study suggest that there have been two principal modes in detrital age dates, one in the Cretaceous and the other in Tertiary. Muscovite grains from both Assam and Bengal basins indicate similar source areas when major streams systems (i.e., paleo-Brahmaputra; Uddin and Lundberg, 1999) developed and drained from northeastern India through Assam and Bengal basins to the proto-Bay of Bengal. These $^{40}Ar/^{39}Ar$ ages from present study match closely with predominant Cretaceous U/Pb detrital zircon dates from same strata of the Assam Basin (Uddin et al., 2006) reinforcing the source terranes as the Gangdese batholith and the MMB.

CHAPTER 9: DISCUSSION

9.1 SYNTHESIS

Bengal and Assam basins are foreland basins south of the eastern Himalayas that hold 20+ km and 10+ km respectively of mostly orogenic sediments derived from the Himalayan and Indo-Burman orogenic belts. These two basins, separated by Precambrian massifs and the Kaladan fault, have experienced varied tectonic histories. Thick Cenozoic sedimentary deposits from these basins record critical information about tectonic events, paleogeography, and sedimentation history of this area. Detrital modal analyses of sandstones and heavy mineral assemblages, geochemical analysis of sandstones, and $^{40}Ar/^{39}Ar$ age dating of detrital muscovites in this study provide insights on the history of these basins.

9.2 BENGAL AND ASSAM SANDSTONES PROVENANCE

9.2.1 Bengal Basin

Sandstones from the Bengal Basin are mostly medium- to fine-grained and quartzolithic with low feldspar contents (Figs. 19, 20, 21, 22, and 23), although Oligocene sandstones are comparatively more quartz rich. All samples from Bengal Basin are dominated mostly by monocrystalline quartz grains. A few detrital chert and polycrystalline quartz grains are present. In the Bengal Basin, feldspars are rare but increase in abundance up-section. The abundance of quartz and scarcity of feldspar grains and lithic fragments in Oligocene sandstones indicate erosion from a low-relief

area under a strong chemical weathering regime. The dominance of monocrystalline quartz and paucity of metamorphic lithic fragments and feldspars suggest erosion from a craton rather than a collisional orogen (Uddin and Lundberg, 1998a). However, Oligocene sandstones from the Bengal Basin have a 'recycled orogenic' signature. Hence, the Indo-Burman Ranges orogenic belt may have contributed detritus to the basin during the Oligocene. Aitchison et al. (2007) suggested that the collision between the Indian plate and Eurasian plates may have initiated in early Eocene time approximately 55 Ma ago. Post-Oligocene sandstones from the Bengal Basin are much more feldspathic than those of the Oligocene Barail units. The increase in both feldspars and lithic fragments signals the initial input from an orogenic source to the Bengal Basin. Lithic fragments are most commonly sedimentary and low- to medium-grade metamorphic lithic fragments. The change in sandstone modes from the Oligocene to the post-Oligocene may record the commencement of uplift and erosion of Himalayas. The Indo-Burman Ranges also contributed sediments to the Bengal Basin during the post-Oligocene (Uddin and Lundberg, 1998a).

Heavy mineral assemblages in the Bengal Basin sediments are dominated by opaque and ultrastable minerals. Among the ultrastable minerals, rutile is more abundant than tourmaline and zircon in the Oligocene strata. Chrome spinels, rich in Cr and depleted in Al, are present in substantial amounts. The presence of abundant opaque minerals in the Oligocene units indicates input from a basaltic source, possibly the Rajmahal Trap located adjacent to the northwestern part of the basin. The presence of garnets, epidote, and aluminosilicates in all post-Oligocene sandstones in the Bengal Basin suggest input from the Himalayan and Indo-Burman Ranges (Uddin and Lundberg, 1998b; Kumar, 2004; Zahid, 2005).

9.2.2 Assam Basin

All sandstones from the Assam basin are quartzolithic in composition (Figs. 24, 25, 26, 27, and 28) and low in feldspar content. The Eocene Disang sandstones are mostly fine grained and rich in lithic fragments. Compared with the Oligocene sandstones from the Bengal Basin, the Oligocene Barail sands from Assam contain more lithic grains and fewer feldspar grains. The Disang sediments were deposited in deep-marine environments close to an arc-trench system during the Eocene (Rangarao, 1983; Kumar, 2004). Mafic rock fragments in Eocene sediments of the Assam Basin suggest an ophiolitic source. This source was the most likely from the Indo-Burman Ranges; ophiolite belts were obducted over the Burmese continent close to the Assam Basin during Cretaceous-Eocene time (Saikia, 1999). Depositional facies changed from deep marine to deltaic environments during the Oligocene when sediments of the Barail Group were deposited (Rangarao, 1983). Contribution from the ophiolite belt of the Indo-Burman Ranges is indicated by the presence of chert in the Oligocene sandstones from the Assam Basin. Miocene Sandstones of the Surma Group probably were derived from the eastern Himalayas and Indo-Burman Ranges (Kumar, 2004). The Mio-Pliocene Tipam Sandstone contains abundant plagioclase feldspar, which indicates a contribution from Higher Himalayan crystalline rocks and from the Indo-Burman Ranges (DeCelles et al., 1998; Mitchell et al., 2007). The heavy-mineral assemblage in the Eocene Oligocene Barail Group is dominated by mostly ultrastable grains such as zircon, tourmaline, and rutile (ZTR) with other grains such as chrome spinel, staurolite, apatite and opaque minerals suggesting an ophiolite source from the Indo-Burman Ranges. In contrast, Miocene and Mio-Pliocene sandstones of the Assam Basin contain more diverse heavy mineral suites.

This suggests derivation from a diverse suite of source rocks exposed to erosion in both the Himalayan and Indo-Burman Ranges.

9.3 MICROPROBE ANALYSIS

9.3.1 Garnet

Garnets are rare in the Eocene Disang Formation of Assam Basin and in the Oligocene Barail Group of both basins, but become very common in post-Oligocene sandstones. Detrital garnets analyzed from the Assam and Bengal basins sandstones are mostly almandine-rich. Pyrope content is usually low, whereas the grossular component is minor. With few exceptions, the spessartine content is very low for both the Bengal and Assam basins. All these garnets suggest derivation from a garnet-mica schist of a low- to medium-grade metamorphic facies. Consequently, garnets from both basins are thought to have derived from various regional metamorphic belts of the Himalayan and Indo-Burman Ranges (Upreti, 1999; Mitchell et al., 2007). The Indian continent could be a source of the Oligocene garnets from the Bengal Basin (Amano and Taira, 1992).

9.3.2 Chrome Spinel

Chrome spinels are very common in the Bengal and Assam basins sandstones. The chromium content of these spinels is high. Other important abundant cations include trivalent Al and Fe^{3+} and divalent Mg and Fe^{2+}. Spinels from the Bengal Basin may have derived either from continental flood basalts of Deccan and Rajmahal Traps, and/or the Indo-Burmese Ranges ophiolites. Chrome spinels from the Assam Basin may have been derived mostly from the ophiolite belts of the Indo-Burman Ranges. However, the Mg-Cr plot (Fig. 43) of spinels from the Bengal and Assam

basins suggests strong chemical similarity with alpine-type ophiolites of the closely located Indo-Burman Ranges. Low Al and Mg contents, together with the wide range in TiO_2 contents of Bengal and Assam chrome spinels, also suggest an Alpine-type ophiolitic source from the Indo-Burman Ranges.

9.3.3 Tourmaline

Al-Fe(tot)-Mg and Ca-Fe(tot)-Mg plots of tourmaline show that most of the grains were sourced from metapelites and metapsammites. Some were derived from Ca-poor metapelites, metapsammites, and quartz-tourmaline rocks. Others were derived from Li-poor granitoids and associated pegmatites. Hence, there are at least two distinct sources for the tourmalines; some tourmalines likely derived from recycled sedimentary rocks in an orogenic belt, while others may have sourced from plutonic rocks. Sediments from the Bengal and Assam basins apparently had a dominantly metasedimentary provenance, with minor contribution from granitic and pegmatitic rocks from the Himalayan and Indo-Burman Ranges.

9.4 WHOLE-ROCK CHEMISTRY

Whole-rock analysis of Bengal Basin sediments clearly documents that the post-Oligocene sandstones accumulated in ‘active continental margin’ tectonic settings. CIA (Chemical Index Alteration value; appendix C) derived from Oligocene sediments of the Bengal Basin suggest detrital grains went through intense chemical weathering, as consistent with the basin’s close proximity to the equator. CIA values strongly depend on the abundance of clay minerals. High CIA contents in Oligocene sediments from the Bengal Basin may be the result of chemical weathering of feldspars eroded from the Indian craton (Uddin and Lundberg, 1998a). Some of the

matrix-rich sandstones from the Bengal and Assam basins fall close to the granitic provenance field in the ternary plot proposed by Taylor and McLennan (1985), suggesting contribution of sediments from granitic source terranes in Tibet, the Himalayas, or the Indo-Burman Ranges.

9.5 $^{40}Ar/^{39}Ar$ MUSCOVITE DATING

Assam Oligocene $^{40}Ar/^{39}Ar$ muscovite cooling ages range from 35 Ma to 205 Ma with strong modes at 70 Ma to 80 Ma. Copeland and others (1995) produced ages focusing on the low temperature (100-350°C) cooling history of the Gangdese batholiths and found ages generally from 70 to 40 Ma. The data of the present research are consistent with a source for the deepest sample (B 2) as the country rock to or an upper level of the Gangdese plutons, in which muscovite reached isotopic closure prior to those samples collected in surface exposures by Copeland and Harrison (1995). The Gangdese batholiths in the southern Tibetan Plateau and/or Mogok Metamorphic Belt of Indo-Burman Ranges are possible sources of muscovite grains found in the Oligocene strata of Assam that are older than ~ 100 Ma. Miocene muscovite grains from the Assam Basin (28 Ma to 81 Ma) may have been derived from several sources, including the Eohimalayan events (Hodges et al., 1994) of the eastern Himalayas, the Tibetan Plateau, and the Indo-Burman Ranges. Figure 55 shows muscovite cooling age distributions from Oligocene and Miocene strata of Assam and some previous published studies on regional detrital age. Laser $^{40}Ar/^{39}Ar$ dating of individual detrital muscovites from the Miocene sequences from the Bengal Basin yielded cooling ages between ca 12 Ma to 516 Ma, with conspicuous modes of 17 Ma and 26 Ma. This suggests a combination of sources (Uddin et al., 2005; in pers. comm., 2008).

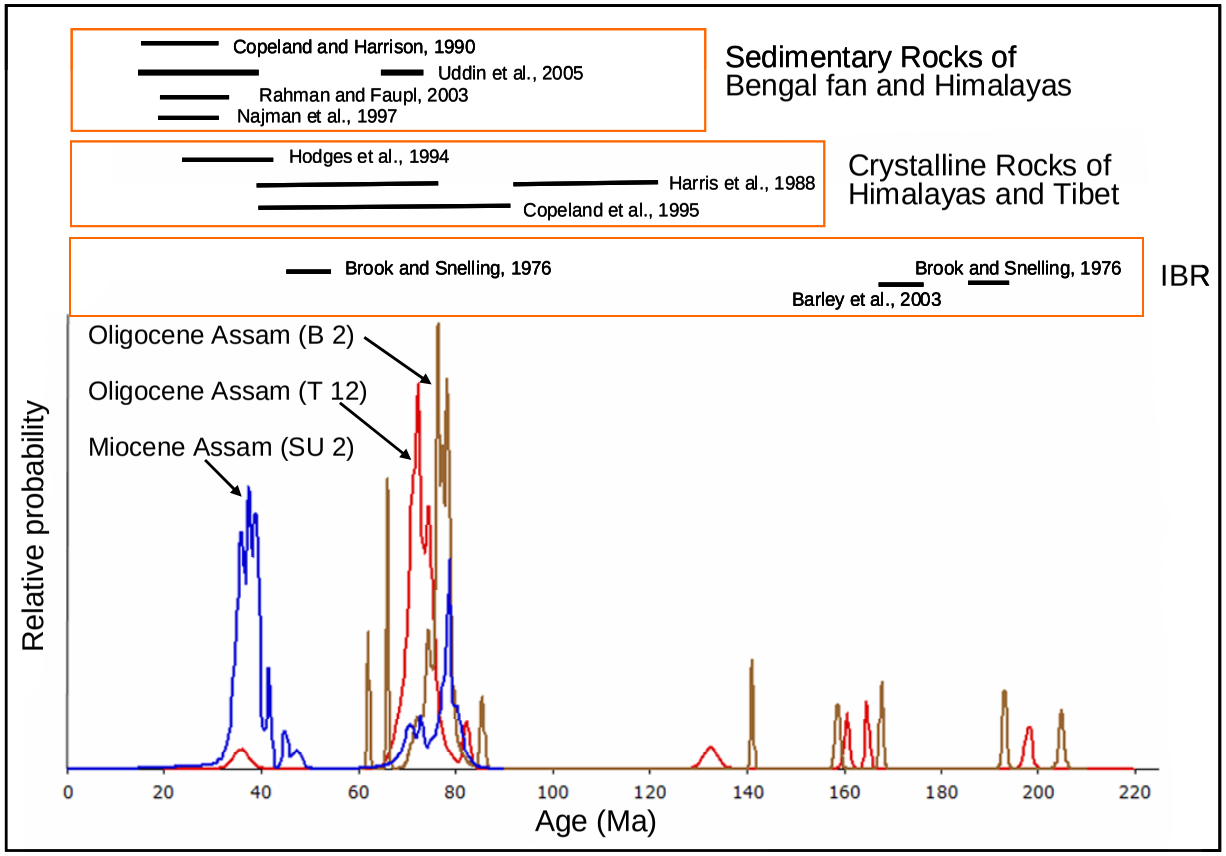

Figure 55. $^{40}Ar/^{39}Ar$ cooling ages of single crystal muscovite from Oligocene and Miocene sequences from the Assam Basin. Both Oligocene and Miocene muscovite dates suggest that there are two principal modes in detrital age dates, one in the Cretaceous and the other in Tertiary. The data are compared with regional studies as cited (IBR: Indo-Burman Ranges).

9.6 PALEOTECTONIC SETTING

Detrital modal analyses of sandstones show variations in provenance history for the Bengal and Assam foreland basins in the eastern Himalayas. Almost all the sand(stone) samples from these two basin are quartzolithic. Only Oligocene sands of the Barail Group are mostly quartzose and contain low lithic fragments with rare to no feldspar. The abundance of quartz and paucity of lithic fragments and feldspars suggest that the nearby Indian Craton was the principal source of sediments. High ZTR indices and dominance of opaque minerals also support this interpretation. During the Eocene-Oligocene, the Bengal Basin was probably located far south from it present location at the continental margin of the Indian plate. In contrast, the location of the Assam Basin during the Eocene-Oligocene was probably similar to that of post-Oligocene time (Fig 56A). The more distal paleogeographic location of the Bengal Basin during the Oligocene probably did not allow Himalayan sediments to reach the basin. The Bengal Basin most likely was closer to the Indo-Burman Ranges, which contributed recycled sediments. Whole-rock chemical analyses of sandstones from the Bengal Basin also show that Oligocene sediments of the Bengal Basin experienced intense chemical weathering associated with close proximity to the equator.

Post-Oligocene sandstones from Bengal Basin record different signatures to that of the Oligocene (Fig. 56B). They are more quartzolithic and contain more lithic fragments and feldspars than the Oligocene strata. They are more similar to the Assam sandstones. By the Miocene, the Indian continent had collided with the Eurasian plate and, hence, the influx of clastic sediments into the basin from the north and the east increased markedly at this time. Hence, the Bengal Basin had moved closer to the Himalayan and the Indo-

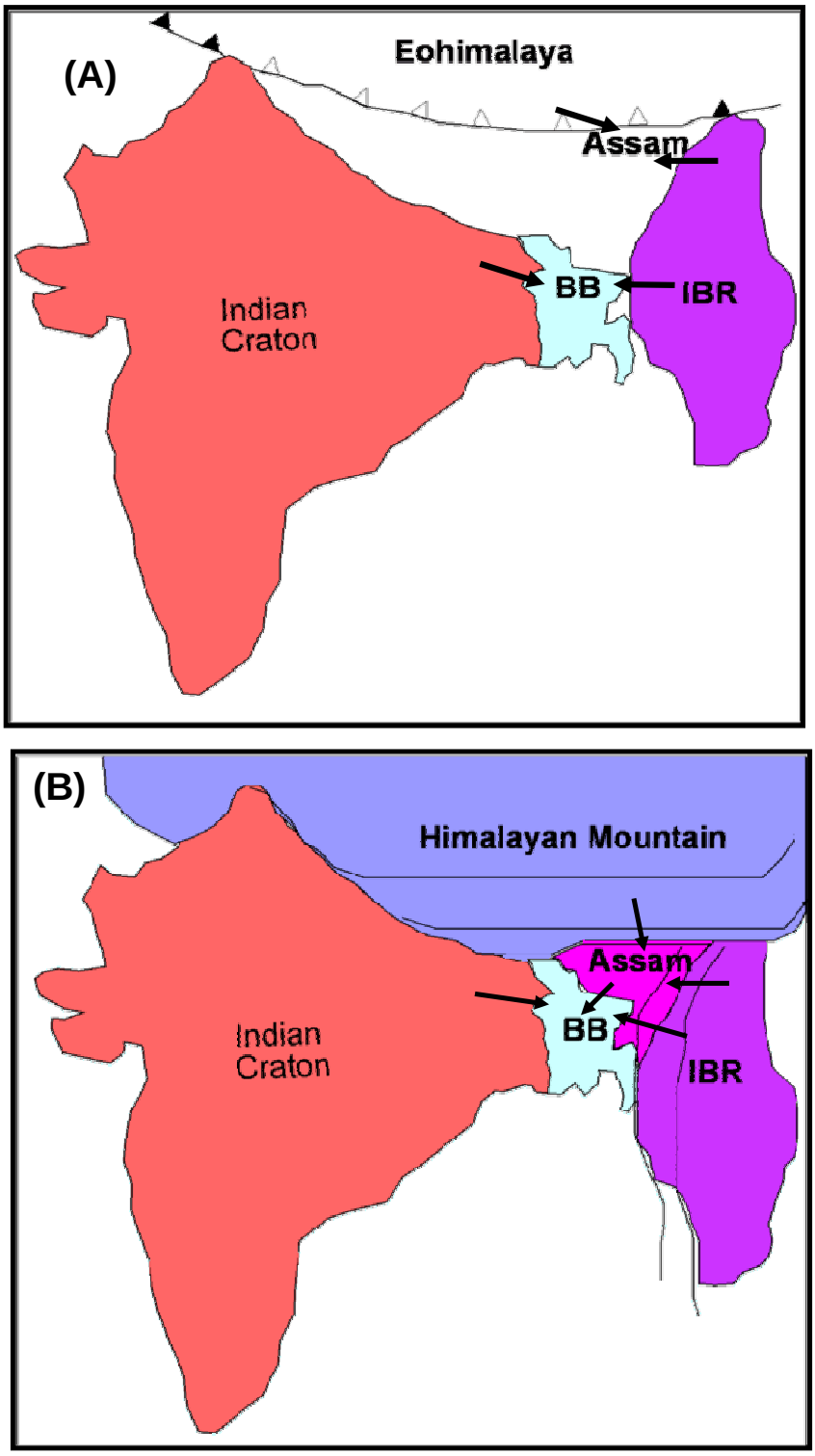

Figure 56. Paleotectonic setting of Bengal and Assam basins during (A) Eocene-Oligocene time, and (B) Post-Oligocene time (after Rangarao, 1983; Uddin and Lundberg, 1998a). BB: Bengal Basin, IBR: Indo-Burman Ranges, and arrows are indicating sediment contribution from the source areas.

Burman Ranges. Contribution of sediments from the Himalayan and Indo-Burman Ranges into the Assam Basin remained consistent since the Eocene.

The locus of sedimentation in the foreland basins of the eastern Himalayas progressed generally west and south through time. Sedimentary deposits were thick in Assam during the Paleogene and in the Bengal Basin during the Neogene. Current sedimentation of the Himalayan-Assam-Bengal system is in the Bay of Bengal enroute to the Bengal deep sea fan. As the orogenic belts (Himalayas and the Indo-Burman Ranges) continued to uplift, the foreland basins kept on shifting towards the south and west. Paleogene depocenters of the Assam and the Bengal basins were far apart resulting in differences in sediment composition and thickness. The right-lateral Kaladan fault may have brought these two depositional systems close to each other, resulting in orogenic sedimentation from both the Himalayas and the Indo-Burman Ranges.

9.7 CONCLUSIONS

The following conclusions can be drawn based on studies of detrital mineralogy, geochemistry and geochronology of sandstones from Bengal and Assam basins:

1. Oligocene sediments from the Bengal Basin are quartzolithic, and contain some orogenic signature. These strata contain mostly monocrystalline quartz; feldspar contents are low. This suggests that Oligocene sands from the Bengal Basin accumulated during a period of intense chemical weathering associated with proximity to the equator, and may have been derived from the Indian craton to the west and Indo-Burman Ranges to the east. Post-Oligocene sediments have much higher feldspar contents

compared to Oligocene sediments, indicating input from evolving orogenic sources from the Himalayas to north and Indo-Burman Ranges to the east.

2. All Tertiary sandstones from the Assam Basin are quartzolithic containing abundant lithic grains. These sandstones clearly show an orogenic provenance, suggesting that the eastern Himalayas and/or Indo-Burman Ranges were uplifted by the early Eocene.

3. Heavy mineral assemblages of Oligocene sediments in the Bengal Basin have high ZTR indices and are dominated by opaque grains. In contrast, Miocene sediments are characterized by low ZTR indices and fewer opaque grains. This suggests that source areas of sediments became more diverse by the Miocene. Also, this indicates that chemical weathering was not as intense in the Miocene as it was during the Oligocene. Heavy mineral assemblages in the Assam Basin show similar trends in composition but do not reflect such as an obvious change in composition between the Miocene and pre-Miocene sediments as observed in the Bengal Basin.

4. Garnets in Bengal and Assam basins are rich in almandine. Garnet composition indicates derivation mostly from low- to medium-grade regional metamorphic sources in the Himalayas and Indo-Burman Ranges.

5. High Cr, low Mg and Fe, and varied TiO_2 contents of chrome spinels may indicate derivation from the Rajmahal Trap and Indo-Burman ophiolites

for the Bengal Basin, and from the Indo-Burman Ranges for the Assam Basin.

6. Whole-rock chemistry data indicate that Oligocene sandstones from the Bengal Basin went through intense weathering. Sandstones from both Bengal and Assam basins may have been derived from granitic sources located in the Higher Himalayas, Indian craton, and Indo-Burman Ranges.

7. $^{40}Ar/^{39}Ar$ muscovite cooling age data suggest that the Oligocene and Miocene muscovites of the Assam Basin may have been derived from the Gangdese batholiths, the southern Tibetan Plateau, and/or Mogok Metamorphic Belt in the Indo-Burman Ranges. Muscovite grains from Miocene sandstones from the Bengal Basin were derived mostly from Himalayan sources.

REFERENCES

Ahmed, A., 1983, Oligocene stratigraphy and sedimentation in the Surma Basin, Bangladesh: [unpublished M.Sc. thesis], University of Dhaka, 96 p.

Aitchison, J.C., Ali, J.R., and Davis, A.M., 2007, When and where did India and Asia collide?: Journal of Geophysical Research, vol. 112, B05423 (doi: 10.1029/2006JB004706).

Alam, M., 1972, Tectonic classification of the Bengal Basin: Geological Society of America Bulletin, v. 83, p. 519–522.

Alam, M.M., 1991, Paleoenvironmental study of the Barail succession exposed in northeastern Sylhet, Bangladesh: Bangladesh Journal of Scientific Research, v. 9, p. 25– 32.

Alam, M., 1989, Geology and depositional history of Cenozoic sediments of the Bengal Basin of Bangladesh: Palaeogeography, Palaeoclimetology, Palaeoecology, v. 69, p. 125- 139.

Alam, M., Alam, M.M., Curray, J.R., Chowdhury, M.L.R., and Gani, M.R., 2003, An overview of the sedimentary geology of the Bengal Basin in relation to the regional tectonic framework and basin-fill history: Sedimentary Geology, v. 155, p. 179-208.

Amano, K., and Taira, A., 1992, Two-phase uplift of Higher Himalayas since 17 Ma: Geology, v. 20, p. 391-394.

Arai, S., 1992, Chemistry of chromian spinel in volcanic rocks as a potential guide to magma chemistry: Mineralogical Magazine, v. 56, p. 173-184.

Bakhtine, M.I., 1966, Major tectonic features of Pakistan, Part II, The Eastern Province: Science and Industry, Karachi, Pakistan, v. 4, no. 2, p. 89-100.

Baksi, S.K., 1965, Stratigraphy of Barail series in southern part of Shillong Plateau, Assam, India: Geological Notes, v. 49, p. 2282-2288.

Banerji, R.K., 1981, Cretaceous–Eocene sedimentation, tectonism and biofacies in the Bengal basin, India: Palaeogeography Palaeoclimatology Palaeoecology, v. 34, p. 57-85.

Basu, A., 1976, Petrology of Holocene alluvial sand derived from plutonic source rocks; implication to paleoclimate interpretation: Journal of Sedimentary Petrology, v. 4, p. 694-709.

Barley, M.E., Doyle, M.G., Khin Zaw, Pickard, A.L., and Rak, P., 2003, Jurassic to Miocene magmatism and metamorphism in the Mogok metamorphic belt and the India–Eurasia collision in Myanmar: Tectonics, v. 22, p. 1–11.

Bernet, M., Kapoutsos, D., and Bassett, K., 2007, Diagenesis and provenance of Silurian quartz arenites in the south-eastern New York State: Sedimentary Geology, v. 201, p. 43-55.

Bhandari, L.L., Fuloria, R.C., and Sastri, V.V., 1973, Stratigraphy of Assam Valley, India: American Association of Petroleum Geologists Bulletin, v. 57, p. 642-654.

Bhatia, M.R., 1983, Plate tectonics and geochemical composition of sandstones: Journal of Geology, v. 91, p. 611–627.

Bhatia, M.R., and Crook, K.A.W., 1986, Trace element characteristics of graywackes and tectonic setting discrimination of sedimentary basins: Contributions to Mineralogy and Petrology, v. 92, p. 181-193.

Brook, M., and Snelling, N.J, 1976, K/Ar and Rb/Sr age determinations on rocks and minerals from Burma: Report No. 76/12, Institute of Geological Sciences, London.

Brunnschweiler, R.O., 1974, Indo-Burman ranges, *in* Spencer, M.A., ed., Mesozoic-Cenozoic orogenic belts: Geological Society of London, Special Publication, v. 4, p. 279-299.

Catlos, E.J., Harrison, T.M., Kohn, M.J., Grove, M., Ryerson, F.J., Manning, C.E., and Upreti, B.N., 2001, Geochronologic and thermoberometric constrains on the evolution of the Main Central Thrust, Central Nepal Himalayas: Journal of Geophysical Research, v. 106, p. 16177-16204.

Chaudhri, R.S., 1972, Heavy minerals from Siwalik formations of the northwestern Himalayas: Sedimentary Geology, v. 8, p. 77-82.

Chowdhury, K.R., Haque, M., Nasreen, N., and Hasan, R., 2003, Distribution of planktonic foraminifera in the northern Bay of Bengal: Sedimentary Geology, v. 155, p. 393-405.

Cerveny, P.F., Johnson, N.M., Tahirkheli, R.A.K., and Bonis, N.R., 1989, Tectonic and geomorphic implications of Siwalik Group heavy minerals, Tectonics of western Himalayas: Geological Society of America Special Paper, v. 232, p. 129-136.

Cookenboo, H.O., Bustin, R.M., and Wilks, K.R., 1997, Detrital chromian spinel compositions used to reconstruct the tectonic setting of provenance: Implications for orogeny in the Canadian Cordillera: Journal of Sedimentary Research, v. 67, p. 116-123.

Copeland, P., and Harrison, T.M., 1990, Episodic rapid uplift in the Himalaya revealed by $^{40}Ar/^{39}Ar$ analysis of detrital K-feldspar and muscovite, Bengal Fan: Geology, v. 18, p. 354-357.

Copeland, P., Harrison, T.M., Yun, P., Kidd, W.S.F., Roden, M., and Yuquan, Z., 1995, Thermal evolution of the Gangdese batholith, southern Tibet: A history of episodic unroofing: Tectonics, v.14, no. 2, p.223-236.

Curray, J.R., 1991, Geological history of the Bengal geosyncline: Journal of Association of Exploration Geophysics, v. 12, p. 209-219.

Curray, J.R., Emmel, F.J., Moore, D.G., and Raitt, R.W., 1982, Structure, tectonics and geological history of the northeastern Indian Ocean: *In*: Nairn, A.E.M., Stehli, F.G. (Eds.), The Ocean Basins and Margins: The Indian Ocean, vol. 6. p. 399-450.

Curray, J.R., and Moore, D.G., 1974, Sedimentary and tectonic processes of the Bengal deep-sea fan and geosyncline: in Burk, C.A., and Drake, C.L., eds., The Geology of Continental Margins: New York, Springer-Verlag, p. 617-628.

Curray, J.R., Moore, D.G., Lawyer, L.A., Emmel, F.J., Raitt, R.W., Henry, M., and Kieckhefer, R., 1979, Tectonics of the Andaman Sea and Burma, Geological and Geophyscial Investigations of Continental Margins, in Watkins, J.S., Montadert, J., and Dickerson, P.W., eds., American Association of Petroleum Geologists Memoir, v. 29, p. 189-198.

Curray, J.R., and Munasinghe, T., 1989, Timing of intraplate deformation, northeastern Indian Ocean: Earth and Planetary Science Letters, v. 94, p. 71-77.

Das Gupta, A.B., and Biswas, A.K., 2000, Geology of Assam, Geological Society of India, 169 p.

DasGupta, S., 1984, Tectonic trends in Surma basin and possible genesis of folded belt: Geological Survey of India, Memoir, v. 113, p. 58-61.

Dasgupta, S., and Nandy, D.R., 1995, Geological framework of the Indo-Burmese convergent margin with special reference to ophiolitic emplacement: Indian Journal of Geology, v. 67, p. 110– 125.

DeCelles, P.G., Gehrels, G.E., Quade, J., Ojha, T.P., Kapp, P.A., and Upreti, B.N., 1998, Neogene foreland basin deposits, erosional unroofing, and the kinematic history of the Himalayan fold-thrust belt, western Nepal: Geological Society of America Bulletin, v. 110, p. 2-21.

DeCelles, P.G., Robinson, D.M., Quade, J., Ojha, T.P., Garzione, C.N., Copeland, P., and Upreti, B.N., 2001, Stratigraphy, structure, and tectonic evolution of the Himalayan fold-thrust belt in western Nepal: Tectonics, v. 20, p. 487-509.

Deer, W.A., Howie, R.A., and Zussman, J., 1992, An introduction to the rock-forming minerals: Longman Scientific Technical, Harlow, United Kingdom, 696 p.

Dick, H.J.B., and Bullen, T., 1984, Chromian spinel as a petrogenetic indicator in abyssal and alpine-type peridotites and spatially associated lavas: Contributions to Mineralogy and Petrology, v. 86, p. 54-76.

Dickin, A.P., 1995, Radiogenic Isotope Geology: New York, Cambridge Press, 452 p.

Dickinson, W.R., 1970a, Tectonic setting and sedimentary petrology of the Great Valley sequence: Geological Society of America - Abstracts with Programs, v. 2, p. 86-87.

—, 1970b, Interpreting detrital modes of graywacke and arkose: Journal of Sedimentary Petrology, v. 40, p. 695-707.

—, 1982, Composition of sandstones in circum-Pacific subduction complexes and fore-arc basins: American Association of Petroleum Geologists Bulletin, v. 66, p. 121-137.

—, 1985, Interpreting provenance relations from detrital modes of sandstones, *in* Zuffa, G.G., ed., Reading Provenance from Arenites: Dordecht, The Netherlands, Riedel, p. 333-361.

Dickinson, W.R., and Suczek, C., 1979, Plate tectonics and sandstone compositions: American Association of Petroleum Geologists Bulletin, v. 63, p. 2164-2182.

Dickinson, W.R., Ingersoll, R.V., Cowan, D.S., Helmold, K.P., and Suczek, C.A., 1982, Provenance of Franciscan graywackes in coastal California: Geological Society of America Bulletin, v. 93, p. 95-107.

Dorsey, R.J., 1988, Provenance evolution and unroofing history of a modern arc-continent collision: Evidence from petrography of Plio-Pleistocene sandstones, eastern Taiwan: Journal of Sedimentary Petrology, v. 58, p. 208-218.

Duarah, R., Saikia, M.M., and Bhattacharya, C.C., 1983, Occurrence of radiolarian cherts in flysch-ophiolite succession of Indo-Burman orogen: Geological Magazine, v. 120, p. 178-182.

Evans, P., 1964, The tectonic framework of Assam: Journal of the Geological Society of India, v. 5, p. 80-96.

Faure, G., 1986, Principles of Isotope Geology, second edition: New York, John Wiley and Sons, 589 p.

Fleet, W.F., 1926, Petrological notes on the Old Red Sandstones of the West Midlands: Geological Magazine, v. 63, p. 505-516.

Gansser, A., 1964, Geology of the Himalayas: Interscience, London, p. 289 p.

Garzanti, E., Vezzoli, G., Ando, S., Lave, J., Attal, M., France-Lanord, C., and DeCelles, P., 2007, Quantifying sand provenance and erosion (Marsyandi River, Nepal Himalaya): Earth and Planetary Science Letters, v. 258, p. 500-515.

Godwin, T., Uddin, A., Sarma, and J.N., 2001, Provenance history of Neogene sandstones from the Assam Basin, India: Abstracts with Programs - Geological Society of America, v. 33, p. 72.

Graham, S.A., Dickinson, W.R., and Ingersoll, R.V., 1975, Himalayan-Bengal model for flysch dispersal in the Appalachian-Ouachita system: Geological Society of America Bulletin, v. 86, p. 273-286

Graham, S.A., Ingersoll, R.V., and Dickinson, W.R., 1976, Common provenance for lithic grains in Carboniferous sandstones from Ouachita Mountains and Black Warrior Basin: Journal of Sedimentary Petrology, v. 46, p. 620-632.

Hames, W.E. and Bowring, S.A., 1994, An empirical evaluation of the argon diffusion geometry in muscovite: Earth and Planetary Science Letters, v. 124, p. 161-167.

Harris, N.B.W., Ronghua, X., Lewis, C.L., and Chengwei, J., 1988, Plutonic rocks of the 1985 Tibet Geotraverse, Lhasa to Golmud, *Philos. Trans. Royal Society of London, A327*, p. 145-168

Harrison, T.M., Ryerson, F.J., Le Fort, P., Yin, A., Lovera, O.M., and Catlos, E.J., 1997, A late Miocene-Pliocene origin for the Central Himalayan inverted metamorphism: Earth and Planetary Science Letters, v. 22, p. 1-8.

Henry, D.J., and Dutrow, B.L., 1992, Tourmaline as a low grade clastic metasedimentary rock: an example of the petrogenetic potential of tourmaline: Contributions to Mineralogy and Petrology, v. 112, p. 203-218.

Henry, D.J., and Guidotti, C.V., 1985, Tourmaline as a petrogenetic indicator mineral: an example from the staurolite grade metapelites of NW Maine: American Mineralogists, v. 70, p. 1-15.

Hess, H.H., 1966, Notes on operation of Frantz isodynamic magnetic separator, Princeton University: User manual guide, p. 1-6.

Hiller, K., and Elahi, M., 1984, Structural development and hydrocarbon entrapment in the Surma Basin, Bangladesh (northwest Indo–Burman Fold belt): Proceedings of the 4th Offshore Southeast Asia Conference, Singapore, p. 6-50 – 6-63.

Hodges, K.V., Hames, W.E., Olszewski, W., Burchfiel, B.C., Royden, L.H., and Chen, Z., 1994, Thermobarometric and $^{40}Ar/^{39}Ar$ geochronologic constraints on Eohimalayan metamorphism in the Dinggye area, Southern Tibet: Contributions to Mineralogy and Petrology, v. 117, p. 151-163.

Hodges, K.V., Rhul, K.W., Wobus, C.W., and Pringle, M.S., 2005, $^{40}Ar/^{39}Ar$ thermochronology of the detrital minerals, *in* Thermochronology, Reviews in Mineralogy and Geochemistry, Reiners, P.W., and Ehlers, T.A., eds., Mineralogical Society of America, Washington, D.C., v. 58, p. 235-257.

Holtrop, J.F., and Keizer, J., 1970, Some aspects of stratigraphy and correlation of the Surma Basin wells, East Pakistan: New York, United Nations, ECAFE Mineral Resources Development Series no. 36, p. 143-155.

Hoque, M., 1982, Tectonic set-up of Bangladesh and its relation to hydrocarbon accumulation: Center for Policy Research, Dhaka, Bangladesh, 177 p.

Hubbard, M.S., and Harrison, T.M., 1989, $^{40}Ar/^{39}Ar$ age constraints on deformation and metamorphism on the Main Central Thrust zone and Tibetan slab, eastern Nepal Himalaya: Tectonics, v. 8, p. 865-880

Hutchinson, C.S., 1975, Ophiolites in southeast Asia: Geological Society of America Bulletin, v. 80, p. 797-806.

Hutchison, C.S, 1989, Geological evolution of South East Asia: Oxford Monographs on geology and geophysics, Oxford, Clarendon Press, 368 p.

Ingersoll, R.V., 1978, Petrofacies and petrologic evolution of the Late Cretaceous fore-arc basin, northern and central California: Journal of Geology, v. 86, p. 335-352.

Ingersoll, R.V., Bullard, T.F., Ford, R.L., Grimm, J.P., Pickle, J.D., and Sares, S.W., 1984, The effect of grain size on detrital modes: A test of the Gazzi-Dickinson point-counting method: Journal of Sedimentary Petrology, v. 54, p. 103-116.

Ingersoll, R.V., and Eastmond, D.J., 2007, Composition of modern sand from the Sierra Nevada, California, USA: Implications for actualistic petrofacies of continental-margin magmatic arcs: Journal of Sedimentary Research, v. 77, p. 784-796.

Ingersoll, R.V., Graham, S.A., and Dickinson, W.R., 1995, Remnant ocean basins *in* Busby, C.I., and Ingersoll, R.V., eds., Tectonics of sedimentary basin: Cambridge, Massachusetts, Blackwell Science, p. 363-391.

Ingersoll, R.V., and Suczek, C.A., 1979, Petrology and provenance of Neogene sand from Nicobar and Bengal Fans, DSDP sites 211 and 218: Journal of Sedimentary Research, v. 49, p. 1217-1228.

Irvine, T.N., 1974, Petrology of the Duke Island ultramafic complex, southern Alaska: Geological Society of America Bulletin, v. 138, p. 240.

—, 1977, Origin of chromite layers in the Muskox Intrusion and other stratiform intrusions; a new interpretation: Geology, v. 5, p. 273-277.

Johnson, S.Y., and Nur Alam, A.M., 1991, Sedimentation and tectonics of the Sylhet Trough, Bangladesh: Geological Society of America Bulletin, v. 103, p. 1513-1527.

Kent, W.N., and Dasgupta, U., 2004, Structural evolution in response to fold and thrust belt tectonics in northern Assam. A key to hydrocarbon exploration in the Jaipur anticline area: Marine and Petroleum Geology, v. 21, p. 785–803.

Kent, R.W., Pringle, M.S., Muller, R.D., Saunders, A.D., and Ghose, N.C., 2002, Ar/Ar geochemistry of the Rajmahal Basalts, India, and their relationship to the Kerguelen Plateau, Journal of Petrology, v. 43, no. 7, p. 1141-1153.

Khin, J., 1990, Geological, petrological and geochemical characteristics of granitoid rocks in Burma with special reference to the associated W-Sn mineralization and there tectonic setting: Journal of Southeast Asian Earth Sciences, v. 4, no.4, p. 293-304.

Khan, M.A.M., Ismail, M., and Ahmad, M., 1988, Geology of hydrocarbon prospects of the Surma Basin, Bangladesh: Proceedings of the 7th Offshore South East Asia Conference, Singapore, p. 364-387.

Khan, M.R., and Muminullah, M., 1980, Stratigraphy of Bangladesh, *in* petroleum and mineral resources of Bangladesh: Seminar and exhibition: Dhaka, Bangladesh Ministry of Mineral Resources, Bangladesh, p. 35-40.

Khandoker, R.A., 1989, Development of major tectonic elements of the Bengal basin: a plate tectonic appraisal: Bangladesh Journal of Scientific Research, v. 7, p. 221–232.

Kumar, P., 2004, Provenance history of Cenozoic sediments near Digboi-Margherita area, eastern syntaxis of the Himalayas, Assam, northeast India [M.S. Thesis]: Auburn University, Auburn, Alabama, 131 p.

Le Dain, A.Y., Tapponnier, P., and Molnar, P., 1984, Active faulting and tectonics of Burma and surrounding regions: Journal of Geophysical Research, v. 89, p. 453-472.

Le Fort, P., 1996, Evolution of the Himalaya, in Yin, A., and Harrison, M., eds., The tectonic evolution of Asia: New York, Cambridge University Press, World and Regional Geology Series, p. 95-109.

Lindsay, J.F., Holliday, D.W., and Hulbert, A.G., 1991, Sequence stratigraphy and the evolution of the Ganges–Brahmaputra Delta complex: American Association of Petroleum Geologists Bulletin, v. 75, p. 1233-1254.

Ludwig, K.R., 2003, User's manual for Isoplot, v. 3.0, a geochronological toolkit for Microsoft Excel: Berkeley Geochronological Center, Special Publication no. 4.

Mahoney, J.J., Macdougall, J.D., Lugmair, G.W. and Gopalan, K., 1983. Kerguelen hotspot source for Rajmahal Traps and Ninetyeast Ridge?: Nature, v. 303, p. 385-389.

Mange, M.A., and Maurer, H.F.W., 1992, Heavy minerals in color: Chapman & Hall, London, 147 p.

Mange, M.A., and Morton, A.C., 2007, Geochemistry of heavy minerals: *in* Mange, M.A., and Wright, D.T., eds., Heavy minerals in use: Developments in Sedimentology, v. 58, p. 345-391.

McDougall, I., and Harrison, M.T., 1999, Geochronology and thermochronology by the $^{40}Ar/^{39}Ar$ method: New York, Oxford University Press, 269 p.

McLennan, S.M., Hemming, S., McDaniel, D.K., and Hanson, G.N., 1993, Geochemical approaches to sedimentation, provenance and tectonics: *in* Johnsson, M.J., Basu, A., eds., *Processes controlling the composition of clastic sediments*, Geological Society of America Special Paper 284, p. 21-40.

Merrihue, C., and Turner, G., 1966, Potassium-argon dating by activation with fast neutrons: Journal of Geophysical Research, v. 71, p. 2852-2856.

Mirkhamidov, F.M., and Mannan, M.M., 1981, Nature of the gravity field and its relation with geotectonics at Bangladesh: Unpublished report, Petrobangla, Dhaka.

Milliken, K.L., 2007, Provenance and diagenesis of heavy minerals, Cenozoic units of the northwestern Gulf of Mexico sedimentary basin: *in* Mange, M.A., and Wright, D.T., eds., Heavy minerals in use: Developments in Sedimentology, v. 58, p. 247-261.

Mitchell, A.H.G., Htay, M.T., Htun, K.M., Win, M.N., Oo, T., and Hlaing, T., 2007, Rock relationship in the Mogok metamorphic belt, Tatkon to Mandalay, Central Myanmar: Journal of Asian Earth Sciences, v. 29, p. 891-910.

Molnar, P., 1984, Structure and tectonics of the Himalaya: Constraints and implications of geophysical data: Annual Review of Earth and Planetary Sciences, v. 12, p. 489-518.

Morton, A.C., 1985, Heavy minerals in provenance studies *in* Zuffa, G.G. ed., provenance of arenites: Boston, Reidel publishing, p. 249-277.

—, 1992, New trends in heavy mineral analysis: NERC News, v. 21, p. 8-10.

Morton, A.C., Davies, J.R., and Waters, R.A., 1992, Heavy minerals as a guide to turbidity provenance in the lower Palaeozoic southern Welsh Basin; a pilot study, Geological Magazine, v. 129, p. 573-580.

Morton, A.C., and Hallsworth, C.R., 1999, Processes controlling the composition of heavy mineral assemblages in sandstones: Sedimentary Geology, v. 124, p. 3-30.

Morton, A.C., and Hallsworth, C., 2007, Stability of detrital heavy minerals during burial diagenesis: *in* Mange, M.A., and Wright, D.T., eds., Heavy minerals in use: Developments in Sedimentology, v. 58, p. 215-345.

Morton, A.C., and Taylor, P.N., 1991, Geochemical and isotopic constraints on the nature and age of basement rocks from Rockall Bank, NE Atlantic: Journal of the Geological Society, London, v. 148, p. 630-634.

Murthy, M.V.N., Chakrabarti, C., and Talukdar, S.E., 1976, Stratigraphic revision of the Cretaceous-Tertiary sediments of the Shillong Plateau: Geological Survey of India Records, v. 107, p. 80-90.

Nanayama, F., 1997, An electron microprobe study of the Amazon Fan: Proceedings of the Ocean Drilling Program, Scientific Results, v. 155, p. 147-168.

Nandi, K., 1967, Garnets as indices of progressive regional metamorphism: Mineralogical Magazine, v. 36, p. 89-93.

Najman, Y., and Garzanti, E., 2000, Reconstructing early Himalayan tectonic evolution and paleogeography from Tertiary foreland basin sedimentary rocks, northern India: Geological Society of America Bulletin, v. 112, p. 435-449.

Najman, Y.M.R., Pringle, M.S., Johnson, M.R.W., and Robertson, A.H.F., 1997, Laser $^{40}Ar/^{39}Ar$ dating of single detrital muscovite grains from early foreland-basin sedimentary deposits in India: Implication for early Himalayan evolution, Geology, v. 25, p.535-538.

Nesbitt, H.W., and Young, G.M., 1984, Prediction of some weathering trends of plutonic and volcanic rocks based on thermodynamic and kinetic considerations: Geochim. Cosmochim. Acta, v. 48, p.1523–1548.

Nixon, G.T., Cabri, L.J., and Laflamme, J.H.G., 1990, Platinum-group-element mineralization in lode and placer deposits associated with the Tulameen alaskan-type complex, British Columbia: The Canadian Mineralogist, v. 28, p. 503-535.

Ni, J.F., Guzman-Speziale, M., Holt, W.E., Wallace, T.C., and Seager, W.R., 1989, Accretionary tectonics of Burma and the three dimensional geometry of the Burma subduction zone: Geology, v. 17, p. 68-71.

Press, S., 1986, Detrital spinels from alpinotype source rocks in Middle Devonian sediments of the Rhenish Massif: Geologische Rundschau, v. 75, p. 333-340.

Rahman, S., 1999, The Precambrain rocks of the Khasi Hills, Meghalaya, Shillong Plateau, in Verma, P.K., ed., Geological Studies in the eastern Himalayas: Delhi, Pilgrims Book (Pvt.) Ltd., p. 59-65.

Rahman, M.J.J., and Faupl, P., 2003, $^{40}Ar/^{39}Ar$ multigrain dating of detrital white mica of sandstones of the Surma Group in the Sylhet Trough, Bengal Basin, Bangladesh: Sedimentary Geology, v. 155, p. 383-392.

Rangarao, A., 1983, Geology and hydrocarbon potential of a part of Assam-Arakan Basin and its adjacent area: Petroleum Asia Journal, v. 6, p. 127-158.

Reimann, K.U., 1993, Geology of Bangladesh: Berlin, Gebruder Borntraeger, 160 p.

Renne, P.R., Swisher, C.C., Deino, A.L., Karner, D.B., Owens, T.L., and DePaolo, D.J., 1998, Intercalibration of standards, absolute ages, and uncertainties in $^{40}Ar/^{39}Ar$ dating: Chemical Geology, v. 145, p. 117-152.

Rieu, R., Allen, P.A., Plotze, M., and Pettke, T., 2007, Compositional and mineralogical variations in a Neoproterozoic glacially influenced succession, Mirbat area, south Oman: Implications for paleo-weathering conditions: Precambrian Research, v. 154, p. 248–265.

Roser, B.P., and Korsch, R.J., 1988, Provenance signatures of sandstone-mudstone suites determined using discriminant function analysis of major-element data: Chemical Geology, v. 67, p. 119-139.

Rowley, D.B., 1996, Age of initiation of collision between India and Asia: A review of stratigraphic data: Earth and Planetary Science Letters, v. 145, p. 1-13.

Saikia, M.M., 1999, Indo-Burman orogenic belt, its plate tectonic evolution, *in* Verma, P.K., ed., Geological Studies in the Eastern Himalayas: Delhi, Pilgrims Book (Pvt.) Ltd., p. 19-39.

Salt, C.A., Alam, M.M., and Hossain, M.M., 1986, Bengal Basin: current exploration of the hinge zone area of southwestern Bangladesh: Proceedings of 6th Offshore Southeast Asia Conference, Singapore, p. 55-57.

Sclater, J.G., and Fisher, R.L., 1974, The evolution of the east central Indian Ocean, with emphasis on the tectonic setting of the Ninetyeast Ridge: Geological Society of America Bulletin, v. 85, p. 683-702.

Selley, R.C., 1998, Elements of petroleum geology: 2nd edition, Academic Press, London, 470 p.

Sengupta, S., Ray, K.K., Acharyya, S.K., and de Smith, J.B., 1990, Nature of ophiolite occurrence along the eastern margin of the Indian plate and their tectonic significance: Geology, v. 18, p. 439-442.

Shamsuddin, A.H.M., Abdullah, S.K.M., 1997, Geological evolution of the Bengal Basin and its implication in hydrocarbon exploration in Bangladesh: Indian Journal of Geology, v. 69, p. 93–121.

Shamsuddin, A.H.M., Brown, T.A., Lee, S., and Curiale, J., 2001, Petroleum systems of Bangladesh: Proceedings of the 13th SEAPEX Exploration Conference, April, 2001, Singapore.

Sinha, R.N., and Sastri, V.V., 1973, Correlation of the Tertiary geosynclinal sediments of the Surma Valley, Assam, and Tripura state (India): Sedimentary Geology, v. 10, p. 107-134.

Spear, F.S., 1993, Metamorphic phase equilibria and pressure-temperature-time paths: Mineralogical Society of America, Washington, DC, 799 p.

Sturt, B.A., 1962, The composition of garnets from pelitic schists in relation to the grade of regional metamorphism: Journal of Petrology, v. 3, p. 181-191.

Suttner, L.J., 1974, Sedimentary petrographic provinces: An evaluation, *in* Ross, C.A., ed., Paleogeographic provinces and provinciality: Special Publication- Society of Economic Paleontologists and Mineralogists, no. 21, p. 75-84.

Taylor, S.R., and McLennan, S.M., 1985, The continental crust: its composition and evolution: an examination of the geochemical record preserved in sedimentary rocks: Blackwell Scientific Publication, 312 p.

Taylor, S.R., and McLennan, S.M., 1995, The geochemical evolution of the continental crust: Reviews of Geophysics, v. 33, p. 241-265.

Tucker, M., 1988, Techniques in Sedimentology: Blackwell Scientific Publications, London, 395 p.

Uddin, A., and Lundberg, N., 1998a, Cenozoic history of the Himalayan-Bengal system: Sand composition in the Bengal basin, Bangladesh: Geological Society of America Bulletin, v. 110, p. 497-511.

—, 1998b, Unroofing history of the eastern Himalaya and the Indo-Burman ranges: Heavy-mineral study of Cenozoic sediments from the Bengal Basin, Bangladesh: Journal of Sedimentary Research, v. 68, p. 465-472.

—, 1999, A paleo-Brahmaputra? Subsurface lithofacies analysis of Miocene deltaic sediments in the Himalayan–Bengal system, Bangladesh: Sedimentary Geology, v. 123, p. 239-254.

—, 2004, Miocene sedimentation and subsidence during continent–continent collision, Bengal Basin, Bangladesh: Sedimentary Geology, v. 164, p. 131-146.

Uddin, A., Burchfiel, B.C., Geissman, J.W., and Lundberg, N., 2002, Tectonic configuration of the Bengal Basin: Miocene juxtaposition with Assam, India: Geological Society of America - Abstracts with Programs, v. 34. p. 509.

Uddin, A., Hames, W., and Zahid, K.M., 2005, Detrital mineral chemistry and age constraints on Tertiary source terrain evolution for the Bengal basin: Abstracts with Programs - Geological Society of America, v. 37, n. 7, p. 561.

Uddin, A., Bowring, S., Crowley, J., and Ramezani, J., 2006, U-Pb zircon constraints on provenance of Cenozoic sediments of the Assam-Bengal system, eastern Himalayas: Abstracts with Programs - Geological Society of America, v. 38, n. 7, p. 239.

Uddin, A., Kumar, P., Sarma, J.N., and Akhter, S.H. 2007, Heavy-mineral constraints on provenance of Cenozoic sediments from the foreland basins of Assam, India and Bangladesh: Erosional history of the eastern Himalayas and the Indo-Burman ranges, *in* Mange, M.A., and Wright, D.T., eds., Heavy minerals in use: Developments in Sedimentology, v. 58, p. 823-847.

Upreti, B.N., 1999, An overview of the stratigraphy and tectonics of the Nepal Himalaya: Journal of Asian Earth Sciences, v. 17, p. 577-606.

Venkataramana, P., Dutta, A.K., and Acharyya, S.K., 1986, Petrography and petrochemistry of the ophiolite suite: *in* Geology of Nagaland Ophiolite, Geological Survey of India - Memoir, v. 119: Bangalore, p. 33-63.

Wanas, H.A., and Abdel-Maguid, N.M., 2006, Petrography and geochemistry of the Cambro-Ordovician Wajid Sandstone, southwest Saudi Arabia: Implications for provenance and tectonic setting: Journal of Asian Earth Science, v. 27, p. 416-429.

Yokoyama, K., Taira, A., and Saito, Y., 1990, Mineralogy of silts from the Bengal Fan: Proceedings of Ocean Drilling Programs, Scientific Results, v. 116, p. 59-73.

Zahid, K.M., 2005, Provenance and basin tectonics of Oligocene-Miocene sequences of the Bengal Basin, Bangladesh [M.S. Thesis]: Auburn University, Auburn, Alabama, 142 p.

Zhu, B., Delano, J.W., and Kidd, S.F.W., 2005, Magmatic compositions and source terranes estimated from melt inclusions in detrital Cr-rich spinels: An example from mid-Cretaceous sandstones in the eastern Tethys Himalaya: Earth and Planetary Science Letters, v. 233, p. 295-309.

Zutshi, P.L., 1993, Tectonics and hydrocarbon of Cachar - Tripura, eastern Region, India: Bulletin of the Oil and Natural Gas Corporation Limited, v. 30, p. 97-137.

APPENDICES

Appendix-A

Garnet data from Bengal Basin (SBR-Oligocene Barail, SBK-Miocene Surma, STM-Mio-Pliocene Tipam, and SD-Pliocene Dupi Tila)

	Garnet Standard	SBR 1	SBR2	SBK1	SBK2	SBK4	STM1	STM2	SD1	SD2
SiO2	41.33	37.63	36.53	99.20	35.90	36.45	36.23	35.81	36.46	36.75
TiO2	0.70	0.01	0.07	0.00	10.45	0.01	0.03	0.03	0.02	0.05
Al2O3	21.97	22.15	21.30	0.06	17.70	21.44	21.64	20.94	21.24	21.86
FeO	9.33	29.74	33.79	0.59	10.25	33.01	35.97	38.04	19.14	36.11
MnO	0.25	1.30	0.76	0.07	0.08	0.58	0.66	1.81	13.18	0.04
MgO	20.62	9.09	1.81	0.00	0.00	3.49	3.07	2.42	1.62	4.48
CaO	4.29	1.05	5.37	0.06	25.58	4.95	2.39	0.95	8.33	0.71
TOTAL	98.49	100.98	99.64	99.98	99.96	99.93	99.99	100.00	100.00	99.99
Si	5.98	5.82	5.92	11.96	5.56	5.86	5.85	5.86	5.87	5.88
Ti	0.08	0.00	0.01	0.00	1.22	0.00	0.00	0.00	0.00	0.01
Al	3.75	4.04	4.07	0.01	3.23	4.06	4.12	4.04	4.03	4.13
Fe	1.13	3.85	4.58	0.06	1.33	4.43	4.86	5.21	2.58	4.84
Mn	0.03	0.17	0.10	0.01	0.01	0.08	0.09	0.25	1.80	0.00
Mg	4.45	2.10	0.44	0.00	0.00	0.84	0.74	0.59	0.39	1.07
Ca	0.66	0.17	0.93	0.01	4.25	0.85	0.41	0.17	1.44	0.12
TOTAL	16.07	16.16	16.04	12.04	15.60	16.11	16.08	16.12	16.11	16.05
Endmembers										
Py	70.91	33.34	7.23	0.00	0.00	13.48	12.12	9.50	6.28	17.73
Alm	18.00	61.18	75.64	80.63	23.78	71.51	79.62	83.78	41.56	80.18
Gro	10.60	2.76	15.40	10.18	76.03	13.74	6.78	2.68	23.17	2.01
Sp	0.49	2.71	1.72	9.18	0.20	1.27	1.48	4.04	28.98	0.08
Total	100.00	100.00	100.00	100.00	100.00	100.00	100.00	100.00	100.00	100.00

Appendix-A continued:

Garnet data from Assam Basin (AD-Eocene Disang, ABR-Oligocene Barail, ASU-Miocene Surma and ATM-Mio-Pliocene Tipam).

	Garnet Standard	AD-6	ABR1	ABR2	ASU1	ASU2	ATM 1	ATM 2	ATM 4	ATM 5	ATM 6	ATM 7	ATM 8	ATM 9	ATM 10	ATM 11
SiO2	41.33	41.44	37.13	37.18	37.22	37.08	40.99	36.54	36.22	37.42	36.48	37.00	36.51	36.37	36.61	39.63
TiO2	0.70	0.41	0.00	0.00	0.03	0.02	0.28	0.10	0.12	0.13	0.07	0.09	0.09	0.00	0.11	0.14
Al2O3	21.97	30.37	21.99	21.96	21.77	21.31	32.29	20.92	21.38	21.14	21.52	21.24	21.34	21.28	21.02	24.64
FeO	9.33	18.30	33.47	34.08	34.91	36.09	15.26	29.24	30.58	25.90	4.60	30.55	26.98	34.52	32.94	8.45
MnO	0.25	0.05	2.49	2.48	0.59	0.42	0.00	2.15	0.37	5.28	33.80	3.82	5.01	1.45	0.41	0.37
MgO	20.62	7.88	4.34	4.12	1.90	1.94	8.84	1.01	1.37	0.84	0.96	1.68	1.25	1.99	1.64	2.67
CaO	4.29	1.43	1.44	1.42	4.49	4.31	2.34	10.01	9.90	9.26	2.56	5.56	8.74	4.31	7.25	24.04
TOTAL	98.49	99.88	100.86	101.21	100.91	101.16	100.00	99.97	99.94	99.97	99.99	99.94	99.91	99.92	99.99	99.94
Si	5.98	6.00	5.89	5.89	5.94	5.94	5.86	5.90	5.84	6.00	5.93	5.96	5.88	5.90	5.91	5.94
Ti	0.08	0.04	0.00	0.00	0.00	0.00	0.03	0.01	0.01	0.02	0.01	0.01	0.01	0.00	0.01	0.02
Al	3.75	5.18	4.11	4.10	4.10	4.02	5.44	3.98	4.06	3.99	4.12	4.03	4.05	4.07	4.00	4.35
Fe	1.13	2.21	4.44	4.52	4.66	4.83	1.82	3.95	4.12	3.47	0.62	4.12	3.64	4.68	4.45	1.06
Mn	0.03	0.01	0.33	0.33	0.08	0.06	0.00	0.29	0.05	0.72	4.65	0.52	0.68	0.20	0.06	0.05
Mg	4.45	1.70	1.03	0.97	0.45	0.46	1.88	0.24	0.33	0.20	0.23	0.40	0.30	0.48	0.40	0.60
Ca	0.66	0.22	0.25	0.24	0.77	0.74	0.36	1.73	1.71	1.59	0.45	0.96	1.51	0.75	1.25	3.86
TOTAL	16.07	15.37	16.05	16.06	16.01	16.05	15.39	16.10	16.12	15.99	16.01	16.01	16.08	16.07	16.08	15.87
Endmembers																
Py	70.91	41.04	16.98	16.05	7.60	7.61	46.33	3.92	5.30	3.36	3.91	6.72	4.89	7.89	6.43	10.74
Alm	18.00	53.46	73.44	74.47	78.18	79.33	44.85	63.51	66.36	58.06	10.49	68.60	59.33	76.61	72.27	19.04
Gro	10.60	5.34	4.06	3.98	12.88	12.14	8.82	27.85	27.52	26.59	7.49	15.99	24.62	12.25	20.38	69.39
Sp	0.49	0.16	5.52	5.50	1.33	0.93	0.00	4.72	0.82	11.99	78.10	8.69	11.16	3.25	0.92	0.83
Total	100.00	100.00	100.00	100.00	100.00	100.00	100.00	100.00	100.00	100.00	100.00	100.00	100.00	100.00	100.00	100.00

Appendix-B

Chrome spinel data from Bengal Basin (SBR-Oligocene Barail, SBK-Miocene Surma, STM-Mio-Pliocene Tipam, and SD-Pliocene Dupi Tila)

	Chrome Standard	SBR1	SBR2	SBR3	SBR4	SBR5	SBR6	STM1	STM2
SiO2	0.04	0.04	0.03	0.02	0.02	0.06	0.07	0.04	0.03
TiO2	0.12	0.00	0.12	0.32	0.06	0.00	0.05	0.28	0.10
Al2O3	23.27	22.12	27.34	13.97	38.29	13.79	20.80	11.96	21.10
Cr2O3	47.60	47.42	40.44	50.51	30.28	50.97	48.61	56.67	46.98
V2O3	0.00	0.00	0.00	0.00	0.00	0.00	0.00	0.00	0.00
FeO	11.97	17.21	18.09	26.51	15.58	23.51	16.93	21.23	19.43
MnO	0.27	0.21	0.34	0.35	0.15	0.88	0.28	0.29	0.12
MgO	16.69	12.87	13.22	8.10	15.26	9.86	13.24	9.25	12.08
CaO	0.00	0.00	0.01	0.02	0.00	0.00	0.02	0.04	0.00
ZnO	0.04	0.13	0.41	0.19	0.36	0.94	0.00	0.26	0.15
TOTAL	100.00	100.00	99.99	99.99	100.01	100.01	100.00	100.01	99.99
Si	0.01	0.01	0.01	0.01	0.01	0.02	0.02	0.01	0.01
Ti	0.02	0.00	0.02	0.06	0.01	0.00	0.01	0.05	0.02
Al	6.56	6.42	7.75	4.32	10.28	4.22	6.05	3.71	6.18
Cr	9.00	9.23	7.69	10.49	5.46	10.47	9.49	11.80	9.23
V	0.00	0.00	0.00	0.00	0.00	0.00	0.00	0.00	0.00
Fe	2.39	3.54	3.64	5.82	2.97	5.11	3.50	4.67	4.04
Mn	0.05	0.04	0.07	0.08	0.03	0.19	0.06	0.07	0.03
Mg	5.95	4.73	4.74	3.17	5.18	3.82	4.87	3.63	4.48
Ca	0.00	0.00	0.00	0.00	0.00	0.00	0.01	0.01	0.00
Zn	0.01	0.02	0.07	0.04	0.06	0.18	0.00	0.05	0.03
TOTAL	24.00	24.00	24.00	24.00	24.00	24.00	24.00	24.00	24.00
Fe(ii)	2.02	3.22	3.14	4.78	2.74	3.82	3.09	4.31	3.50
Fe(iii)	0.37	0.33	0.50	1.05	0.23	1.28	0.40	0.36	0.54
Fe2/(Fe2+Fe3)	0.84	0.91	0.86	0.82	0.92	0.75	0.88	0.92	0.87
Fe3/(Fe3+Fe2)	0.16	0.09	0.14	0.18	0.08	0.25	0.12	0.08	0.13
Cr/Cr+Al	0.58	0.59	0.50	0.71	0.35	0.71	0.61	0.76	0.60

Appendix-B continued:

Chrome spinel data from Assam Basin (AD-Eocene Disang, ABR-Oligocene Barail, ASU-Miocene Surma and ATM-Mio-Pliocene Tipam).

	Chrome Standard	AD1	AD2	ABR1	ASU1	ASU2	ASU4	ATM1	ATM2
SiO2	0.04	0.04	0.05	0.07	0.00	0.07	0.05	0.00	0.03
TiO2	0.12	0.02	0.08	0.12	0.33	0.05	0.11	0.31	0.11
Al2O3	23.27	24.70	17.64	41.85	18.42	51.49	13.53	18.42	17.43
Cr2O3	47.60	43.40	49.17	27.73	47.58	16.07	53.80	45.65	49.57
V2O3	0.00	0.00	0.00	0.00	0.00	0.00	0.00	0.00	0.00
FeO	11.97	18.56	23.27	12.45	23.25	12.92	21.88	27.52	22.55
MnO	0.27	0.22	0.38	0.18	0.29	0.11	0.39	0.39	0.19
MgO	16.69	12.88	9.02	17.52	10.04	19.02	10.21	7.62	9.95
CaO	0.00	0.00	0.07	0.01	0.00	0.00	0.03	0.02	0.00
ZnO	0.04	0.17	0.32	0.05	0.10	0.26	0.00	0.07	0.17
TOTAL	100.00	100.00	100.00	99.99	100.01	100.00	100.00	100.00	100.00
Si	0.01	0.01	0.01	0.02	0.00	0.02	0.01	0.00	0.01
Ti	0.02	0.00	0.02	0.02	0.06	0.01	0.02	0.06	0.02
Al	6.56	7.09	5.35	10.95	5.52	12.89	4.14	5.61	5.25
Cr	9.00	8.36	10.00	4.87	9.57	2.70	11.04	9.33	10.03
V	0.00	0.00	0.00	0.00	0.00	0.00	0.00	0.00	0.00
Fe	2.39	3.78	5.00	2.31	4.95	2.30	4.75	5.95	4.82
Mn	0.05	0.05	0.08	0.03	0.06	0.02	0.09	0.09	0.04
Mg	5.95	4.68	3.46	5.80	3.81	6.03	3.95	2.94	3.79
Ca	0.00	0.00	0.02	0.00	0.00	0.00	0.01	0.00	0.00
Zn	0.01	0.03	0.06	0.01	0.02	0.04	0.00	0.01	0.03
TOTAL	24.00	24.00	24.00	24.00	24.00	24.00	24.00	24.00	24.00
Fe(ii)	2.02	3.26	4.41	2.19	4.17	1.94	3.99	5.02	4.16
Fe(iii)	0.37	0.52	0.60	0.12	0.78	0.36	0.76	0.93	0.67
Fe2/(Fe2+Fe3	0.84	0.86	0.88	0.95	0.84	0.84	0.84	0.84	0.86
Fe3/(Fe3+Fe2	0.16	0.14	0.12	0.05	0.16	0.16	0.16	0.16	0.14
Cr/Cr+Al	0.58	0.54	0.65	0.31	0.63	0.17	0.73	0.62	0.66

Appendix-C

Tourmaline data from Bengal Basin (SBR-Oligocene Barail, SBK-Miocene Surma, STM-Mio-Pliocene Tipam, and SD-Pliocene Dupi Tila)

	Tourmaline Standard	SBR1	SBR2	SBR3	SBR4	SBR5	SBK1	SBK2	SBK3	STM1	STM2	SD1	SD2
SiO2	40.42	39.61	40.82	42.04	39.92	38.96	41.30	42.40	41.89	41.86	41.59	40.00	40.46
TiO2	4.90	0.08	0.86	1.06	0.61	1.49	0.68	0.74	0.62	0.56	0.83	1.32	0.59
Al2O3	14.84	40.50	39.71	38.68	37.79	34.21	37.84	40.30	41.05	37.88	36.85	38.68	35.14
FeO	10.77	17.26	10.21	5.79	15.10	16.29	4.50	3.30	4.61	6.75	9.91	13.86	13.01
MnO	0.14	0.16	0.01	0.03	0.19	0.18	0.05	0.06	0.10	0.00	0.00	0.06	0.01
MgO	12.94	0.18	5.51	8.99	3.36	4.88	11.32	9.60	8.60	9.36	7.60	3.51	7.39
CaO	11.21	0.11	0.39	1.27	0.73	1.94	3.33	1.27	1.27	0.88	1.12	0.22	0.52
Na2O	2.54	2.04	2.40	2.01	2.18	1.95	0.87	2.10	1.82	2.62	2.05	2.21	2.84
K2O	2.16	0.03	0.08	0.03	0.05	0.09	0.03	0.04	0.04	0.02	0.05	0.05	0.05
TOTAL	99.91	99.96	99.99	99.91	99.93	99.99	99.92	99.82	99.99	99.92	100.00	99.92	100.00
Si	6.24	5.78	5.79	5.86	5.81	5.76	5.76	5.85	5.79	5.87	5.91	5.78	5.86
Ti	0.57	0.01	0.09	0.11	0.07	0.17	0.07	0.08	0.06	0.06	0.09	0.14	0.06
Al	2.70	6.97	6.64	6.36	6.48	5.96	6.22	6.55	6.69	6.26	6.17	6.58	6.00
Fe	1.39	2.11	1.21	0.68	1.84	2.01	0.52	0.38	0.53	0.79	1.18	1.67	1.58
Mn	0.02	0.02	0.00	0.00	0.02	0.02	0.01	0.01	0.01	0.00	0.00	0.01	0.00
Mg	2.98	0.04	1.17	1.87	0.73	1.08	2.35	1.97	1.77	1.96	1.61	0.76	1.60
Ca	1.85	0.02	0.06	0.19	0.11	0.31	0.50	0.19	0.19	0.13	0.17	0.03	0.08
Na	0.76	0.58	0.66	0.54	0.62	0.56	0.24	0.56	0.49	0.71	0.57	0.62	0.80
K	0.42	0.01	0.01	0.01	0.01	0.02	0.01	0.01	0.01	0.00	0.01	0.01	0.01
TOTAL	16.93	15.52	15.63	15.62	15.69	15.88	15.68	15.59	15.55	15.79	15.70	15.60	15.98
Al	-	46.43	45.89	45.45	45.50	44.26	44.81	45.88	46.03	45.06	44.93	45.78	44.16
Al50Fe(tot)50	-	30.23	27.13	25.14	29.20	29.61	24.30	24.27	24.85	25.38	26.75	28.71	27.88
Al50Mg50	-	23.34	26.97	29.41	25.31	26.13	30.89	29.85	29.12	29.57	28.32	25.52	27.96
Total	-	100.00	100.00	100.00	100.00	100.00	100.00	100.00	100.00	100.00	100.00	100.00	100.00
Ca	-	0.77	2.46	6.95	4.22	9.06	14.74	7.39	7.56	4.57	5.78	1.41	2.46
Fe(tot)	-	97.45	49.71	24.69	68.57	59.28	15.54	14.97	21.37	27.48	39.80	67.92	48.46
Mg	-	1.78	47.83	68.36	27.20	31.66	69.72	77.64	71.07	67.95	54.42	30.67	49.08
Total	-	100.00	100.00	100.00	100.00	100.00	100.00	100.00	100.00	100.00	100.00	100.00	100.00

Appendix-C continued:

Tourmaline data from Assam Basin (AD-Eocene Disang, ABR-Oligocene Barail, ASU-Miocene Surma and ATM-Mio-Pliocene Tipam).

	Tourmaline Standard	AD1	AD2	ABR1	ABR2	ASU1	ASU2
SiO2	40.05	40.65	41.51	41.17	41.88	41.24	39.97
TiO2	4.94	0.38	0.38	0.65	0.21	0.51	0.28
Al2O3	14.83	30.26	35.83	38.88	37.11	38.79	31.75
FeO	11.40	17.04	9.22	9.58	7.58	10.41	14.91
MnO	0.06	0.01	0.02	0.08	0.02	0.02	0.00
MgO	12.84	7.64	9.34	6.58	9.72	6.13	8.74
CaO	10.92	1.45	1.13	0.54	0.83	0.62	2.29
Na2O	2.74	2.31	2.48	2.39	2.52	2.14	2.05
K2O	2.09	0.04	0.04	0.07	0.03	0.06	0.02
TOTAL	99.87	99.78	99.95	99.94	99.91	99.92	100.00
Si	6.20	6.04	5.91	5.83	5.90	5.86	5.88
Ti	0.58	0.04	0.04	0.07	0.02	0.05	0.03
Al	2.71	5.30	6.01	6.49	6.16	6.49	5.51
Fe	1.48	2.12	1.10	1.14	0.89	1.24	1.84
Mn	0.01	0.00	0.00	0.01	0.00	0.00	0.00
Mg	2.97	1.69	1.98	1.39	2.04	1.30	1.92
Ca	1.81	0.23	0.17	0.08	0.12	0.09	0.36
Na	0.82	0.66	0.68	0.66	0.69	0.59	0.58
K	0.41	0.01	0.01	0.01	0.01	0.01	0.00
TOTAL	16.98	16.10	15.90	15.68	15.84	15.64	16.13
Al	-	42.38	44.32	45.57	44.68	45.55	42.72
Al50Fe(tot)50	-	29.66	26.21	26.77	25.58	27.11	28.48
Al50Mg50	-	27.96	29.47	27.66	29.74	27.33	28.80
Total	-	100.00	100.00	100.00	100.00	100.00	100.00
Ca	-	5.71	5.31	3.14	4.07	3.56	8.77
Fe(tot)	-	52.40	33.74	43.54	29.19	47.04	44.61
Mg	-	41.89	60.94	53.32	66.74	49.39	46.62
Total	-	100.00	100.00	100.00	100.00	100.00	100.00

Appendix-D

Whole rock data from Bengal Basin (SBR-Oligocene Barail, SBH/SBK-Miocene Surma, UTM/STM-Mio-Pliocene Tipam, and SD-Pliocene Dupi Tila)

Major element (%)	SBR-2	SBR-12	SBR-14	SBH-1	SBH-3	SBK-1	SBK-2	STM-3	UTM-1	UTM-2	UTM-3	SD-1	SD-2
SiO2	87.72	78.32	62.08	74.82	69.28	71.90	73.70	78.47	76.93	76.48	78.84	79.28	75.50
Al2O3	3.89	9.89	16.60	11.50	12.29	11.61	11.08	9.84	10.23	10.35	9.81	10.01	12.11
Fe2O3	3.66	3.45	7.20	4.19	4.67	4.50	4.03	2.93	3.34	3.94	2.84	2.58	2.58
MgO	0.17	0.48	1.32	0.89	1.91	1.53	1.05	0.50	0.70	0.70	0.83	0.49	0.72
CaO	0.01	0.04	0.15	0.12	1.81	1.82	1.71	0.42	0.79	1.44	1.09	0.64	1.17
Na2O	0.04	0.15	0.37	0.35	1.53	1.67	2.05	0.61	1.08	1.55	1.39	0.98	1.34
K2O	0.60	1.61	2.57	2.28	2.47	1.85	1.49	2.29	1.95	1.80	2.11	2.26	2.14
TiO2	1.02	1.01	1.20	0.66	0.71	0.76	0.60	0.56	0.50	0.73	0.52	0.39	0.38
P2O5	0.07	0.07	0.15	0.08	0.15	0.15	0.20	0.07	0.05	0.09	0.06	0.04	0.04
MnO	0.01	0.02	0.05	0.02	0.07	0.08	0.08	0.21	0.04	0.06	0.04	0.05	0.04
Cr2O3	0.02	0.02	0.02	0.01	0.02	0.02	0.01	0.03	0.01	0.02	0.01	0.01	0.01
LOI	2.50	4.70	8.10	4.90	4.90	3.90	3.80	4.00	4.30	2.60	2.30	3.10	3.80
SUM	100.03	99.92	99.92	99.92	99.90	99.90	99.91	100.05	100.04	99.92	99.91	99.92	99.91
CIA	85.68	84.60	84.31	80.70	67.90	68.50	67.85	74.77	72.81	68.36	68.13	72.07	72.26
Trace elements (ppm)													
Ba	135.00	263.00	340.00	381.00	394.00	293.00	228.00	386.00	348.00	288.00	338.00	429.00	383.00
Ni	8.00	19.00	49.00	31.00	37.00	35.00	18.00	42.00	12.00	14.00	11.00	21.00	11.00
Sr	41.00	45.00	97.00	38.00	121.00	140.00	136.00	87.00	103.00	155.00	124.00	106.00	159.00
Zr	2267.00	811.00	320.00	277.00	243.00	388.00	404.00	393.00	432.00	776.00	158.00	182.00	123.00
Y	38.00	35.00	49.00	29.00	29.00	36.00	44.00	37.00	29.00	44.00	20.00	21.00	18.00
Nb	18.00	13.00	15.00	11.00	17.00	15.00	13.00	12.00	10.00	10.00	14.00	7.00	10.00
Sc	5.00	10.00	18.00	10.00	11.00	11.00	9.00	7.00	8.00	9.00	7.00	6.00	8.00

Appendix-D continued:

Whole-rock data from Assam Basin (AD-Eocene Disang, ABR-Oligocene Barail, ASU-Miocene Surma and ATM-Mio-Pliocene Tipam).

Major element (%)	AD-6	AD-8	ABR-2	ABR-7	ASU-1	ASU-2	ATM-1	ATM-3
SiO2	81.99	78.96	82.52	69.39	84.83	92.01	62.36	69.51
Al2O3	8.36	9.01	6.60	11.84	3.65	2.36	15.04	13.22
Fe2O3	3.56	4.26	2.47	5.47	0.87	0.36	6.20	4.53
MgO	1.01	1.15	1.07	2.46	0.50	0.10	3.91	2.16
CaO	0.10	0.11	1.03	1.87	4.02	0.04	2.15	1.86
Na2O	1.10	1.09	0.92	2.72	0.05	0.03	2.59	2.38
K2O	1.02	0.84	0.80	0.65	0.39	0.20	2.07	1.85
TiO2	0.60	0.82	0.61	0.45	0.38	0.15	0.59	0.63
P2O5	0.09	0.12	0.09	0.09	0.05	0.02	0.09	0.12
MnO	0.02	0.01	0.03	0.09	0.02	0.01	0.08	0.06
Cr2O3	0.01	0.03	0.04	0.11	0.20	0.07	0.06	0.03
LOI	2.00	3.40	3.60	4.70	4.90	4.70	4.60	3.40
SUM	99.92	99.91	99.89	99.92	99.92	100.06	99.87	99.87
CIA	79.02	81.54	70.59	69.32	45.01	89.73	68.83	68.46
Trace elements (ppm)								
Ba	137.00	123.00	116.00	99.00	83.00	44.00	420.00	360.00
Ni	30.00	57.00	62.00	187.00	14.00	17.00	113.00	103.00
Sr	70.00	73.00	90.00	157.00	89.00	12.00	287.00	241.00
Zr	143.00	450.00	580.00	171.00	344.00	40.00	181.00	274.00
Y	20.00	28.00	24.00	18.00	9.00	<5	21.00	26.00
Nb	6.00	9.00	9.00	<5	6.00	<5	12.00	12.00
Sc	9.00	9.00	5.00	12.00	4.00	2.00	12.00	11.00

Appendix-E:

$^{40}Ar/^{39}Ar$ data for monitor minerals used in $^{40}Ar/^{39}Ar$ geochronology.

Data Monitor Mineral Muscovite FC=2

		^{40}Ar (*+atm)		^{39}Ar(K)		^{38}Ar (Cl+atm)		^{37}Ar(Ca)		^{36}Ar(Atm)		%Rad	R	J-value	%-sd
au9.4i.san	76	1.1E-13 +	6E-17	9.558E-14 +	3.104E-17	2.14E-16 +	7.099E-19	4.777E-16 +	4.323E-18	1.48E-18 +	1.013E-19	0.9960232	1.1460	0.0136582 + 0.00001	0.0006996
	77	5.73E-14 +	4E-17	4.945E-14 +	3.63E-17	1.235E-16 +	6.841E-19	2.911E-16 +	3.244E-18	1.199E-18 +	8.417E-20	0.9938144	1.1511	0.0135986 + 0.00001	0.0010932
	78	9.6E-14 +	7E-17	8.049E-14 +	2.983E-17	2.314E-16 +	1.367E-18	4.193E-16 +	3.924E-18	1.154E-17 +	1.994E-19	0.9644647	1.1497	0.0136141 + 0.00001	0.0010909
	79	7.6E-14 +	3E-17	6.532E-14 +	4.956E-17	1.662E-16 +	1.085E-18	3.339E-16 +	5.071E-18	1.531E-18 +	1.141E-19	0.9940452	1.1563	0.0135368 + 0.00001	0.0009854
	80	6E-14 +	5E-17	5.163E-14 +	3.64E-17	1.246E-16 +	5.434E-19	2.768E-16 +	2.656E-18	3.9E-19 +	6.865E-20	0.9980796	1.1600	0.0134941 + 0.00002	0.0011402
														0.013580 + 0.00003	**0.21%**
au9.3i.san	86	1.28E-13 +	2E-16	1.104E-13 +	1.834E-16	2.823E-16 +	1.168E-18	6.843E-16 +	9.862E-18	1.63E-18 +	1.283E-19	0.9962265	1.152	0.0135921 + 0.00003	0.002124
	87	7.41E-14 +	6E-17	6.379E-14 +	7.328E-17	1.604E-16 +	8.886E-19	3.559E-16 +	3.556E-18	6.861E-19 +	9.98E-20	0.9972622	1.1577	0.013521 + 0.00002	0.0015103
	88	9.39E-14 +	4E-17	8.067E-14 +	6.806E-17	2.069E-16 +	9.793E-19	4.548E-16 +	3.903E-18	2.651E-18 +	1.323E-19	0.9916602	1.1548	0.0135543 + 0.00001	0.0010579
	89	1.2E-13 +	9E-17	1.021E-13 +	5.093E-17	2.7E-16 +	1.027E-18	6.209E-16 +	6.968E-18	4.877E-18 +	1.311E-19	0.9879887	1.1615	0.0134764 + 0.00001	0.0009784
	90	1.32E-13 +	7E-17	1.132E-13 +	3.387E-17	2.855E-16 +	1.608E-18	6.439E-16 +	4.47E-18	4.245E-18 +	1.378E-19	0.9904709	1.1520	0.0135876 + 0.00001	0.0006882
														0.0135463 + 0.00002	**0.16%**
au9.2i.san	91	3.5E-14 +	2E-17	2.802E-14 +	1.499E-17	6.453E-17 +	3.055E-19	1.728E-16 +	2.773E-18	8.502E-18 +	1.805E-19	0.9282442	1.16	0.0134964 + 0.00003	0.0018908
	92	8.45E-14 +	5E-17	7.218E-14 +	3.073E-17	1.658E-16 +	6.893E-19	3.99E-16 +	4.185E-18	5.732E-18 +	1.823E-19	0.9799653	1.148	0.0136359 + 0.00001	0.0009939
	93	7.59E-14 +	6E-17	6.391E-14 +	2.953E-17	1.54E-16 +	9.827E-19	4.966E-16 +	1.086E-17	7.122E-18 +	1.975E-19	0.972273	1.155	0.0135554 + 0.00002	0.0012694
	94	8.02E-14 +	5E-17	6.857E-14 +	5.714E-17	1.589E-16 +	8.492E-19	3.936E-16 +	6.409E-18	3.391E-18 +	2.208E-19	0.9875099	1.156	0.0135462 + 0.00002	0.0013621
	95	7.18E-14 +	5E-17	6.235E-14 +	5.175E-17	1.443E-16 +	5.88E-19	3.378E-16 +	2.608E-18	1.136E-18 +	1.343E-19	0.9953291	1.147	0.0136483 + 0.00002	0.0012537
														0.0135764 + 0.00003	**0.21%**
au9.1j.san	96	5.24E-14 +	3E-17	4.439E-14 +	3.53E-17	1.064E-16 +	7.292E-19	3.344E-16 +	4.569E-18	1.724E-18 +	8.803E-20	0.9902725	1.168	0.0133956 + 0.00002	0.0011332
	97	5.47E-14 +	3E-17	4.646E-14 +	2.281E-17	1.28E-16 +	8.064E-19	4.543E-16 +	2.803E-18	2.288E-18 +	9.702E-20	0.9876367	1.163	0.0134619 + 0.00001	0.0009684
	98	6.6E-14 +	8E-17	5.45E-14 +	5.227E-17	1.827E-16 +	1.161E-18	6.82E-16 +	4.238E-18	7.567E-18 +	1.13E-19	0.9661296	1.17	0.0133736 + 0.00002	0.0016308
	99	1.08E-13 +	1E-16	9.121E-14 +	6.799E-17	2.449E-16 +	6.84E-19	5.553E-16 +	6.239E-18	9.469E-18 +	1.523E-19	0.9741922	1.158	0.0135167 + 0.00002	0.0013424
	100	1.12E-13 +	4E-17	9.293E-14 +	4.099E-17	2.378E-16 +	1.03E-18	5.753E-16 +	5.445E-18	9.903E-18 +	2.113E-19	0.9739067	1.175	0.0133177 + 0.00001	0.0008041
														0.0134131 + 0.00003	**0.26%**
au9.3g.san	71	1.59E-13 +	4E-17	1.36E-13 +	4.109E-17	3.829E-16 +	8.675E-19	8.156E-16 +	5.129E-18	2.526E-18 +	1.045E-19	0.9953125	1.166	0.0134263 + 6.1E-06	0.0004563

Notes:

1 ^{40}Ar *atm, ^{40}Ar produced from radioactive decay and atmosphere; $^{39}Ar_K$, ^{39}Ar produced from ^{39}K; ^{38}Ar atm.cl, ^{38}Ar produced from atmosphere and chlorine; ^{37}Ar Ca, ^{37}Ar produced from calcium; ^{36}Ar atm, atmospheric ^{36}Ar.

2 All data are in moles

3 All uncertainities are quotes at one standard deviation (1σ)

4 J values calculated assuming an age of 28.02±0.09 Ma (after Renne et al., 1998)

5 Monitor prepared by New Mexico Tech; 20-28 mesh size

6 All data are corrected for mass discrimination and interferring argon isotopes produced during $^{39}Ar_K$

7 %Rad, the percentage of radiogenic ^{40}Ar for $^{40}Ar_{total}$; R, the ratio of radiogenic ^{40}Ar to $^{39}Ar_K$

Appendix-E continued:

Assam Basin Oligocene muscovite cooling age data.

		^{40}Ar (*+atm)		^{39}Ar(K)		^{38}Ar (Cl+atm)		^{37}Ar(Ca)		^{36}Ar(Atm)		%Rad	R	Age (Ma)		%-sd
Assam Barail	1	1.674E-14	+ 1.529E-17	4.98E-15	+ 9.4E-18	1.09E-17	+ 1.21E-19	3E-18	+ 7.59E-19	1.59E-18	+ 1.37E-19	0.971851	3.263938	78.052823	+ 0.257066	0.003293
B2 Muscovite	2	2.739E-15	+ 7.139E-18	8.82E-16	+ 3E-18	2.02E-18	+ 5.06E-20	9.82E-19	+ 6.37E-19	2.94E-19	+ 1.3E-19	0.968281	3.007606	72.043696	+ 1.094993	0.015199
(95°42'30"E	3	8.876E-15	+ 2.044E-17	2.78E-15	+ 6.1E-18	5.71E-18	+ 8.57E-20	1.99E-18	+ 8.11E-19	7.93E-19	+ 1.44E-19	0.973592	3.103266	74.288572	+ 0.439059	0.00591
27°16'10"N)	4	1.351E-14	+ 1.81E-17	3.97E-15	+ 8E-18	8.6E-18	+ 1.02E-19	2.59E-18	+ 7.47E-19	1.49E-18	+ 1.34E-19	0.967325	3.295985	78.802705	+ 0.309561	0.003928
	5	1.391E-14	+ 1.834E-17	5.26E-15	+ 8.9E-18	1.29E-17	+ 1.55E-19	2.53E-18	+ 8.98E-19	1.16E-18	+ 1.32E-19	0.975407	2.581282	62.004947	+ 0.224977	0.003628
	6	6.813E-17	+ 1.325E-18	3.53E-18	+ 3.5E-19	8.86E-20	+ 1.17E-19	1.88E-18	+ 8.68E-19	2.14E-19	+ 6.06E-20	0.072997	1.407608	34.076055	+ 138.9184	4.076717
	7	1.038E-14	+ 1.34E-17	3.21E-15	+ 7.7E-18	8.87E-18	+ 1.64E-19	1.88E-18	+ 8.69E-19	4.63E-19	+ 6.85E-20	0.986823	3.192091	76.370567	+ 0.258529	0.003385
	8	1.026E-14	+ 1.929E-17	3.66E-15	+ 1.2E-17	1.03E-17	+ 1.94E-19	4.88E-18	+ 1.53E-18	6.48E-19	+ 7.34E-20	0.981353	2.751025	66.008611	+ 0.285973	0.004332
	9	1.112E-14	+ 1.001E-17	3.89E-15	+ 4.5E-18	8.19E-18	+ 5.05E-20	1.23E-18	+ 6.75E-19	1.46E-18	+ 7.47E-20	0.961325	2.750317	65.99194	+ 0.169791	0.002573
	10	3.006E-14	+ 4.18E-17	4.14E-15	+ 5.9E-18	1.25E-17	+ 1.62E-19	4.64E-18	+ 9.55E-19	9.09E-19	+ 7.33E-20	0.991068	7.190733	167.69043	+ 0.358202	0.002136
	11	2.513E-14	+ 3.735E-17	3E-15	+ 3.5E-18	6.28E-18	+ 7.36E-20	1.25E-18	+ 9.66E-19	4.65E-19	+ 6.68E-20	0.994537	8.338228	193.06509	+ 0.398071	0.002062
	12	2.497E-14	+ 3.404E-17	4.12E-15	+ 4.5E-18	8.74E-18	+ 1.09E-19	2.47E-18	+ 1.06E-18	8.94E-19	+ 7.93E-20	0.989419	6.003819	141.06308	+ 0.283298	0.002008
	13	5.304E-15	+ 1.55E-17	1.45E-15	+ 3.5E-18	2.89E-18	+ 5.88E-20	7.44E-19	+ 1.27E-18	3.23E-19	+ 5.79E-20	0.981988	3.582356	85.489675	+ 0.431891	0.005052
	14	6.271E-15	+ 6.172E-17	1.89E-15	+ 1.9E-17	3.27E-18	+ 8.87E-20	1.73E-18	+ 1.05E-18	2.68E-19	+ 6.2E-20	0.987391	3.268263	78.154058	+ 1.122759	0.014366
	15	5.141E-15	+ 7.018E-18	1.55E-15	+ 2.3E-18	3.62E-18	+ 6.84E-20	2.86E-18	+ 1.47E-18	7.19E-19	+ 6.94E-20	0.958642	3.18504	76.205378	+ 0.355639	0.004667
	16	1.067E-14	+ 3.781E-17	3.26E-15	+ 1.9E-17	6.95E-18	+ 1.08E-19	2.83E-18	+ 1.19E-18	6.09E-19	+ 9.44E-20	0.983142	3.214502	76.895462	+ 0.56633	0.007365
	17	3.063E-14	+ 4.087E-17	3.41E-15	+ 6.8E-18	1.17E-17	+ 1.88E-19	2.76E-18	+ 1.11E-18	1.22E-18	+ 9.36E-20	0.988205	8.872356	204.75569	+ 0.52909	0.002584
	18	2.039E-14	+ 2.081E-17	2.99E-15	+ 7.8E-18	6.01E-18	+ 8.31E-20	3.73E-18	+ 8.99E-19	4.13E-19	+ 8.53E-20	0.994015	6.786739	158.67123	+ 0.487974	0.003075
	19	4.358E-15	+ 5.139E-18	1.3E-15	+ 3.9E-18	2.64E-18	+ 6.21E-20	1.39E-19	+ 9.23E-19	2.92E-19	+ 9.18E-20	0.980178	3.283786	78.517297	+ 0.561762	0.007155
	20	5.465E-15	+ 8.532E-18	1.68E-15	+ 3.7E-18	3.45E-18	+ 4.61E-20	3.1E-19	+ 9.38E-19	2.52E-19	+ 8.96E-20	0.986375	3.214223	76.888928	+ 0.43179	0.005616
	21	7.597E-15	+ 1.05E-17	2.36E-15	+ 7.4E-18	4.8E-18	+ 8.14E-20	4.44E-18	+ 9.1E-19	3E-19	+ 6.71E-20	0.98832	3.185161	76.208212	+ 0.332311	0.004361
	22	3.627E-15	+ 8.942E-18	1.1E-15	+ 4.1E-18	1.86E-18	+ 6.71E-20	2.72E-19	+ 9.72E-19	4.57E-20	+ 6.35E-20	0.996275	3.293309	78.740084	+ 0.54131	0.006875
	23	1.721E-14	+ 2.449E-17	5.24E-15	+ 1.2E-17	1.39E-17	+ 2.18E-19	3.83E-18	+ 1.18E-18	8.7E-19	+ 7.16E-20	0.985063	3.233176	77.332752	+ 0.234311	0.00303
	24	8.048E-15	+ 1.704E-17	2.43E-15	+ 5.3E-18	6.34E-18	+ 1.26E-19	5.76E-19	+ 1.09E-18	3.04E-19	+ 6.38E-20	0.988841	3.269559	78.184374	+ 0.302618	0.003871
	27	2.344E-15	+ 9.599E-18	7.52E-16	+ 1.9E-18	1.7E-18	+ 3.88E-20	-2.7E-19	+ 8E-19	-2.6E-20	+ -9E-20	1.003216	3.129528	74.904381	+ 0.919989	0.012282
	28	1.413E-15	+ 2.463E-18	4.5E-16	+ 2E-18	3.88E-19	+ 1.54E-20	-9.7E-19	+ 9.36E-19	-8E-20	+ -6.5E-20	1.016686	3.194403	76.424707	+ 1.078253	0.014109
	31	6.945E-16	+ 2.881E-18	1.96E-16	+ 2E-18	7.57E-19	+ 3.98E-20	-9E-19	+ 9.04E-19	1.9E-19	+ 6.67E-20	0.919106	3.2561	77.869375	+ 2.580006	0.033132
	32	8.935E-16	+ 2.896E-18	2.43E-16	+ 2E-18	7.38E-19	+ 3.9E-20	-2.7E-19	+ 7.9E-19	2.97E-19	+ 6.72E-20	0.901802	3.31292	79.198831	+ 2.106507	0.026598
	33	1.046E-15	+ 3.81E-18	2.82E-16	+ 1.4E-18	5.97E-19	+ 3.57E-20	-5.9E-19	+ 8.88E-19	4.68E-19	+ 6.8E-20	0.867749	3.222988	77.094197	+ 1.795958	0.023296
	34	1.148E-15	+ 4.949E-18	3.22E-16	+ 1.6E-18	5.84E-19	+ 1.94E-20	-1.1E-18	+ 7.87E-19	5.71E-19	+ 6.53E-20	0.853073	3.03745	72.744347	+ 1.543624	0.02122
	35	9.545E-16	+ 3.34E-18	2.71E-16	+ 2.8E-18	4.47E-19	+ 2.4E-20	-6.1E-19	+ 9.67E-19	3.15E-19	+ 6.36E-20	0.902472	3.179561	76.077012	+ 1.894002	0.024896

Appendix-E continued:

Assam Basin Oligocene muscovite cooling age data.

		^{40}Ar (*+atm)		^{39}Ar(K)		^{38}Ar (Cl+atm)		^{37}Ar(Ca)		^{36}Ar(Atm)		%Rad	R	Age (Ma)	
Assam Barail	2	5.57E-16 +	3.79E-18	3.59E-16 +	1.59E-18	1.24E-18 +	4.1E-20	8.88E-19 +	8.11E-19	8.94E-20 +	7.41E-20	0.952567	1.477004	35.73949 +	1.511286
T-12 Muscovite	3	4.03E-15 +	6.48E-18	1.24E-15 +	4.62E-18	3.1E-18 +	6.07E-20	7.18E-18 +	7.12E-19	4.82E-19 +	7.21E-20	0.964664	3.148547	75.35022 +	0.5224
(95°52'00"E	4	1.18E-16 +	2.27E-18	2.56E-17 +	9.54E-19	3.06E-19 +	9.75E-20	1.34E-18 +	7.89E-19	-1.1E-19 +	-7.3E-20	1.264492	5.812835	136.7416 +	20.24134
27°18'10"N)	5	9.7E-15 +	1.45E-17	1.4E-15 +	2.84E-18	3.07E-18 +	5.34E-20	3.22E-18 +	1.12E-18	2.76E-19 +	7.19E-20	0.991583	6.872181	160.5825 +	0.542014
	6	3.77E-15 +	5.16E-18	1.24E-15 +	3.7E-18	2.85E-18 +	6.31E-20	2.17E-18 +	1.18E-18	3.61E-19 +	1.03E-19	0.971727	2.956811	70.85054 +	0.633901
	7	3.66E-15 +	7.01E-18	1.07E-15 +	2.81E-18	2.8E-18 +	5.54E-20	2.95E-18 +	9.78E-19	1.59E-18 +	1.13E-19	0.871492	2.992521	71.68945 +	0.797128
	8	1.42E-15 +	4.96E-18	4.6E-16 +	1.87E-18	1.26E-18 +	5.47E-20	2.96E-18 +	1.1E-18	3.73E-19 +	1.06E-19	0.922478	2.854924	68.45488 +	1.686375
	9	1.39E-15 +	7.04E-18	4.51E-16 +	1.85E-18	1.21E-18 +	5.26E-20	1.84E-18 +	8.93E-19	3.07E-19 +	1.1E-19	0.934582	2.871255	68.83908 +	1.802183
	10	9.97E-17 +	1.9E-18	2.36E-17 +	7.71E-19	2.71E-19 +	1.12E-19	1.69E-18 +	1.01E-18	1.1E-19 +	6.88E-20	0.672699	2.839154	68.0838 +	21.11041
	11	3.92E-15 +	1.76E-17	1.22E-15 +	3.87E-18	2.21E-18 +	3.79E-20	3.96E-18 +	9.81E-19	8.1E-19 +	1.83E-19	0.938898	3.011225	72.12867 +	1.144225
	12	3.68E-15 +	8.3E-18	1.18E-15 +	3.78E-18	3.06E-18 +	5.96E-20	7.87E-19 +	8.55E-19	5.37E-20 +	1.78E-19	0.99569	3.099108	74.19107 +	1.106904
	14	2.25E-15 +	4.81E-18	6.71E-16 +	1.83E-18	1.59E-18 +	4.81E-20	3.05E-17 +	8.47E-19	2.11E-19 +	1.72E-19	0.972299	3.256134	77.87018 +	1.914682
	15	7.21E-15 +	1.43E-17	2.07E-15 +	4.03E-18	4.97E-18 +	4.12E-20	3.15E-18 +	7.43E-19	3.19E-19 +	1.8E-19	0.98694	3.443105	82.24115 +	0.657636
	16	2.81E-15 +	2.21E-17	8.47E-16 +	3.57E-18	2.36E-18 +	6.15E-20	1.4E-18 +	1.09E-18	4.16E-19 +	8.56E-20	0.956276	3.172062	75.90131 +	1.006758
	17	1.36E-14 +	2.89E-17	4.38E-15 +	9.7E-18	1.06E-17 +	5.86E-20	2.94E-17 +	1.04E-18	1.43E-18 +	8.69E-20	0.969085	3.019135	72.31441 +	0.268658
	19	2.62E-14 +	3.19E-17	3.67E-15 +	7.85E-18	8.19E-18 +	9.73E-20	9.13E-18 +	8.54E-19	7.43E-19 +	7.97E-20	0.991603	7.061502	164.8102 +	0.435457
	20	8.53E-16 +	3.53E-18	2.47E-16 +	1.15E-18	7.05E-19 +	3.7E-20	1.17E-18 +	8.18E-19	2.97E-19 +	7.56E-20	0.897072	3.100094	74.21419 +	2.231716
	21	3.39E-15 +	6.6E-18	1.05E-15 +	2.07E-18	2.57E-18 +	5.37E-20	4.28E-19 +	1.29E-18	7.43E-19 +	1.1E-19	0.935145	3.01862	72.30231 +	0.769986
	22	3.04E-15 +	3.13E-18	9.96E-16 +	3.44E-18	2.42E-18 +	5.35E-20	-1.1E-18 +	1.1E-18	2.65E-19 +	1.08E-19	0.974203	2.974306	71.26159 +	0.811472
	23	7.96E-15 +	9.6E-18	2.4E-15 +	6.15E-18	5.54E-18 +	6.78E-20	1.47E-18 +	1.02E-18	1.67E-18 +	1.15E-19	0.938035	3.111442	74.48031 +	0.406276
	24	1.15E-16 +	2.06E-18	1.93E-17 +	7.59E-19	2.41E-19 +	5.37E-20	-2.1E-18 +	1.01E-18	1.47E-19 +	1.05E-19	0.619768	3.673003	87.60118 +	38.66931
	25	1.36E-14 +	1.35E-17	1.58E-15 +	3.73E-18	3.71E-18 +	5.14E-20	-2.4E-18 +	1.14E-18	2.58E-19 +	1.04E-19	0.994388	8.561864	197.9691 +	0.679349
	26	4.46E-15 +	7.13E-18	1.46E-15 +	5.42E-18	3.41E-18 +	5.05E-20	3.37E-18 +	7.4E-19	4.11E-19 +	1.6E-19	0.972761	2.97295	71.22972 +	0.832851
	27	1.64E-15 +	6.06E-18	4.98E-16 +	1.16E-18	1.76E-18 +	6.12E-20	1.23E-18 +	6.93E-19	3.63E-19 +	1.25E-19	0.934534	3.080285	73.74953 +	1.815946
	28	4.99E-15 +	5.44E-18	1.59E-15 +	6.4E-18	4.33E-18 +	9.15E-20	2.43E-18 +	6.42E-19	2.67E-19 +	1.3E-19	0.984226	3.096074	74.11991 +	0.660355
	29	3.74E-15 +	3.24E-18	1.18E-15 +	2.33E-18	2.82E-18 +	8.28E-20	6.54E-18 +	1.07E-18	2.64E-19 +	1.06E-19	0.979086	3.112823	74.51271 +	0.662753
	30	2.57E-15 +	1.01E-17	8.44E-16 +	2.29E-18	2.23E-18 +	6.7E-20	2.39E-18 +	1.4E-18	3.29E-19 +	1.03E-19	0.962161	2.930167	70.22437 +	0.935615
	33	2.72E-15 +	1.04E-17	8.43E-16 +	2.01E-18	1.98E-18 +	3.59E-20	1.13E-18 +	9.11E-19	4.15E-19 +	9.37E-20	0.954871	3.075892	73.64648 +	0.860301
	34	3.12E-15 +	5.45E-18	1E-15 +	2.08E-18	2.15E-18 +	4.78E-20	6.63E-18 +	9.96E-19	2.6E-19 +	9.53E-20	0.975344	3.028401	72.53195 +	0.70623
	36	1.43E-15 +	6.3E-18	4.75E-16 +	1.13E-18	8.91E-19 +	4.07E-20	5.14E-19 +	8.55E-19	9E-20 +	1.54E-19	0.981414	2.954098	70.78679 +	2.322787
	37	2.1E-15 +	7.5E-18	6.9E-16 +	1.9E-18	1.53E-18 +	4.06E-20	5.11E-18 +	9.35E-19	2.14E-19 +	1.56E-19	0.969837	2.944469	70.56052 +	1.641178
	38	1.99E-15 +	5.53E-18	6.54E-16 +	2.16E-18	1.63E-18 +	4.52E-20	2.48E-18 +	7.52E-19	1.43E-19 +	1.53E-19	0.978684	2.976027	71.30201 +	1.697326
	39	3.14E-15 +	4.34E-18	9.97E-16 +	1.6E-18	2.62E-18 +	5.18E-20	2.35E-18 +	7.74E-19	4.22E-19 +	1.51E-19	0.960275	3.024421	72.4385 +	1.088534
	40	4.29E-15 +	4.79E-18	7.52E-16 +	1.43E-18	1.49E-18 +	3.18E-20	4.08E-20 +	8.11E-19	1.98E-19 +	1.52E-19	0.986356	5.626824	132.5226 +	1.436481

Appendix-E continued:

Assam Basin Miocene muscovite cooling age data.

		^{40}Ar (*+atm)		^{39}Ar(K)		^{38}Ar (Cl+atm)		^{37}Ar(Ca)		^{36}Ar(Atm)		%Rad	R	Age (Ma)		%-sd
Assam Barail	1	4.529E-15	+ 8.991E-18	2.76E-15	+ 3.8E-18	7.31E-18	+ 1.1E-19	2.35E-18	+ 1.01E-18	9.56E-19	+ 1.49E-19	0.937602	1.540456	37.259091	+ 0.397711	0.010674
SU-2 Muscovite	2	2.155E-15	+ 6.405E-18	9.92E-16	+ 3.3E-18	3.16E-18	+ 9.14E-20	-8.4E-19	+ 9.77E-19	2.12E-18	+ 1.15E-19	0.709694	1.541128	37.275191	+ 0.86314	0.023156
(95°48'30"E	3	7.078E-15	+ 1.21E-17	1.42E-15	+ 3.3E-18	4.72E-18	+ 8.04E-20	-5.4E-19	+ 6.77E-19	8.4E-18	+ 2.19E-19	0.649156	3.229504	77.24677	+ 1.14397	0.014809
27°16'30"N)	4	8.428E-15	+ 1.049E-17	4.77E-15	+ 1.3E-17	1.14E-17	+ 1.2E-19	7.02E-19	+ 8.05E-19	4.53E-18	+ 1.94E-19	0.841304	1.486759	35.973183	+ 0.319052	0.008869
	5	3.905E-15	+ 4.87E-18	2.16E-15	+ 4.5E-18	5.47E-18	+ 8.67E-20	3.51E-19	+ 8.54E-19	1.72E-18	+ 1.7E-19	0.8696	1.571239	37.995864	+ 0.572069	0.015056
	6	5.812E-16	+ 2.551E-18	9.58E-18	+ 4.4E-19	4.1E-19	+ 1.05E-19	3.02E-18	+ 1.16E-18	1.92E-18	+ 1.65E-19	0.024449	1.482856	35.879674	+ 155.258	4.327186
	7	1.102E-14	+ 1.305E-17	1.07E-15	+ 4.1E-18	6.68E-18	+ 1.1E-19	2.16E-18	+ 1.11E-18	2.68E-17	+ 5.44E-19	0.281209	2.90508	69.634595	+ 3.808115	0.054687
	8	1.894E-14	+ 2.332E-17	3.63E-15	+ 5.3E-18	1.77E-17	+ 1.63E-19	1.43E-18	+ 9.75E-19	4.51E-17	+ 3E-19	0.295993	1.545821	37.387517	+ 0.651632	0.017429
	9	4.389E-15	+ 1.058E-17	7.54E-16	+ 3.8E-18	3.71E-18	+ 8.11E-20	1.75E-18	+ 1.09E-18	1.12E-17	+ 2.62E-19	0.246217	1.433553	34.698136	+ 2.666167	0.076839
	10	8.947E-15	+ 1.048E-17	3.43E-15	+ 8E-18	1.04E-17	+ 6.94E-20	-6.1E-20	+ 8.73E-19	1.15E-17	+ 1.53E-19	0.620454	1.617697	39.107218	+ 0.363249	0.009289
	11	3.85E-15	+ 7.444E-18	2.27E-15	+ 4.5E-18	5.73E-18	+ 9.66E-20	-1.3E-18	+ 1.03E-18	5.12E-19	+ 8.11E-20	0.960692	1.630107	39.403971	+ 0.279463	0.007092
	12	4.679E-15	+ 1.256E-17	2.52E-15	+ 8E-18	5.45E-18	+ 6.5E-20	2.47E-18	+ 1.03E-18	1.08E-18	+ 1.31E-19	0.93171	1.729447	41.7777	+ 0.415453	0.009944
	13	1.222E-14	+ 1.836E-17	3.64E-15	+ 6.5E-18	8.46E-18	+ 9.78E-20	9.93E-19	+ 8.21E-19	9.09E-19	+ 1.06E-19	0.978017	3.280354	78.43698	+ 0.27706	0.003532
	14	5.321E-15	+ 7.602E-18	2.95E-15	+ 7.4E-18	8.62E-18	+ 1.91E-19	8.35E-19	+ 8.43E-19	9.15E-19	+ 1.15E-19	0.949205	1.713079	41.386788	+ 0.306019	0.007394
	15	9.358E-15	+ 1.228E-17	5.42E-15	+ 8.2E-18	1.58E-17	+ 1.3E-19	1.99E-18	+ 7.99E-19	2.21E-18	+ 1.62E-19	0.930081	1.607203	38.856248	+ 0.229597	0.005909
	16	1.181E-15	+ 3.413E-18	6.67E-16	+ 3.5E-18	1.13E-18	+ 4.71E-20	1.37E-18	+ 7.64E-19	6.52E-19	+ 1.35E-19	0.836684	1.481827	35.855041	+ 1.472336	0.041064
	17	1.81E-15	+ 5.265E-18	1.07E-15	+ 4.7E-18	2.1E-18	+ 4.32E-20	-2.8E-19	+ 4.97E-19	8.08E-19	+ 1.39E-19	0.868027	1.464482	35.439433	+ 0.952173	0.026868
	18	5.039E-15	+ 5.165E-18	2.49E-15	+ 4E-18	5.5E-18	+ 1.01E-19	2.73E-19	+ 7.61E-19	3.58E-18	+ 2.06E-19	0.790294	1.596929	38.610502	+ 0.597137	0.015466
	19	1.447E-14	+ 1.58E-17	1.78E-15	+ 3.5E-18	4.12E-18	+ 6.82E-20	1.06E-18	+ 8.84E-19	7E-19	+ 1.1E-19	0.985715	7.991957	185.44549	+ 0.598263	0.003226
	20	1.735E-14	+ 1.331E-17	2.37E-15	+ 7.2E-18	5.8E-18	+ 9.27E-20	1.75E-18	+ 5.53E-19	7.78E-19	+ 1.03E-19	0.986749	7.231888	168.60668	+ 0.613189	0.003637
	21	1.544E-15	+ 3.37E-18	9.36E-16	+ 3.5E-18	2.09E-18	+ 6.58E-20	7.27E-19	+ 6.52E-19	4.56E-19	+ 1.32E-19	0.912828	1.505284	36.416922	+ 1.024561	0.028134
	23	1.575E-15	+ 3.04E-18	9.22E-16	+ 3.1E-18	2.14E-18	+ 7.13E-20	5.75E-20	+ 1.02E-18	6.13E-19	+ 1.27E-19	0.884938	1.510712	36.546918	+ 1.001125	0.027393
	24	8.035E-16	+ 4.83E-18	4.43E-16	+ 2.4E-18	1.11E-18	+ 4.35E-20	2.11E-19	+ 6.84E-19	5.55E-19	+ 1.03E-19	0.795954	1.443466	34.935768	+ 1.700716	0.048681
	25	2.136E-15	+ 8.041E-18	1.36E-15	+ 2.8E-18	2.47E-18	+ 4.64E-20	6.59E-19	+ 6.56E-19	5.34E-19	+ 1.21E-19	0.926156	1.449937	35.090855	+ 0.655782	0.018688
	26	9.428E-15	+ 8.433E-18	5.69E-16	+ 1.9E-18	8.22E-19	+ 1.82E-20	-5.4E-20	+ 4.03E-19	4.54E-19	+ 1.02E-19	0.985765	16.33477	360.62739	+ 1.738886	0.004822
	27	1.943E-15	+ 3.255E-18	1.14E-15	+ 5.3E-18	2.52E-18	+ 6.93E-20	-2E-18	+ 9.24E-19	8.78E-19	+ 1.04E-19	0.86644	1.474607	35.682052	+ 0.68375	0.019162
	28	2.45E-15	+ 3.592E-18	1.59E-15	+ 6.8E-18	4.7E-18	+ 1.34E-19	-8E-19	+ 5.68E-19	4.36E-19	+ 1.12E-19	0.947421	1.460771	35.350517	+ 0.531799	0.015044
	29	2.973E-16	+ 2.858E-18	1.49E-16	+ 1.2E-18	4.55E-19	+ 4.32E-20	4.3E-19	+ 4.82E-19	4.14E-19	+ 1.27E-19	0.588809	1.171744	28.410842	+ 6.144804	0.216284
	31	9.285E-16	+ 1.938E-18	2.78E-16	+ 1.5E-18	5.39E-19	+ 4.56E-20	6.38E-19	+ 9.39E-19	2.47E-20	+ 1.1E-19	0.992145	3.318612	79.331965	+ 2.863978	0.036101
	32	6.956E-15	+ 1.377E-17	2.04E-15	+ 2.5E-18	6.51E-18	+ 1.32E-19	1.29E-18	+ 8.53E-19	8.39E-19	+ 1.17E-19	0.964359	3.294436	78.766457	+ 0.449868	0.005711
	33	6.143E-15	+ 1.065E-17	1.96E-15	+ 4.7E-18	3.73E-18	+ 6.34E-20	1.59E-18	+ 7.28E-19	5.45E-19	+ 1.17E-19	0.973766	3.044667	72.913746	+ 0.476376	0.006533
	34	2.567E-14	+ 3.972E-17	7.7E-15	+ 1.2E-17	2.06E-17	+ 3E-19	2.94E-18	+ 8.65E-19	8.99E-19	+ 1.15E-19	0.989651	3.299411	78.88285	+ 0.204804	0.002596
	35	2.831E-15	+ 5.911E-18	8.3E-16	+ 3.4E-18	2.67E-18	+ 6.89E-20	9.25E-19	+ 1.04E-18	2.15E-19	+ 1.07E-19	0.977567	3.33418	79.696002	+ 0.982788	0.012332
	36	4.362E-15	+ 7.111E-18	1.31E-15	+ 3.8E-18	2.75E-18	+ 3.41E-20	2.14E-18	+ 9.52E-19	5.04E-19	+ 1.34E-19	0.965859	3.219327	77.008465	+ 0.774436	0.010056
	37	3.433E-15	+ 7.624E-18	1.05E-15	+ 5E-18	1.9E-18	+ 3.21E-20	-6.9E-19	+ 7.38E-19	4.77E-19	+ 1.28E-19	0.958956	3.13678	75.074403	+ 0.957292	0.012751
	38	9.629E-15	+ 1.278E-17	5.59E-15	+ 1.4E-17	1.35E-17	+ 1.25E-19	3.82E-18	+ 8.18E-19	2.56E-18	+ 1.85E-19	0.921498	1.588419	38.406909	+ 0.265177	0.006904
	39	1.315E-15	+ 2.051E-18	8.53E-16	+ 4.6E-18	2.06E-18	+ 5.08E-20	-1.3E-18	+ 7.7E-19	1.9E-19	+ 1.5E-19	0.957364	1.476763	35.733711	+ 1.272359	0.035607
	40	1.19E-15	+ 3.893E-18	3.33E-16	+ 2.4E-18	3.2E-19	+ 2.03E-20	-1.5E-18	+ 7.27E-19	6.82E-19	+ 1.41E-19	0.830757	2.969787	71.155418	+ 3.070437	0.043151
	42	1.362E-15	+ 3.008E-18	8.71E-16	+ 3.4E-18	1.61E-18	+ 3.79E-20	9.91E-19	+ 5.05E-19	4.27E-19	+ 1.2E-19	0.907289	1.419944	34.371853	+ 1.00202	0.029152
	44	9.537E-16	+ 2.643E-18	3.83E-16	+ 2.7E-18	7.83E-19	+ 4.89E-20	2.88E-19	+ 7.34E-19	1.26E-18	+ 1.55E-19	0.61	1.51669	36.69008	+ 2.937229	0.080055
	45	2.704E-15	+ 6.379E-18	8.67E-16	+ 5.3E-18	1.17E-18	+ 4.28E-20	7.62E-19	+ 6.25E-19	4.96E-19	+ 1.04E-19	0.945814	2.949344	70.675073	+ 0.981085	0.013882
	46	4.997E-15	+ 1.339E-17	2.89E-16	+ 2.5E-18	9.7E-19	+ 7.27E-20	2.36E-18	+ 1.2E-18	1.08E-18	+ 1.38E-19	0.936217	16.18847	357.69745	+ 4.704122	0.013151
	47	3.633E-15	+ 8.885E-18	1.88E-15	+ 4.4E-18	4.67E-18	+ 8.86E-20	9.38E-19	+ 5.81E-19	4.53E-19	+ 1.29E-19	0.963153	1.857908	44.842621	+ 0.514639	0.011477
	48	1.374E-14	+ 9.164E-18	8.52E-16	+ 4.1E-18	2.31E-18	+ 4.77E-20	2.83E-19	+ 6.57E-19	5.49E-19	+ 1.64E-19	0.988188	15.94794	352.87008	+ 2.135046	0.006051
	49	1.212E-15	+ 3.846E-18	7E-16	+ 1.9E-18	2.52E-18	+ 7.03E-20	5.38E-19	+ 7.86E-19	4.25E-19	+ 9.42E-20	0.896323	1.552251	37.541438	+ 0.977714	0.026044
	50	2.105E-15	+ 9.061E-18	6.72E-16	+ 2.5E-18	2.13E-18	+ 5.13E-20	-4E-19	+ 7.99E-19	4.35E-19	+ 1.25E-19	0.938983	2.942311	70.509791	+ 1.387584	0.019679
	91	2.139E-15	+ 8.73E-18	6.22E-16	+ 2.1E-18	1.03E-18	+ 2.74E-20	-3.9E-19	+ 6.54E-19	6.82E-20	+ 1.09E-19	0.990571	3.403787	81.322861	+ 1.309717	0.016105
	92	1.292E-15	+ 2.872E-18	6.72E-16	+ 3E-18	1.82E-18	+ 7.62E-20	-1.7E-19	+ 8.08E-19	-7.9E-20	+ -9.5E-20	1.018025	1.957861	47.223784	+ 1.038129	0.021983
	93	1.925E-15	+ 4.357E-18	9.05E-16	+ 4.1E-18	2.02E-18	+ 5.13E-20	-1.2E-18	+ 6.92E-19	1.72E-18	+ 1.66E-19	0.736374	1.566529	37.883164	+ 1.335005	0.03524
	94	5.276E-15	+ 1.92E-17	1.55E-15	+ 3E-18	3.58E-18	+ 6.09E-20	2.82E-18	+ 6.94E-19	6.23E-19	+ 1.43E-19	0.965094	3.280237	78.43424	+ 0.731996	0.009333
	95	2.042E-15	+ 1.616E-17	1.18E-15	+ 6.9E-18	2.91E-18	+ 5.29E-20	8.05E-19	+ 8.27E-19	3.26E-19	+ 1.27E-19	0.952834	1.651955	39.926303	+ 0.875663	0.021932
	96	8.95E-15	+ 1.883E-17	5.58E-15	+ 8.6E-18	1.24E-17	+ 9.13E-20	3.24E-18	+ 6.17E-19	1.03E-18	+ 1.86E-19	0.966108	1.549148	37.467159	+ 0.259202	0.006918
	97	6.327E-15	+ 1.848E-17	1.85E-15	+ 4.7E-18	3.93E-18	+ 6.32E-20	1.75E-18	+ 6.44E-19	3.58E-19	+ 1.5E-19	0.983302	3.362284	80.353045	+ 0.655177	0.008154
	98	1.26E-15	+ 1.573E-17	7.7E-16	+ 2.9E-18	2.15E-18	+ 6.29E-20	1.3E-18	+ 8.31E-19	7.09E-20	+ 1.34E-19	0.98337	1.609642	38.914595	+ 1.352944	0.034767
	99	1.31E-15	+ 3.253E-18	7.28E-16	+ 5.3E-18	1.67E-18	+ 4.1E-20	-3.8E-19	+ 7.75E-19	4.72E-19	+ 1.54E-19	0.893515	1.608471	38.886571	+ 1.54678	0.039777
	100	4.839E-15	+ 8.713E-18	1.44E-15	+ 5.7E-18	3.04E-18	+ 3.2E-20	1.22E-18	+ 7.89E-19	4.8E-19	+ 9.21E-20	0.97	3.252231	77.778836	+ 0.568163	0.0073

Appendix-E continued:

Photomicrographs of muscovite grains of the samples (SU-2: Miocene; T-12 and B-2: Oligocene) analyzed for this study.